ACOUSTIC PROPERTIES OF RESERVOIR FLUIDS

A DISSERTATION
SUBMITTED TO THE DEPARTMENT OF GEOPHYSICS
AND THE COMMITTEE ON GRADUATE STUDIES
OF STANFORD UNIVERSITY
IN PARTIAL FULFILLMENT OF THE REQUIREMENTS
FOR THE DEGREE OF
DOCTOR OF PHILOSOPHY

By
Yuguang Liu
June, 1998

© Copyright 1998 by Yuguang Liu
All Rights Reserved

I certify that I have read this thesis and that in my opinion it is fully adequate, in scope and in quality, as a dissertation for the degree of Doctor of Philosophy.

Dr. Amos Nur
(Principal adviser)

I certify that I have read this thesis and that in my opinion it is fully adequate, in scope and in quality, as a dissertation for the degree of Doctor of Philosophy.

Dr. Gerald M. Mavko

I certify that I have read this thesis and that in my opinion it is fully adequate, in scope and in quality, as a dissertation for the degree of Doctor of Philosophy.

Dr. Jack Dvorkin

Approved for the University Committee on Graduate Studies:

Abstract

Both water and hydrocarbons are important resources in reservoir exploration. Hydrocarbons are basic constituents of oil, and water forms the basis of gas hydrate. These real reservoirs behave as mixtures or solutions including dissolved gases, and the properties of a solvent can be significantly affected by the type and concentration of gas dissolved in it. A crucial part of any reservoir monitoring research program must experimentally determine the acoustic velocities, compressibilities, and densities of various gas-fluid solutions at varying temperatures, pressures, and concentrations.

Several theoretical methods are used to estimate these quantities. The properties in a certain phase have long been calculated using the Equation of State (EOS). By thermodynamic theory, EOS can be derived from the acoustic fluid properties that are the function of temperature and pressure under special conditions. Another technique, molecular-level study, yields a statistical picture of the bulk properties of a fluid. Experimental tools allow us to measure these bulk properties under simplified conditions. The theoretical models help us gain a deeper insight into the mechanisms behind the bulk behavior.

In order to obtain accurate data for these properties of fluids, this thesis has conducted a sensitive measurement using wave interference. We used a double-pulse signal emitted from an ultrasonic transducer, which was located between two reflectors. Using interference between the two reflected signals, we calculated velocity and density with estimated related error below 0.02%.

We started our measurements from simple fluids, for most of which we have handbook data. Pure sample measurement can give not only data at conditions different from those covered in the handbook, but also confidence for verification and calibration of experimental design. Measurement of pure fluids is the first step in obtaining robust and reliable results for unknown gas-fluid solutions. Typical gas solutes, CO_2, CH_4, N_2 and NH_3, and solvents, water and decane, were selected as the samples for the solution study. We discovered that the two solvents showed reverse trends in velocity when gas was dissolved into them. For gas aqueous solution, the sound speed of the solution increases with increasing concentration. Velocity increases up to 50

m/s ($\approx 3\%$) and 140 m/s ($\approx 9\%$) for CO_2 aqueous solution and NH_3 aqueous solution respectively. These results were obtained at room temperature ($\approx 22^oC$) with CO_2 saturated vapor pressure of 400 psi (where CO_2 concentration in mole fraction is about 0.8%), and NH_3 saturated vapor pressure of 70 psi. Velocity increases only slightly for CH_4 and N_2 aqueous solutions (only 1.5 m/s for CH_4 and 2.5 m/s for N_2 at saturated vapor pressures of 700 psi and 850 psi, respectively). Conversely, for gases dissolved in decane, the sound velocity of the solution decreases with increasing concentration. Velocity decreases about 100 m/s for CH_4 ($\approx 8\%$), 130 m/s for CO_2 ($\approx 10\%$), and 47 m/s for N_2 ($\approx 4\%$) at saturated vapor pressures of 500 psi, 400 psi, and 600 psi, respectively. Water yielded anomalous properties while decane gave normal results. Relations between sound velocity and gas concentration have been quantitatively related to the control parameters by considering the experiment conditions, and the dynamic solution process was analyzed with a diffusion model.

We propose a mechanism to interpret the anomalous properties of water during gas dissolution. We base our interpretation on the interstitial ice structure combined with molecular interaction. Gas dissolving into a normal fluid weakens the properties caused by molecular interaction, because the interaction between the gas solute molecule and the solvent molecule is weaker than that between pure fluid solvent molecules. Water behaves abnormally because of its hydrogen bonds and special lattice structure, where a vacancy exists in each bonded unit. Free solute molecules can occupy the vacancies in some of the units to strengthen the entire system. The normal behavior dominates after the solute molecules outnumber the available vacancies in the water structure. The number of vacancies in the water structure is temperature-dependent. Higher temperature breaks some bonds and produces free water molecules. We can extend this interpretation to predict the acoustic properties of gas hydrate.

Acknowledgment

I would like to take this opportunity to give my deeply felt gratitude to the people who have made my initial ideas grow into this dissertation. My first and foremost thanks go to my advisor, Amos Nur, for his encouragement, understanding, invaluable advice, and continuous support throughout my graduate study at Stanford. I am so fortunate to have him as my advisor who always identifies and guides the good ideas of mine, and understands how to provide a relaxed, self-motivating research environment where my creativity can be brought out at its best. I will never forget his efforts to help me come to Stanford and his understanding in critical points of my academic development. As it is coming to the close of my graduate study, I want to let him know that all my progress and innovations as crystallized in this dissertation would be simply impossible without him.

I am also thankful to all the faculty, staff and colleagues for their help in all these years. In particular, Professor Gary Mavko not only provides theoretical inspiration to this study, but also gives very insightful suggestions to my experimental methods. I also want to thank Dr. Jack Dvorkin for his valuable comments and helpful discussions during this study. My committee members, Jerry Harris, Roland Horne, and Howard Zebker, deserve special thanks for their illuminating questions and suggestions to advance the project. I also owe thanks to Zhijing Wang, Hezhu Yin, Frank Liu, Manika Prasad and Masumi Yamashita for their helpful comments from time to time. Margaret Muir has been such a great help in providing what I need for the experiment. She is always so warm and resourceful. All my colleagues in SRB have made the occasionally frustrating research processes more humane and bearable. I am thankful to them for making my years at Stanford such a memorable experience.

Dawn Burgess have provided me with careful editing of this dissertation. Her marvelous understanding of a non-native speaker has made the dissertation more readable. My thanks also go to Xiaowei Luo for her proofreading of this work and helpful tips for my presentation.

My friends have been among my greatest assets. They have been the joy of my life throughout the five years at Stanford. My good friend, Yung-Hung Wang,

has provided me great help and advice both inside and outside my academic life. Xiaowei Luo, Yalei Sun, Yanping Lu and many others have made me realize my own weaknesses and overcome them.

I also want to take this opportunity to thank many of my teachers, who taught and encouraged me throughout my school years. My current achievement would be unimaginable without them. I have benefited so much from Professor Guozhen Zhu when I was at Acoustic Lab, Tsinghua University, China. Ms. Yue Chen also helped immensely with the transducers I used in this dissertation project.

I have stayed in school for about 27 years by now. My parents have always been my greatest spiritual support. I was born in a remote and poor rural area in China. It took deep love, courage and faith for them to support me to strive for academic fulfillment. I can never thank them enough, and I only hope I will never disappoint them.

I am very fortunate to meet Qingdi, who is a student in Caltech, in my last and busiest year at Stanford. She has made the hardest work the sweetest. Without any complaint, she spent her holidays drawing most of the diagrams in this thesis.

Contents

List of Tables

List of Figures

Chapter 1

Introduction

1.1 General Purpose

Seismic methods have been widely used in exploring the earth. To obtain useful information from seismic logs and seismic interpretations, 3-D seismic reservoir images, seismic production monitoring, and enhanced oil recovery (EOR) processes, the acoustic properties of the crust's individual constituents, both rocks and fluids, must be known. To interpret seismic results, many theoretical models, such as Gassmann's relation, Biot's theory, and Squirt theory, have been proposed. These models are strongly influenced by the properties of the saturating fluid, especially under in-situ conditions of high pressure and temperature. However, there are few measurements and data on the acoustic properties of fluids (Clark, 1992).

In hydrocarbon exploration and production, reservoirs are now being discovered deeper and deeper in the earth's crust, where the pressure and temperature become higher and higher. The physics of fluids and gases becomes more complicated, and it may become difficult to distinguish among the various constituents of a mixed oil-gas reservoir.

Hydrocarbons are basic components of oil. The efforts of oil-related studies from several different disciplines were summarized (Montel, 1993). Oil producers use Pressure-Volume-Temperature (PVT) to successfully design production facilities

using predetermined tables. But PVT measurements are cumbersome and complicated to obtain, and are also inaccurate for determining acoustic properties such as velocity, adiabatic modulus, viscosity, etc. Biological markers are sometimes used to reconstruct the process of oil formation to learn about the oil's origin and composition, but such markers represent only a small part of the total oil mass. Physicists try to determine hydrocarbon fluid properties more rigorously to ensure correlation among various empirical tables, but it is still very difficult to characterize the rich mixture of hydrocarbon fluids found in real oil samples. Although equations of state (EOS) have been studied for a long time, their usefulness is still restricted to special conditions or simple fluids. Most of the models are still too simple to solve problems in real oils. Some reservoir fluids' EOS can be designed only by defining mixing rules and given parameters of the various fluids, which can be found individually and experimentally. More general models remain unknown. Challenges also appear in dealing with macroscopic transport problems with no stable equilibrium.

Water is of course the principle constituent of living organisms, which consist of up to 95% water (Franks, 1972), and life cannot exist without water, even for a short time. Fortunately, water is a major constituent of the earth's surface, which contains $1.4 \times 10^{24} g$ in the ocean and $0.8 \times 10^{24} g$ chemically bound to the rock of the crust (Eisenberg, 1969). Studies of water properties have developed from different perspectives, and have revealed many behavioral anomalies in the pure water form. For example, volume decreases after melting, density has a maximum in the liquid state (at $4°C$) rather than in the solid (ice) state, isothermal compressibility has a minimum at $46°C$ of the liquid state; water has anomalously high melting, boiling, and critical points for its molecular weight, it has a high dielectric constant, and so on (Stillinger, 1980). This demonstrates the incredible complexity of both water and its solutions and makes further study necessary for understanding its important role. Gas solutions in water further complicate the picture, and understanding their acoustic properties may give insight into the interactions that make water so unusual and vital.

There is growing interest in the study of gas hydrates, because hydrate reservoirs have been considered as a potential future energy source. Natural gas in its hydrate

form may contain twice the energy of the rest of the earth's total fossil fuel resources put together (Sloan, 1990). The total amount of ocean hydrate can be estimated at around $1.8 \times 10^{16} m^3$ (Kvenvolden, 1988). The energy required for dissociation of methane hydrate is only 10% of the recovered energy (Sloan, 1990). The formation and the stability of gas hydrate must be studied in general before large-scale exploration and production can be effective. The mechanics of gas dissolution and the properties of gas in solution will be important to further understand the formation of and detection of hydrate.

1.2 Review of Available Data

The velocity of sound in water has been well studied under varying temperature and pressure. Wilson (1959) thoroughly investigated the velocity of water as a function of temperature, which ranged from 0 to 100°C, and pressure, which ranged from 0 to 1000 bar. Fine and Millero (1973) extracted an empirical relation from the data. However, the study of hydrous solutions has been limited. A complete data set exists for brine, and an empirical relation has been reported by Bark (1964). In our literature search, we have found no data on the sound speed of gas-water solutions.

Hydrocarbons have been emphasized in the literature because they are the constituents of oils. Wang (1988) made complete measurements on different kinds of real oils and gave an empirical relation between velocity and density (or API) (Batzle, 1992). Because real oils consist of a variety of hydrocarbons, from low molecular weights, which may be in the gaseous state, to high-molecular-weight liquids, the critical effect on velocity cannot be seen easily. The complexity of such mixtures limits their usefulness for explicit study.

1.3 Review of Conventional Measurement Techniques

There are three main methods for measuring velocity (Bhatia, 1967): (a) the interferometric method, (b) the optical method, and (c) the pulse methods. The interferometric method is a standing wave method. The emitted continuous wave interferes with the reflected wave, and a series of maxima (or minima) appears, with the variation of distance being an integer multiple of wavelength. This method is not convenient when absorption is high and the efficiency of electro-mechanic conversion is low, leading to a large difference in amplitude between the emitted and the reflected waves. The optical method relies on diffraction of light passing through a sample. The elastic rarefaction and compression of the fluid change its optical properties, forming a diffraction grating from the maxima and minima of standing sound waves. However, this method can be used only for transparent samples. The pulse method usually determines the velocity by measuring travel-time. There are two requirements for this method: (1) the pulse should have many sinusoidal cycles at a single dominant frequency to avoid dispersion in highly dispersive media, and (2) the pulse width limits the shortest distance that can be measured without forming a standing wave. The first two methods measure the velocity by wavelength and are more accurate. The direct pulse method measures the travel-time and is less accurate. However, the pulse method is the most universal and easiest way to measure velocity. It has been widely used both in the lab and in real field measurements. We propose that the pulse method be combined with the interference method to infer the travel-time with very high accuracy, which may be necessary for precise study of fluid and fluid-gas solutions.

Phase delay measurements are often used in physics. The Michelson interferometer (Michelson, 1902) is a well known, optically precise instrument, which provided the first experimental evidence for Einstein's relativity theory. Phase measurements are easily accomplished using acoustic waves. Some have been used to measure the velocity of gas or fluid. A simple apparatus measuring at up to 10 kbar pressure was developed by Kortbeek (1985), based on the cancellation of a traveling wave train

(Williams, 1958), an accurate method for measuring solid velocity. A more complicated system, used at Acoustic Resonance Spectroscopy Lab, at the University of Florida (Colgate, 1990), measured gas and fluid properties. Such equipment was first established by Mehl (1981), based on spherical resonance theoretical results (Ferris, 1952). The theory relates the resonant frequency to the velocity of the material (gas or liquid) by focusing on only one resonant-frequency change. The phase boundary conditions, such as the bubble point, dew point, and critical point, and also the density and heat capacity, were derived by sonic and thermodynamic connection (Colgate, 1992). For our purposes, we prefer a simpler and more accurate device than the one used by Colgate. This thesis presents our design for such a device, based on Kortbeek's system and some general phase-measurement equipment used in physics. We use two reflectors with a double pulse emission. We find not only the precise velocity, but also the density of our sample by accurately measuring the volume change.

1.4 Review of Analysis Methods

The study of the physical properties of fluids and gases can be traced back to Boyle's law of 1662. This was extended in 1873 to real gases by van der Waals, who introduced the effects of intermolecular forces. The most general expression can be derived from thermodynamics in principle. Phase diagrams were introduced to express the transition between different states, and some properties of samples were derived using thermodynamics (Orr, 1995; McCain, 1990).

In order to understand explicitly the real sample, a vast amount of effort in physical chemistry has shifted to the micro-scale. Real phenomena were explored from the micro-structure of the material. For example, the concept of hydrogen bonding between water molecules was introduced by Latimer and Rodebush (1920) and became key to understanding liquid water and its solutions. Many modern techniques have recently been developed to explore the structure of water. For example, X-ray methods, high-resolution spectroscopy and Nuclear Magnetic Resonance are used to image the position of the water cluster and its orientation, and computer simulation of Monte Carlo methods (Liu, 1996) and molecular dynamics give the molecular

pattern the clusters form. However, there still is not a universally accepted model, and six stable molecular structures (Gregory, 1997) have been proposed by different authors. The structure of a liquid and its solution is a fundamental starting point for exploring or predicting the properties of the samples. There are no direct ways to use the molecular structure to predict the acoustic properties of a solution and its related thermodynamic properties. The solution of gas in liquid has not been studied as much as pure liquid, and the solution mechanics of gas have not been established. Experimental study using several different approaches will help to postulate the mechanics.

1.5 Summary of Chapters

The objective of this thesis is to develop an accurate measurement method to obtain the sound speed in fluids and gas-fluid solutions, and to further understand how a gas dissolves into a liquid. To this end, we performed the following:

- Developed an accurate method for velocity measurement under pressure and temperature, and created a laboratory system to apply the method.
- Measured pure fluid samples with the apparatus, not only to calibrate the system, but also to obtain velocity data of unknown fluids (including fluid-fluid mixtures).
- Developed a reliable protocol to measure velocity of gas-fluid solutions and quantitatively monitor the effect of the gas solution process.
- Developed a theoretical model to understand the mechanics of gas dissolution.

This dissertation is organized according to the above steps.

Chapter 2 is a detailed introduction to our measurement method and the main design of our system. A double-pulse method is used to obtain the travel time with a relative error of $\pm 0.02\%$ in velocity, which is one or two orders of magnitude more accurate than the usual direct travel-time method. The key parts of the system

setup include a simple measurement cell, basic structures for variable pressure and temperature measurements, and software control of the system.

Chapter 3 focuses on pure fluid measurements. Pure water is the most economic starting sample. The well-established data set for water allows us to test and calibrate the system. Brine is our second sample. The confidence we obtain from the close agreement between our results and published measurements moves us to measure the pure hydrocarbon samples. The rough measurement of fluid-fluid mixtures and gas-fluid solutions is a way to develop a proper measurement algorithm. The most reliable procedure for fluid measure is given and is extended for accurate gas-fluid study.

Chapter 4 gives the most important results of this study, measurements on gas-fluid solutions. Two important solvents, water and decane, are selected for study. A reverse trend in velocity is discovered when the same gas is dissolved into the different solvents. Results for CO_2, CH_4, N_2 and NH_3 gases dissolved in water are obtained, as are results for CO_2, CH_4 and N_2 gases dissolved in decane. The relation between velocity and gas content is derived in two different ways. One way estimates directly from the data, and the other uses a physical diffusion model to explore the dynamic dissolution process and quantitatively match the relation.

Chapter 5 is a theoretical study of gas-fluid solutions. The reverse trend in velocity is understood explicitly by considering intermolecular interactions and solution mechanics. Hydrogen bonds play a very important role in the unusual properties of water, including the inverse dependence of velocity on gas solute concentration.

In Chapter 6, we review our results and describe how our original contribution will be useful in the future. We suggest avenues for further study, both experimental and theoretical.

Chapter 2

Measurement Method and System Buildup

2.1 Introduction

In Chapter 1, we discussed the three main methods for velocity measurement. The pulse method has been widely used in seismic and other geophysics fields. It is also the most convenient way to measure fluid acoustic properties. The traditional method is to measure the travel time directly, and this can provide a lot of useful information. However, in reservoir-related studies, the dependence of fluid velocity on composition may be slight. A more accurate way is needed to characterize such samples.

This chapter develops a new, double-pulse method to measure phase difference instead of direct travel time. We start by introducing how the system works and what we can expect. Velocity measurement is the main purpose of this study, but some other parameters, such as density, impedance, and attenuation, may be obtained by proper extension. It is a convenient, accurate measurement method for low-attenuation fluid samples.

In constructing our laboratory equipment, we try to use the simplest design that satisfies the specific requirements. The first component is the physical cell. It must (1) be configured to produce reflected signals, (2) contain the fluid sample, (3) allow convenient changing of samples, (4) allow convenient wiring, and (5) be as small as

possible for laboratory use, especially under high pressure. The second component, the transducer, is the most important part of the system setup. It must avoid several potential problems: (1) Side wall reflections and multiples from the low-attenuation metal walls and reflectors may pose a problem; (2) Bubbles gathering on the transducer surface may attenuate or block the transmitted and received signals; and (3) Brine or ionized fluid samples must be electrically insulated to avoid signal grounding and to increase the signal-to-noise ratio. The third component is a specific waveform generator, needed to make the signal adjustable. The fourth component is the surrounding equipment, such as the temperature system, pressure system, and fluid or gas fill-up system. Finally, the fifth component is a central control system, including hardware and software, which is necessary to handle the tasks of control and data acquisition. How to meet the above requirements will be given in detail later.

2.2 Principle

2.2.1 Velocity measurement

As detailed in the next section on the measurement cell, the cell consists of two reflectors, one on each side, and an ultrasonic transducer somewhere between them. The basic principle is to generate an ultrasonic wave from the transducer, and to measure the phase difference between the reflected waves from either side. When one pulse, modulated by the resonance frequency of the transducer, is applied to the transducer, the same acoustic wave emits in two directions with opposite signs. The waves are reflected by each of the reflectors; the transducer receives the two reflected waveforms at different times, because the two reflectors are different distances from the transducer. The transducer is used as both an emitter and a receiver. Figure 2.1 gives a simple sketch of the system. If only one pulse is used, we must manually measure the time delay between the two reflectors. This introduces several sources of error, including picking the arrival times of the attenuated reflected pulses. To avoid this error, and to use frequency to obtain an accurate time delay, we introduce a double-pulse technique, shown in Figure 2.2.

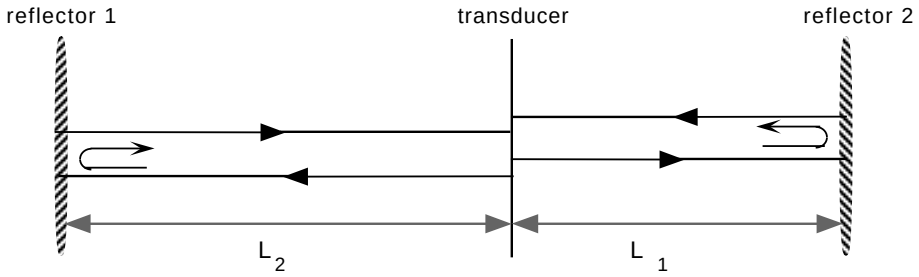

Figure 2.1: Pulse-echo method with two reflectors: L_1 and L_2 are the distance between transducer (in the middle) and reflectors (on both side), respectively.

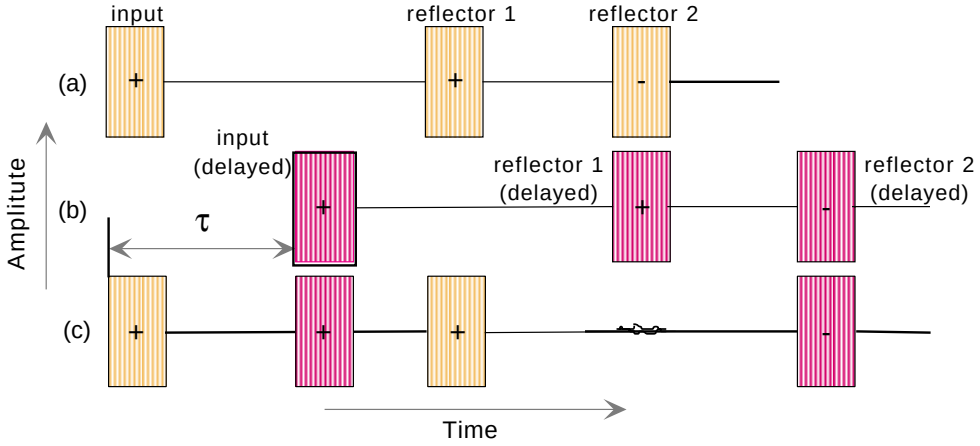

Figure 2.2: Received waveforms from the transducer: (a) waveform from one pulse emission, (b) waveform from delayed pulse emission, (c) cancellation by double pulse.

In Figure 2.2a, the first wavelet is a power signal applied to the transducer, usually at the transducer's resonance frequency for best received efficiency; the second and third wavelets come from shorter and longer reflection paths, respectively. Figure 2.2b shows the same waveforms as Figure 2.2a, but preceded by an adjustable time delay. This is the second, or delayed, pulse in our double-pulse technique. By adjusting the time delay, we can make the first received wave of the delayed emission from reflector 1 (the closer reflector) overlap approximately the reflection of the initial pulse from reflector 2 (the more distant reflector). The two waves interfere with each other, as shown in Figure 2.2c. The phase difference is as follows:

$$\Delta\phi = \omega\tau\,, \tag{2.1}$$

where $\Delta\phi$ is the phase difference, ω is the angular frequency, and τ is the adjustable time delay between pulses.

If two pulses can cancel each other, or $\Delta\phi = 180^\circ$ at frequency $\omega = 2\pi f_n$, then,

$$f_n\tau = n + \frac{1}{2}\,; \qquad n = 0, 1, 2, \cdots, \tag{2.2}$$

where n is the order of the interference index:

$$n = \frac{f_n}{\Delta f_n} - \frac{1}{2}\,,$$

and,

$$\Delta f_n = f_{n+1} - f_n\,.$$

By changing the frequency, we can make the frequency f_n satisfy the cancellation equation Equation 2.2. We can obtain the travel-time difference between reflector 1 and reflector 2 by measuring a series of the cancellation frequencies. The precision of the frequency measurement can reach 0.01%. The velocity is

$$v = \frac{l}{\tau}\,, \tag{2.3}$$

where l, the distance difference between two reflectors, is fixed:

$$l = L_2 - L_1 \,,$$

and can be calibrated by using a standard material at different pressures, p, and temperatures, T.

$$l(p,T) = l_0(1 + \alpha(T)\Delta T)(1 + \beta(p)\Delta p) \,, \tag{2.4}$$

where α is the thermal expansion coefficient, and β is the coefficient of compressibility. The accuracy of the distance measurement can reach 0.01% under high pressure and temperature after calibration. Therefore, the total estimated accuracy of velocity will lie within 0.02%.

2.2.2 Density measurement

If we now let one reflector be movable in the closed device, we can calculate how far the reflector moves under different pressures and temperatures, using the previously measured velocity under the same conditions with the fixed reflector. As

$$l_\rho = v * \tau \,,$$

where $v(p,T)$ and $l(p,T)$ are known, we can get the length change $\Delta l = l_\rho - l$ from the measured τ, and

$$\frac{\Delta\rho}{\rho_0} = -\frac{\Delta V}{V_0} = -\frac{\Delta l}{l} \,, \tag{2.5}$$

where V_0 and ΔV are the initial volume of the cell and volume change after reflector is moved, respectively. ρ_0 is the standard density under certain conditions, including temperature and pressure, and $\Delta\rho$ is the density change after conditions are changed. Therefore, in the closed system with one movable reflector, we can extract both volume and density change.

2.2.3 Impedance and Attenuation

The emission waves can be considered a normal incidental reflection from reflectors. The reflected coefficient is determined by these equations:

$$R_1 = \frac{Z_1 - Z_0}{Z_1 + Z_0}, \tag{2.6}$$

$$R_2 = \frac{Z_2 - Z_0}{Z_2 + Z_0}, \tag{2.7}$$

where Z_1, Z_2, and Z_0 are the first reflector impedance, second reflector impedance, and fluid impedance, respectively. Also,

$$\frac{R_1}{R_2} = \frac{A_1}{A_2} exp[2\alpha(l_1 - l_2)] \tag{2.8}$$

$$= \frac{(Z_1 - Z_0)(Z_2 + Z_0)}{(Z_1 + Z_0)(Z_2 - Z_0)}, \tag{2.9}$$

where A_1 and A_2 are the received amplitudes from the two reflectors, and α is the attenuation coefficient of samples.

2.3 Experimental Setup

2.3.1 Measurement Cell

Figure 2.3 diagrams the measurement cell. The inside dimensions of this cell (diameter $\times$ height) are ϕ2 cm $\times$8 cm. The thickness of the stainless steel cylinder is 1 cm, which can withstand moderately high pressure. The transducer, T, is carefully installed near the middle of the cell with a fixed holder, or step, inside. Two reflectors at the upper and lower ends are screwed and fixed into position. The fixed distances to the transducer from the top and bottom reflectors are about 1 cm and 2 cm respectively, and can be calibrated exactly using a standard sample with known velocity data. A piston, P, is used to transfer pressure between the inside and outside of the cell if the outside pressure is higher. This allows us to make high-pressure measurements by putting the cell into a pressure vessel (Figure 2.4). The reflector nearest the piston

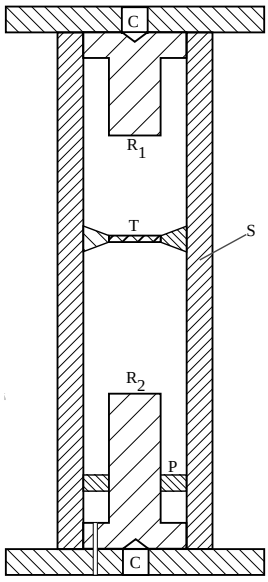

Figure 2.3: Measurement cell: T − transducer, R_1, R_2 − reflectors, C − conical cavity, S − stainless steel cylinder, P − piston.

can be made movable for density measurement by withdrawing screws. The active dimension of the transducer and the reflectors is $\phi 1$ cm (diameter), which has a small side effect of an ultrasonic wave's radiation at a frequency of around 2.5 MHz. The radiation angle θ can be estimated as

$$\theta = \frac{1.22\lambda}{\phi} \approx 4^\circ ,$$

where $\lambda = v/f = 0.6$ mm, $v \approx 1.5 \times 10^5$ cm/s for water and $f \approx 2.5$ MHz. Special conical cavities at the end of each reflector, with an angle of about 104° and a height of about 0.4 cm, are introduced to avoid multi-reflections when the ultrasonic wave is refracted into the metal reflectors, which may have a small attenuation.

Besides considering the radiation effect of the transducer, some specific features are required for the measurement cell. The radiated and received efficiency on both

sides of the transducer, which is used as both emitter and receiver, must be approximately the same so that both reflected waves have approximately the same amplitude. The transducer must be electrically insulated by covering both faces with a special matching layer. The matching layers have a thickness of 1/4 wavelength and intermediate impedance between PZT-5 (the material of the transducer) and detected fluids (which have impedance close to that of pure water) to give the best efficiency and reduce the ringing tail. A special consideration for this vertically erected cell is that the bottom surface of the transducer accumulates gas bubbles easily, which block the signal at the bottom reflector. The proper hole in the transducer is open to let the gas bubble rise up to the top. Careful operation, which we describe in the measurement procedure, does still require keeping the gas bubbles from accumulating. The coated transducer is manufactured by Acoustic Lab, Tsinghua University, Beijing, China.

2.3.2 Structure and Control

The entire system is designed to measure the acoustic properties, and specifically velocity, of fluids and fluid-gas mixtures under pressure and temperature. The system contains several components: (1) The pressure system includes a high-pressure vessel and a controllable pressure pump; (2) The temperature system uses an external heat control, a circulating temperature bath and circulating copper tubing wrapped around the outside of the entire pressure vessel; (3) The gas and fluid fill-up system contains a vacuum pump, a circulation pump under pressure, two hand pumps and numerous pipes for routing; (4) The signal generation system includes a specific waveform generator, which I built myself, and a power amplifier to drive the transducer; and (5) The data acquisition system includes a digital oscilloscope for waveform storage and transfer. The entire system is controlled by a central PC with GPIB standard.

Figure 2.4 diagrams the entire system setup. The measurement cell (marked *1*) lies in the center of the diagram and within a high pressure vessel (*2*) whose pressure tolerance can reach 1 kbar. A helical coil (*3*) made with copper tubing wraps the outside surface of the stainless steel pressure vessel. A temperature bath (*4*) circulates to keep the whole system at the selected temperature. A coat cover (*5*) is wrapped

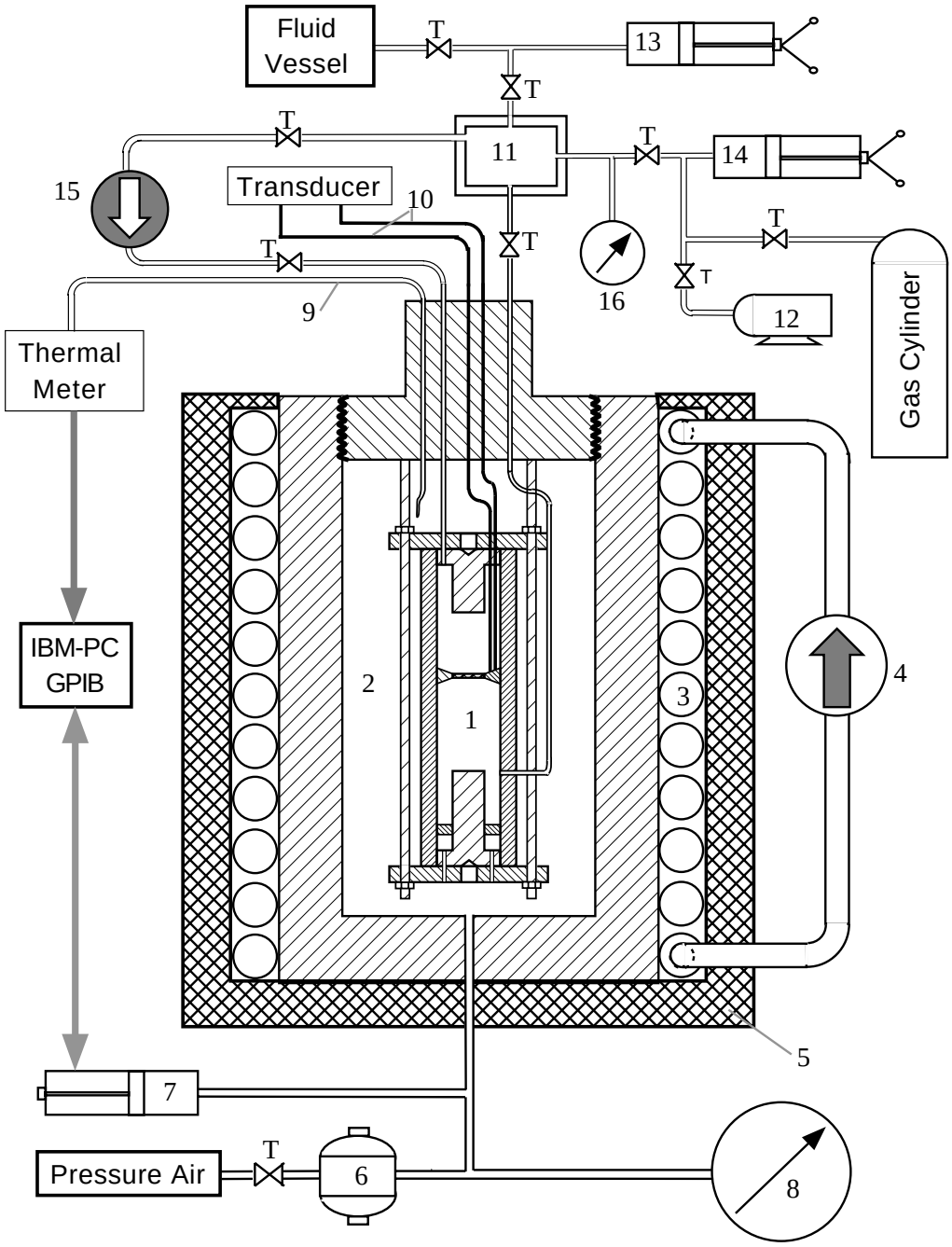

Figure 2.4: Diagram of the entire system setup: *1* – measurement cell, *2* – pressure vessel, *3* – helical coil, *4* – temperature bath/circulation, *5* – coat cover, *6* – pressure pump, *7* – fine pressure pump, *8* – pressure gauge, *9* – thermocouple, *10* – signal wires, *11* – temporal gas/fluid tank, *12* – vacuum pump, *13* – hand pump (fluid), *14* – hand pump (gas), T – tabs.

around for thermal insulation. A gas-driven pressure pump (*6*) pushes oil into the pressure vessel to raise the cell pressure to roughly the correct range. A digitally-controlled fine pressure pump (*7*) is then used to fine-tune the pressure to the desired value and keep it constant, which is necessary for our precise measurement method. A big pressure gauge (*8*) allows a visual check of the current pressure inside the pressure vessel, besides a more precise, digital reading from pump (*7*) which feeds directly to the computer. A thermocouple (*9*) is inserted into the vessel for monitoring the internal temperature. Two wires (*10*) are connected between the transducer and a transducer box, which includes a power amplifier and scopes as in Figure 2.5. A tank (*11*) is an intermediate reservoir for fluid or gas. A digital pressure gauge (*16*) is attached to the gas tank to indicate the pressure in the measurement cell. Two hand pumps (*13* and *14*) are connected to the tank (*11*) to push fluid or gas into the measurement cell when desired. A fluid circulation pump (*15*) is used to mix the fluid in the measurement cell (*1*) when operated. A vacuum pump (*12*) is connected to the gas filling system to evacuate the cell before it is filled with gas, to avoid contamination with air.

The entire system is designed to be controlled by a Pentium PC and can acquire data automatically. As we will see, collecting data under real-time conditions for the interesting parameters takes a long time and generates large data sets, especially for mixture study. Figure 2.5 is a flow chart for the computer control system. The PC communicates with other equipment via GPIB standard protocol in the Labview software environment. The software flow chart for the system operation is introduced in the next section. The thermal meter and pressure sensor send in the current temperature and pressure respectively. The PC sends out a command to set the pressure in the pressure vessel (Figure 2.4(*7*)). The frequency generator is directed to scan in the required frequency range with high resolution. An extra functional frequency generator, the repetitive control (waveform generator), is used to limit the noise in the range of signals back and is required to meet the designed accuracy. The key part of the waveform generator, the specific waveform generator, which I designed and constructed, generates the required waveform as in Figure 2.2.

Figure 2.6 is a sketch of this specific waveform generator. The requirements for

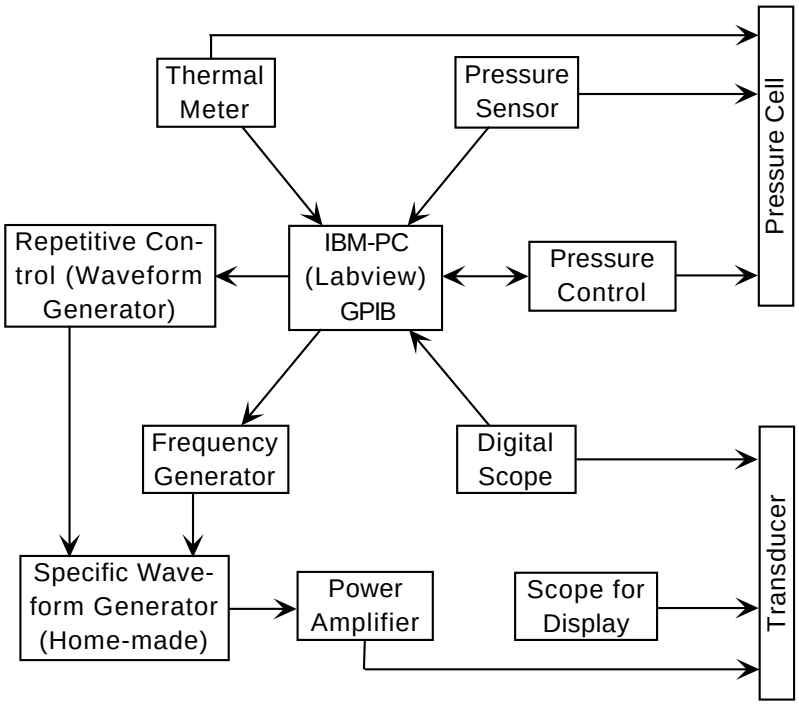

Figure 2.5: Flow chart of the entire system

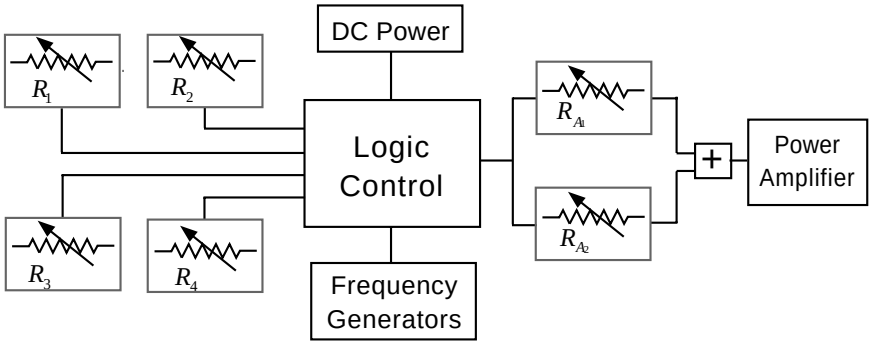

Figure 2.6: Diagram of the special waveform generator: R_1, R_2, R_3, R_4, R_{A_1}, and R_{A_2} are attenuators

the double-pulse method (Figure 2.2) include: (1) that the second impulse be adjustable, in order to let the first reflector signal from second impulse overlap with the second reflector signal; (2) that the number of oscillations in either the first pulse or the second pulse can be set to the desired value; and (3) that the relative amplitudes of the reflected signals from the two reflectors can be adjusted to be the same, to achieve full cancellation and to allow easy reading of the result. R_1 and R_2 in Figure 2.6 accomplish requirement (3) above. R_3 accomplishes requirement (1). R_4 is to control the rate of repetition of the input pulse in Figure 2.2a. R_{A_1} and R_{A_2} accomplish requirement (2) above. The waveform with small amplitude is combined before inputting to the power amplifier as in Figure 2.2c.

A real, established waveform is shown in Figure 2.7. The first two full-scale waveforms in Figure 2.7a are emitted waveforms from the power amplifier at the transducer. The third is a switch-generated waveform, after which we can see the noise level is greatly reduced. Then, the odd-numbered waveforms come from the reflectors or their multi-reflections for the first emitted waveform, and the even-numbered waveforms are reflections of the second emitted waveform. Figure 2.7b is a simple truncated presentation for the two waveforms, which will be moved to overlap each other and to interfere with each other. Figure 2.7c and Figure 2.7d show the conditions of maximum constructive and destructive interference, respectively, achieved by changing the frequency applied in the modulation, after adjusting the delay to overlap the two waveforms in Figure 2.7b.

2.3.3 Software

As shown in Figure 2.5, all equipment is controlled by a central computer with GPIB standard I/O and a Labview-based software environment. It's convenient that most equipment has a GPIB standard port. Figure 2.8 presents a flow chart for managing the equipment. The computer accomplishes the following functions: (1) Sends commands to each piece of equipment for setting up the required conditions; (2) Acquires current conditions of the equipment; and (3) acquires real-time waveforms and calculates mathematical algorithms or functions.

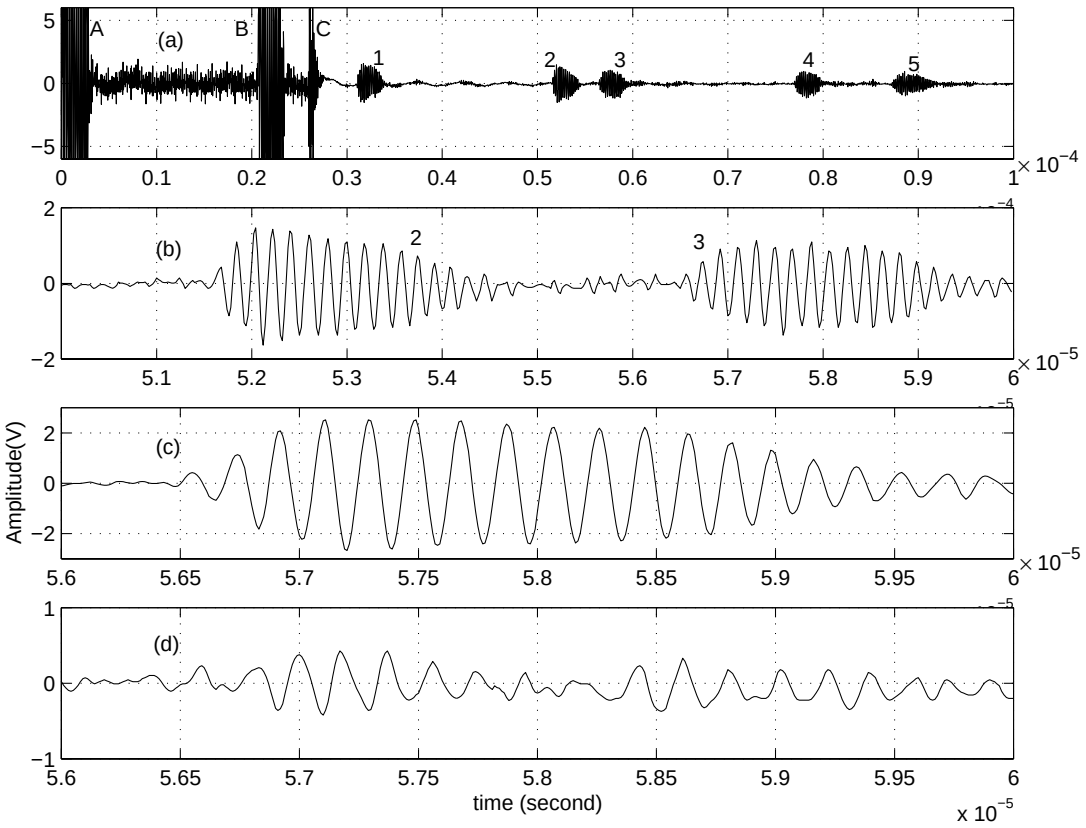

Figure 2.7: Real time waveform in oscilloscope: (a). full scale signals, A & B − emitted waveforms from amplifier, C − noise control jump, 1-5 − waveforms from reflectors; (b). truncated from (a); (c). maximum constructive interference; (d). maximum destructive interference.

Figure 2.9 shows the control panel of the Labview software interface, which includes sample settings for all adjustable parameters, such as transducer frequency, time delay for waveform window, automatic file-name generation, auto time scale, and some current running conditions.

The real accomplished spectrum around the minimum, shown in Figure 2.10, is acquired by Labview and saved to a file for further analysis by Matlab. All results for data analysis in the following chapters are obtained using Matlab. The upper window in Figure 2.10 gives a truncated waveform window around the interference frequency, which is the only area of interest for obtaining the interference frequency. The lower

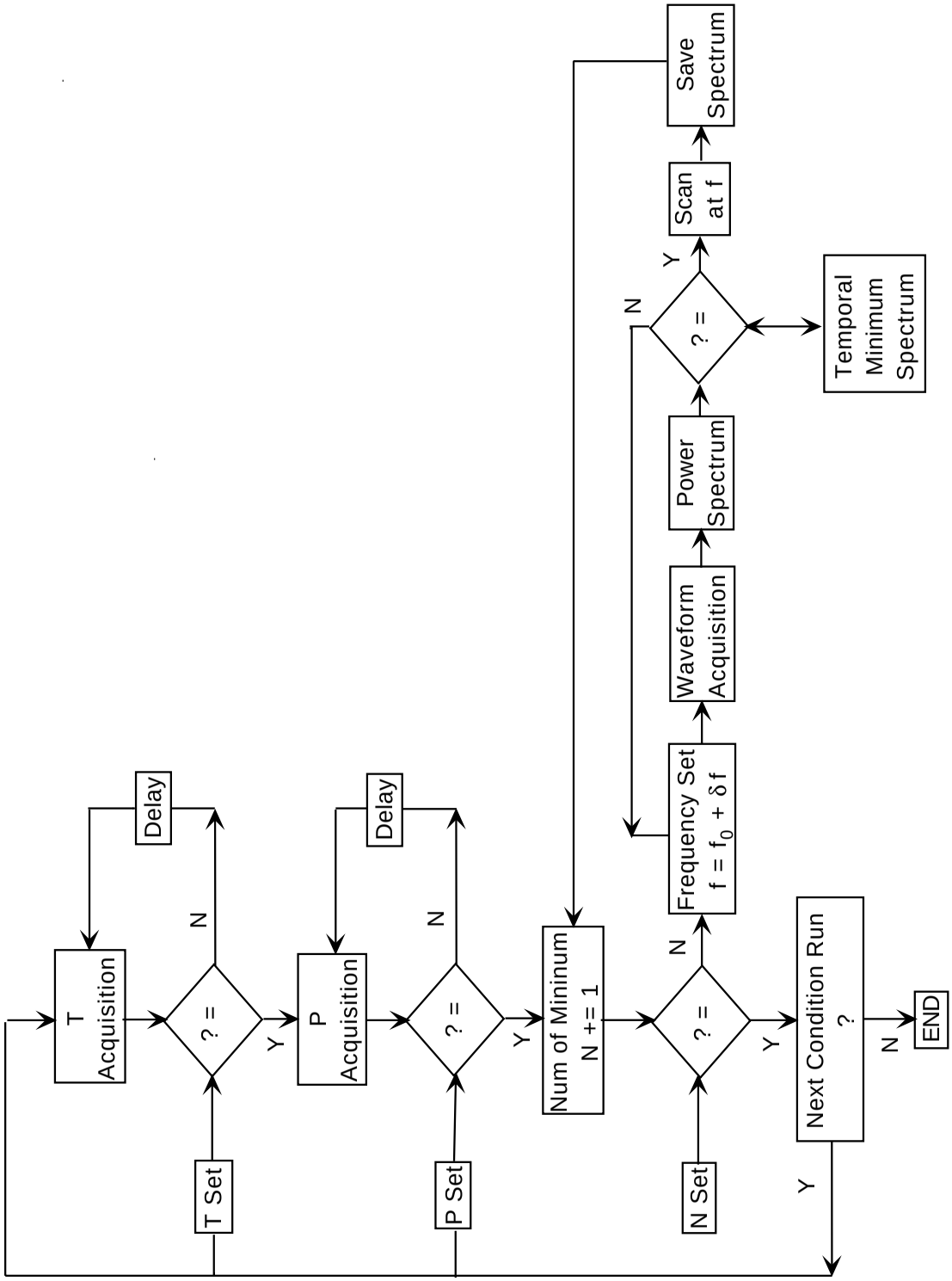

Figure 2.8: Flow chart of software control

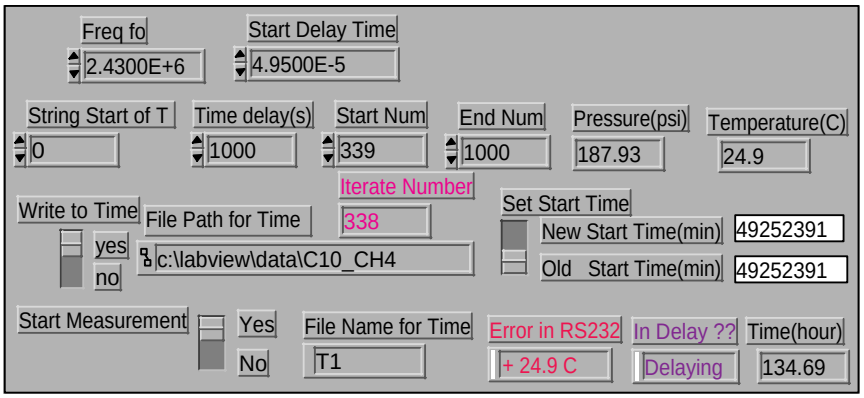

Figure 2.9: Main control Labview panel

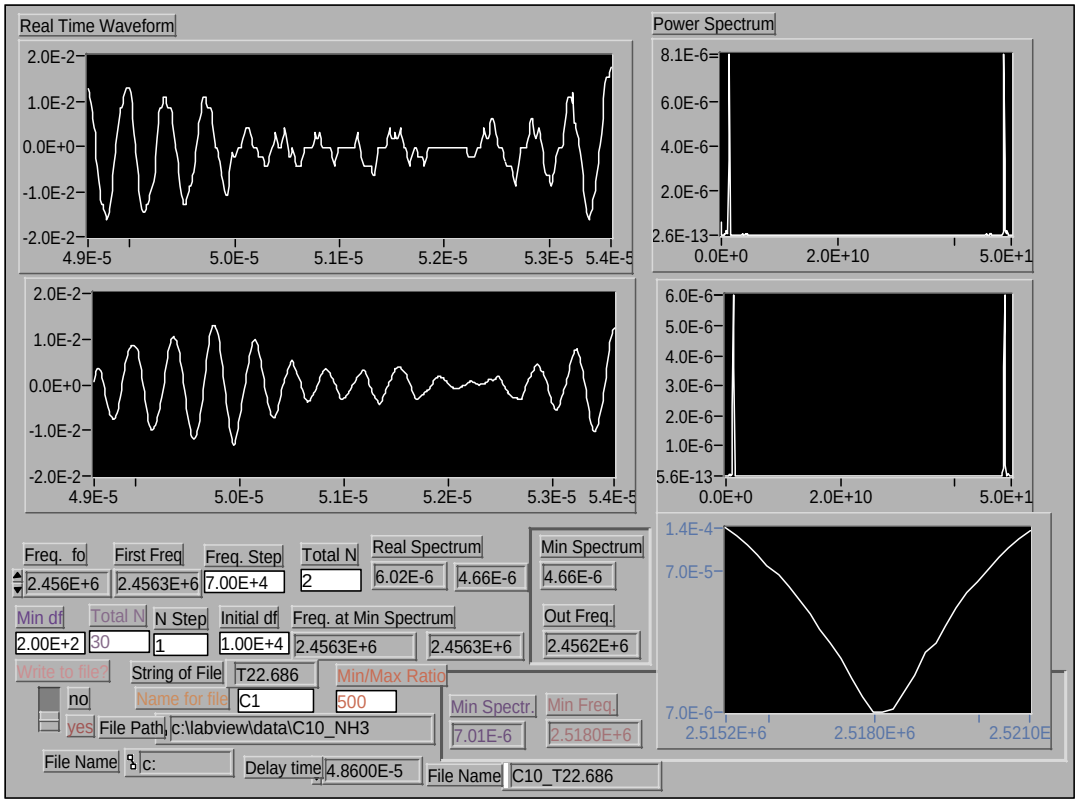

Figure 2.10: Data acquisition Labview panel

window shows the filtered waveform and related power spectrum, which increases the signal-to-noise ratio.

2.4 Conclusion

This chapter gives a detailed description of the most fundamental parts of this thesis: the principle developed and the system built. The new theory determines what the system must accomplish and what we can do. The real system setup makes the proposed accomplishment possible with several specific considerations. Several critical self-made designs make the entire system simple and feasible.

We use the interference method to measure the phase difference instead of travel time directly, which increases the accuracy by about 2 orders of magnitude. We simply use two reflectors and two emitting impulses to accomplish the phase measurement. The accuracy of the velocity measurement can be up to 0.02%. The method can be extended further to measure density with high accuracy and estimate impedance and attenuation of the sample.

The system contains several key parts, including the measurement cell, the transducer and the specific waveform generator. I made or designed these myself. The neat measurement cell is small and has proper connections for electrodes and fluid flow. The transducer is held in position and bubbles are eliminated with high efficiency. The specific waveform generator accomplishes the special requirements, which include (1) double-pulse delay, (2) width of wavelet, (3) signal amplitude adjustment, and (4) noise reduction.

A real waveform of the system is given, which shows its capabilities. Some necessary surrounding systems are briefly described.

Chapter 3

Calibration and Pure Fluid Samples

3.1 Introduction

In Chapter 2, we introduced our system for measuring velocity in fluids with relative errors as low as 0.02% and described some of the equipment used in constructing it. This chapter shows the results of our calibration and testing of the system, beginning with pure fluid samples. This demonstrates the feasibility of the system, and gives us a precise way to explore the unknown properties of some interesting pure fluids.

We start our calibration by using a pure water sample, which is a very important substance to human beings and a most economical sample. The most important reason for us to select this sample for our first test is that a complete data set has been built up for the conditions we intend to use for our system. Thus we can test the accuracy of our method and our equipment by comparing our results to known values.

After pure water, we test our system on brine, or salt water. We test our system at varying temperatures and pressures. This shows how our system works with electrically conductive fluids, and provides another check of our accuracy compared to published data.

Besides water, hydrocarbons are the next most important set of fluid samples for

us, since they are the main constituents of petroleum. There is little published data on the acoustic properties of basic hydrocarbons, since most of the work has been done on real oil samples (Wang, 1988). To avoid the complexity and variability of real oil samples, we examine the simple hydrocarbon decane, the velocity of which has not been well studied, then go on to study its mixtures in the next chapter.

Our initial calibration with pure water was done using a simple temperature-bath setup, and we took measurements at discrete temperatures. Later, we switched to a method requiring less-precise temperature and pressure control. Instead of taking measurements at discrete temperatures and pressures, we took real-time measurements of pressure, temperature and velocity approximately every six minutes. This improved our accuracy and automation, and makes the more complicated mixtures in the next chapters easier to analyze dynamically.

3.2 Pure Water

We started our calibration by measuring the velocity in water with varying temperature at atmospheric pressure. We filled the measurement cell with water and put it into a temperature bath. We measured velocity at a few discrete temperatures: $21°C$, $22°C$, $40°C$, $45°C$, $49°C$, and $59°C$. Figure 3.1a gives the results, in comparison with reference points (Wilson, 1959) and an empirically fitted curve (Fine, 1973). The measurement error is less than $\pm 0.03\%$ as shown in Figure 3.1b.

The main difficulty in velocity measurement is to obtain the data under high pressure. The data for pure water under pressure at room temperature ($22°C$) are shown in Figure 3.2. The upper two charts, (a) and (b), in Figure 3.2 show the direct measurement data for velocity and density under pressure. In practice, the velocity data are obtained first with variable pressure using a fixed reflector. Then we allow the reflector to move as pressure changes to measure density data. Figure 3.2c shows the bulk modulus of water as a function of pressure, calculated using this simple equation:

$$K_s = \rho v^2 \,, \tag{3.1}$$

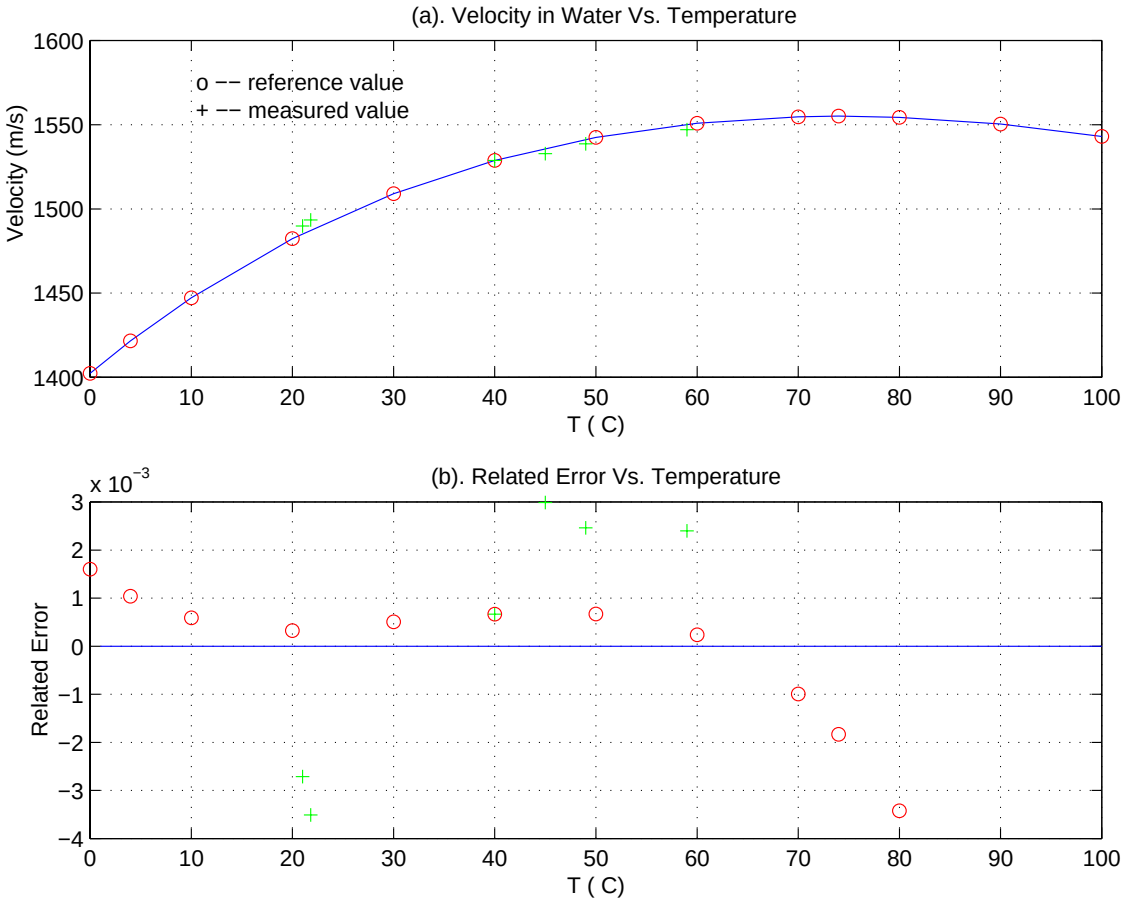

Figure 3.1: Velocity as a function of temperature at 1 bar: o − measured data, +− reference data (Wilson, 1959), solid line − empirical formula (Fine, 1973).

where ρ is density, v is velocity, and K_s is the adiabatic bulk modulus.

The relative errors shown in Figure 3.2d are $0.05\%, 0.05\%$, and 0.1% for velocity, density, and bulk modulus respectively.

3.3 Brine

Figure 3.3 gives the results for velocity in brine with salinity of 20,000, which is simply made by completely mixing 2% salt by weight with pure water. Figure 3.3a shows velocity as a function of temperature. The dash-dot line is from an empirical formula (Chen, 1978); the symbols on each curve represent the measured data; and the solid

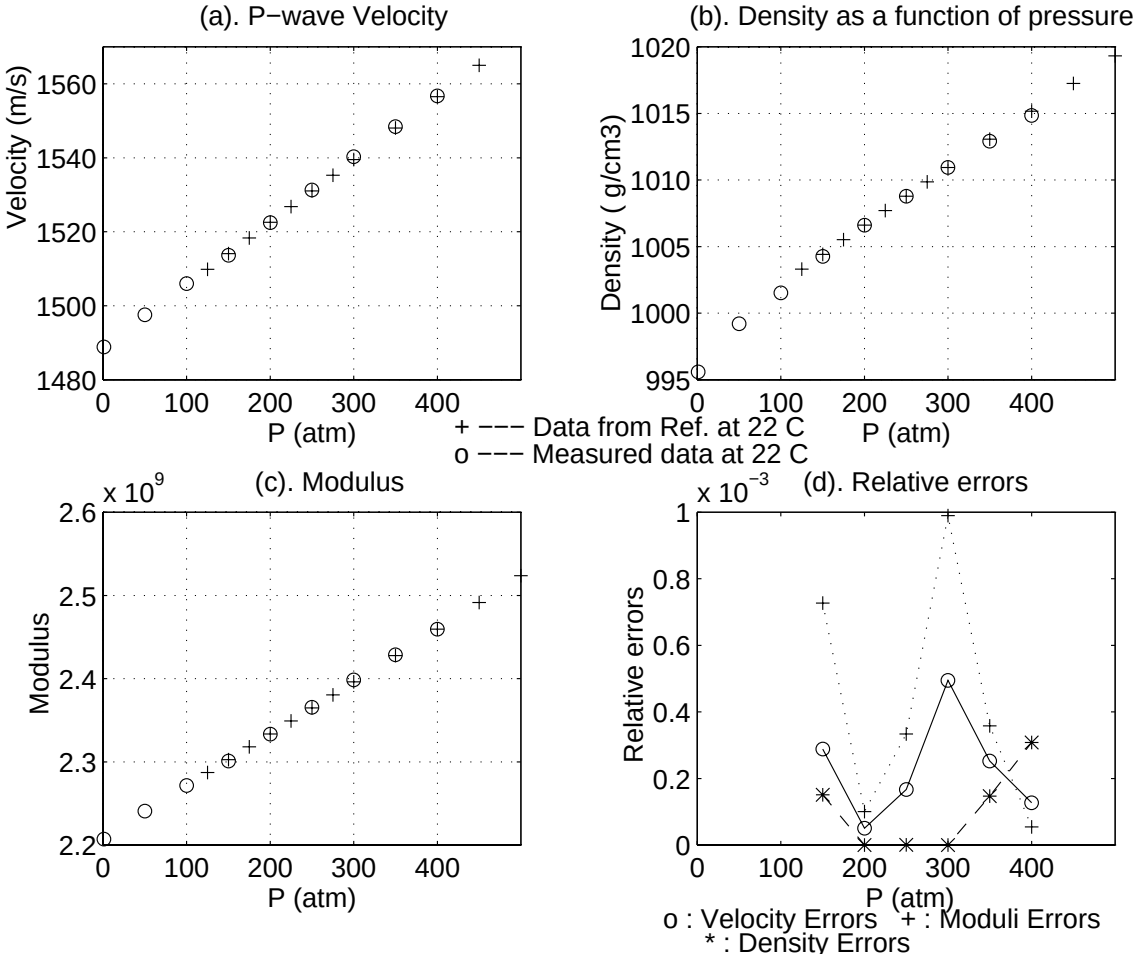

Figure 3.2: Velocity (a), density (b), bulk modulus (c), and their relative errors (d) as functions of pressure at room conditions ($22°C$ and 1 bar).

line is a polynomial fit to the data at each pressure. Another empirical relation (Bark, 1964) has been drawn with a dash-dot line, which gives available data at 1 bar only. These results show consistency with the existing empirical results.

3.4 Simple Hydrocarbon

3.4.1 Fluid-fluid mixture

Figure 3.4 is an early measurement with simple setup, which gives only an occasional measurement result at low resolution for two fluids, decane and hexane, and for their mixtures, at varying pressures. The measurements were made at room temperature which varied somewhat over time, and no record was made of exact operation temperature. The sample was mixed completely before being poured into the cell. The composition shown in the ratio is the volume ratio between the two fluids.

3.4.2 Simple fluid-gas mixture

Figure 3.5 shows a single mixture of pure decane with methane. The measurement cell was filled with methane at a pressure of 200 psi before pure heptane was added to fill the cell. The curve in Figure 3.5 shows that the velocity-versus-pressure curve has a minimum. When methane mixes with heptane under increasing pressure, the velocity first decreases at low pressure, then increases after a certain pressure. The turning point relates to the bubble point. The effect of gas dissolving, which tends to decrease the velocity, competes with that of increasing pressure, which tends to increase the velocity, until the gas is fully dissolved. This result gives us a way to estimate the bubble point of a given amount of gas in a fluid.

3.5 New Way for Pure Fluids

Accurate measurement of pure fluid samples requires good control of temperature and pressure. The results listed above were obtained at room temperature, except for

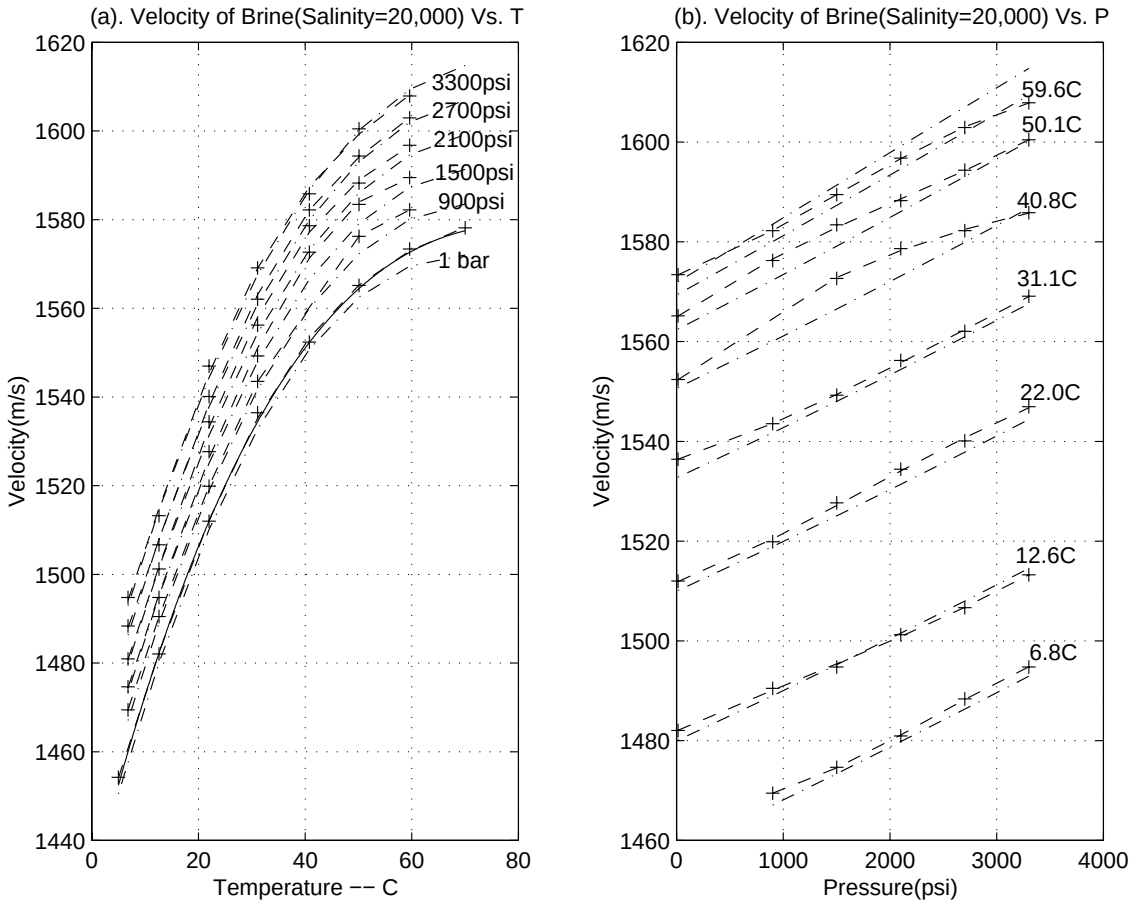

Figure 3.3: Measured velocity for brine with salinity 20,000 as a function of pressure and temperature: the symbols − measured data, dashed line − polynomial fit, dash-dot line − empirical formula (Chen, 1978), solid line − empirical formula (Bark, 1964); (a) velocity vs. temperature at certain pressures, (b) velocity vs. pressure at certain temperatures.

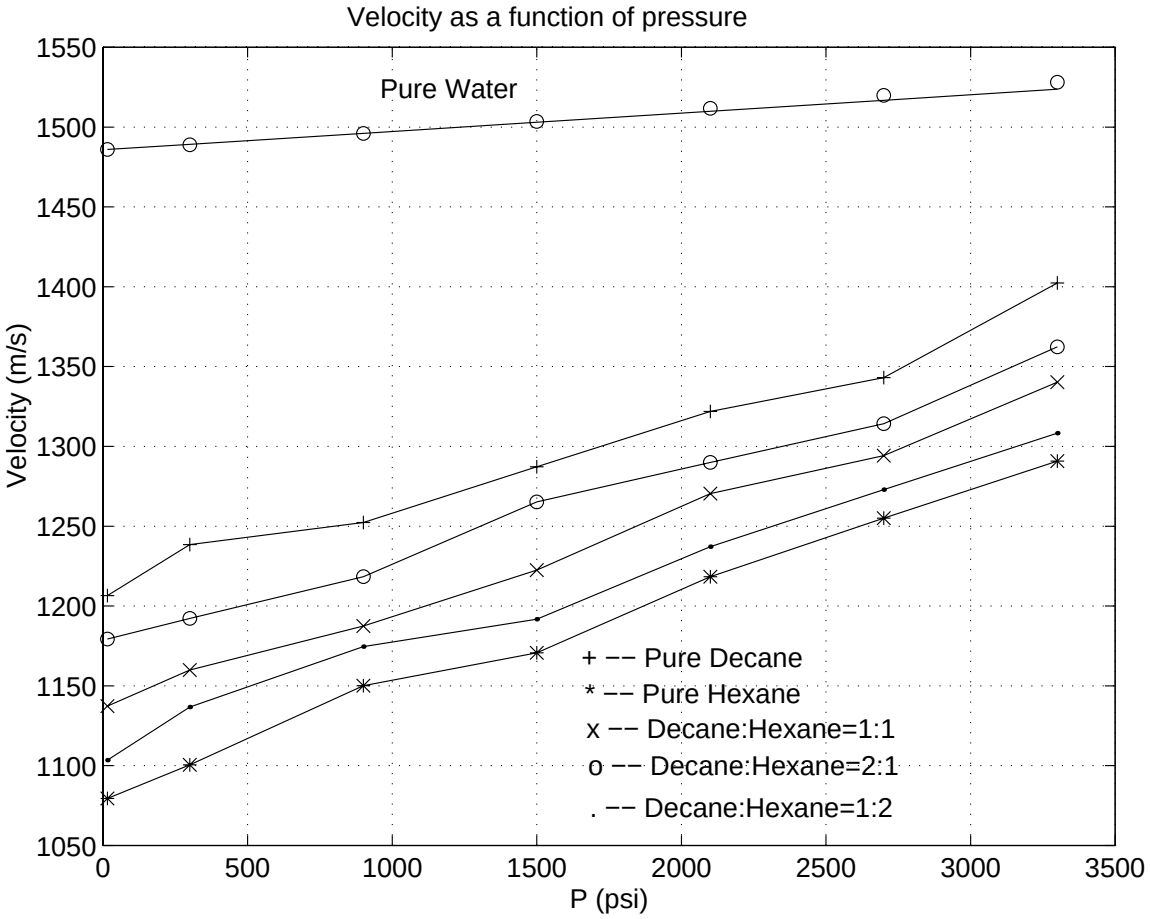

Figure 3.4: Rough velocity of decane, hexane, and their mixture as a function of pressure at room temperature around $21°C$: the ratio is in volume fraction.

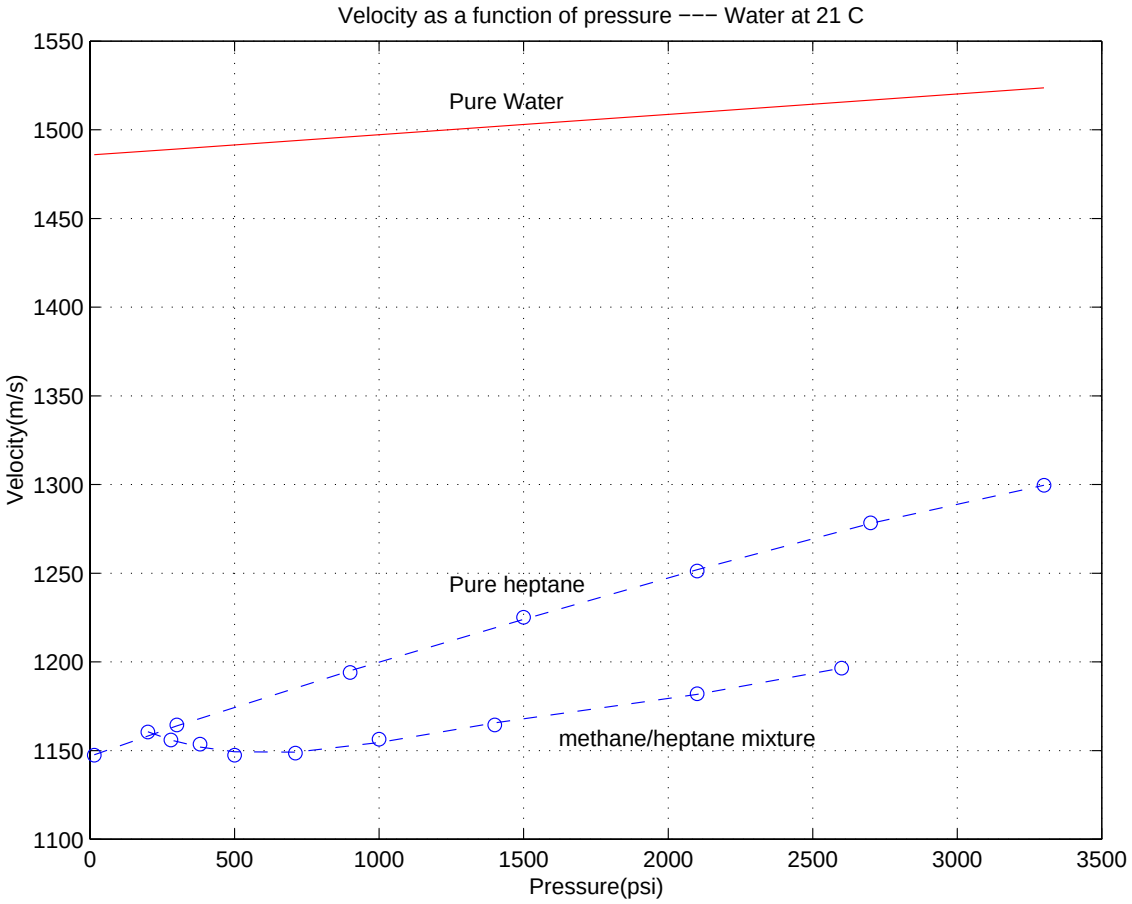

Figure 3.5: Velocity vs. pressure for CH_4 and heptane mixture at room temperature (around $21°C$)

the pure temperature effect measurement in Figure 3.1. Actually, the room temperature may not be exactly constant, and increasing the pressure also may cause the temperature within the system to deviate. The deviations in Figure 3.4 make it clear that we must record the real-time temperature and pressure during each experiment.

The measurement setup without the high pressure pump is shown in Figure 4.1. The pressure and temperature have digital output and can be acquired by computer via GPIB standard. Usually, the results for pure fluid sample were obtained in about 30 hours before mixing was started, and the rate of data collection was about 1 point every 6 minutes. We can see from Figure 3.6 that the velocity in pure decane decreases with increasing temperature at room pressure, which is the reverse of what happens

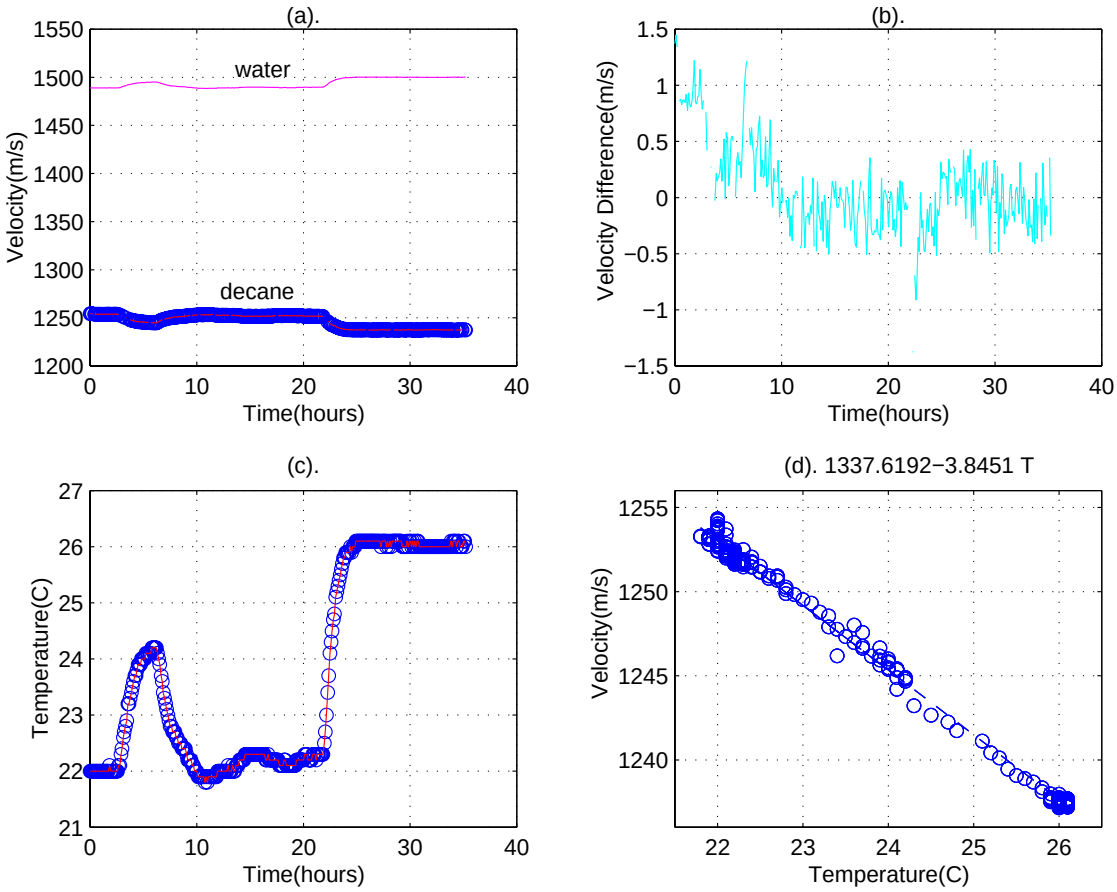

Figure 3.6: Velocity vs. temperature for pure decane: (a) empirical formula data of water and measured data of pure decane, (b) velocity difference between measured data and Equation 3.2, (c) real time temperature, (d) velocity polynomial fit for the measured data.

with pure water. The data can reveal the relation between velocity and temperature.

Now we use this method to examine a less well-characterized fluid, decane, in Figure 3.6, which is truncated from a decane-based CH_4 mixture measurement in Figure 4.10 before CH_4 is filled in. One standard point needs to be set, since we can measure the travel time only with a known distance. This can be calibrated using pure water. Figure 3.6a gives the result of measurements for decane at the recorded temperature. The solid line gives the curve for pure water, calculated from an empirical relation obtained before under similar conditions. Apparently, velocity in

decane has a negative dependence on temperature, while that of water has a positive dependence. The pure decane data were re-plotted by combining Figure 3.6 a and c to produce the graph of velocity vs. temperature shown in Figure 3.6d. The polynomial fit for the data gives the following relation:

$$v = 1337.6 - 3.845T. \tag{3.2}$$

Figure 3.6b gives the absolute error by subtracting the fitted data in Equation 3.2 from the measurement data in Figure 3.6a. The error is below the limit of $\pm$1.0 m/s.

We need to go a little further to obtain the velocity vs. pressure. To avoid the complexity of the high pressure system, we use measurements taken while filling the measurement cell with gas to obtain the pressure effect, When the cell is pressurized with gas, we may assume that the gas takes some time to dissolve, but pressure will increase instantly, at least in comparison to the measurement period in minutes. Figure 3.7 comes from Figure 4.10. Figure 3.7a gives the result with the temperature effect removed, but not the pressure effect. The velocity should be continuous if the pressure effect is subtracted, so the velocity changes caused by pressure can be extracted, as shown in Figure 3.7b. The linear polynomial fit for velocity change with pressure (Figure 3.7d) is as follows:

$$\triangle v = 0.027 + 0.039P. \tag{3.3}$$

By combining the pressure and temperature effects, we find the total velocity:

$$v = 1337.6 - 3.845T + 0.039P \tag{3.4}$$

where v is in m/s, T in $^{\circ}C$, and P in psi.

Figure 3.7b gives the result with both pressure and temperature effects removed using Equation 3.4.

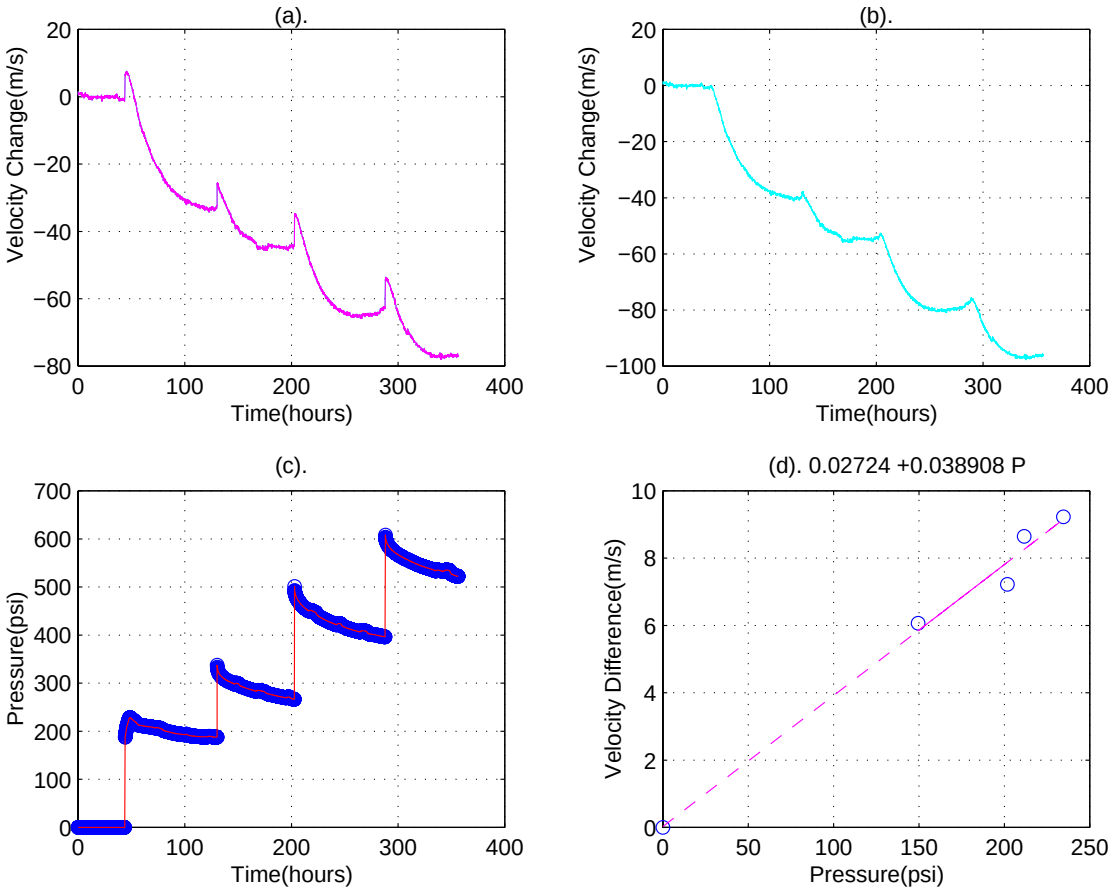

Figure 3.7: Velocity vs. pressure for pure decane: (a) velocity change caused by pressure (temperature effect removed), (b) velocity change caused by gas solution (both temperature and pressure effect removed), (c) real time pressure (1 bar deducted) when gas filled or dissolved, (d) polynomial fit for measured data caused by pressure jump.

3.6 Conclusion

This chapter describes the calibration and testing of the real system we designed. We mainly used fluid samples for which some published data were available. We then extended the method to measure an unknown fluid sample and to determine the bubble point of a simple gas-liquid mixture. We developed a simpler protocol to obtain a pure fluid sample's velocity under varying temperature and pressure with more accuracy and consistency.

Our system has proven to be very accurate and to satisfy our expectations. The overall measurement error for velocity is approximately $\pm 0.5 m/s$, or 0.04% relative error. The pure water result was used to calibrate the system and gave us confidence in our system setup.

In addition to the pure water sample, we presented results for one brine sample under varying temperature and pressure. The results are consistent with the empirical expression. The same procedure was used to measure velocity in a mixture of decane and hexane, with rough control of the temperature and pressure.

A simple procedure was developed for finding the bubble point of a gas-fluid mixture. The velocity curve produced by competition between two effects–velocity decrease with gas dissolution and increase under increasing pressure–showed us a way to identify the bubble point. A simple example was given for a methane- heptane mixture under pressure at room temperature.

A newly developed protocol runs the system more accurately, conveniently and consistently. This procedure will be extended in the next study to a dynamic study of gas-fluid mixtures. Frequent, periodic recording of temperature, pressure, and velocity in real time makes the system consistent and avoids the difficulty of controlling the experimental conditions. A simple example of pure decane mixed with methane was given. A simple relation for velocity vs. temperature and pressure is easily obtained by correlating the large amount of data. This is the most effective way to obtain the temperature and pressure effect for a fluid-gas mixture, which is discussed further in the next chapter.

Chapter 4

Gas-Fluid Solutions

4.1 Introduction

In this chapter, we focus on the quantitative acoustic properties of a gas-fluid solution, which have not been well studied. Some empirical relations for velocity have been reported for real oil samples (Batzle and Wang, 1992), usually measured by the direct travel-time method. It has been widely accepted that the velocity decreases with increasing gas solution. We discover that this is not always the case; the reverse can be true for some samples. As we are interested in hydrate and oil properties, we used pure water or pure hydrocarbons as the solvents for our study, and the gas solutes included CO_2, CH_4, N_2, and NH_3. The results reflect the tendency of velocity to increase or decrease with gas solution. We will use the ideal gas law and pressure change data to estimate the total gas dissolved and compare this estimate to published solubility data.

Studies abound on the solubility of various solutes in water. Table 4.1 gives the mole fraction solubility data of related gases in water under room conditions (25^oC and 1 bar gas partial pressure). Apparently CO_2 and NH_3 are much more soluble in water than CH_4 and N_2.

Some explicit expressions describe the solubility. Battino (1987) gave an equation for methane solubility in water as a function of temperature with a range from 298K

Solute	CO_2	CH_4	N_2	NH_3
Solubility	6.12×10^{-4}	2.42×10^{-5}	1.83×10^{-5}	0.326

Table 4.1: Mole fraction solubility of gas in water under room conditions. (A.G.A, 1965)

to 627K and pressure ranging from 6 to 2000 bars:

$$\ln x_g = -152.777 + \frac{7478.8}{T/K} + 20.6794 \ln(T/K) + 0.75316 \ln(P_t/bar). \tag{4.1}$$

The available expression for CO_2 in water is limited to the function of temperature (Fogg, 1991):

$$\ln x_g = -159.854 + \frac{8741.68}{T/K} + 21.6694 \ln(T/K) - 1.10261 * 10^{-3}(T/K). \tag{4.2}$$

The solubility results are an indirect way for us to estimate how much gas may be dissolved in the solvent when we can not directly know it from the experiment. We may use this relation to estimate the data. For this purpose, it is important to understand the relation between concentration and sound speed change.

4.2 Experimental Procedure

According to our measurement method introduced in chapter 2, the sample to be measured must be in a single state, that is, the liquid state. Gas dissolving into the fluid must not cause any gas bubbles inside the fluid body, so the sample must be carefully prepared to ensure this.

A schematic of the sample cell and its connections appears in Figure 4.1, which presents two main cells. Cell-I is a gas tank and Cell-II is the measurement cell filled with the liquid. A tab T1 is connected to the gas cylinder, C1, and the tab T2 is connected to vacuum pump, V1. The tab T12 is connected to Cell-I to control the gas pressure by adjusting the intensifier I1. A tab T3 connects Cell-I to Cell-II, and

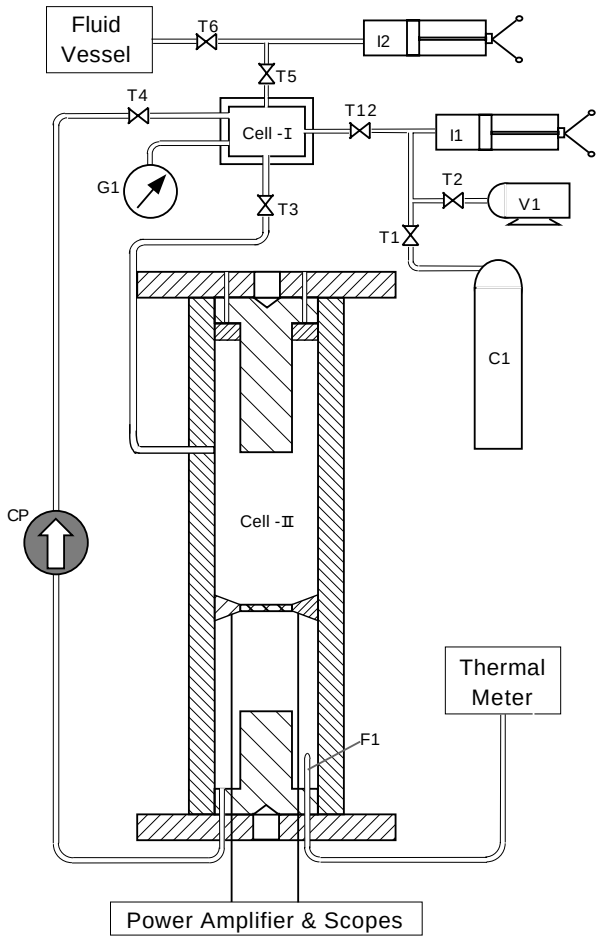

Figure 4.1: Experimental setup for dissolving gas in fluid samples: T1, T2, T12, T3, T4, T5, and T6 – tabs (control gas/fluid flow), I1 and I2 – hand pumps, C1 – gas cylinder, V1 – vacuum pump, G1 – pressure gauge, F1 – thermocouple, CP – circulation pump, Cell-I – gas temporal tank, Cell-II – measurement cell.

is used to start or stop gas flow. A digital pressure gauge, G1, is connected to Cell-I. A thermocouple, F1, is inserted into the fluid from the bottom. Tabs T5 and T6 connect Cell-I with the fluid vessel, which is the reservoir of fluid to be injected into the system. A tab T4 connects Cell-I with a circulation pump, CP, which is optional for fluid circulation in the measurement cell. First, the pure fluid, either water or fluid hydrocarbon, is filled into Cell-II, which has been evacuated to avoid air bubbles gathering inside the cell, especially on the lower surface of the transducer in the middle of the cell, which could reduce the signals from both sides of the transducer. We now run the fluid-filled system for at least 20 hours under room conditions before introducing the gas, for two reasons. The first, as described in chapter 2, is to acquire the pure fluid velocity as a function of temperature, both as a baseline to explore the dependence of velocity on pressure when the gas is added, and to calibrate the system. The other reason is to make sure the system has been set up properly and is stable, by comparing the velocity fluctuation with established empirical relations.

Temperature, pressure, and the frequency response around several interference indices are recorded at a computer preset time interval, with a minimum of 6 minutes between measurements. The first 20 hours are run with tab T3 closed, to calibrate the system by selecting one standard point according to the calibrated length with pure water. The results shown in Figure 4.2 are truncated from Figure 4.3. We can see that the error between the measured data and the empirical data (Chen, 1978) is about $\pm$0.6 m/s, or a relative error of $\pm$0.04%. Cell-I is evacuated before a certain pressure of gas is introduced. The initial gas is filled into Cell-I by turning tabs (T2, T3, T4, T5) closed and tabs (T1, T21) open. The initial pressure, P_o, in the volume, V_o, of Cell-I determines the total amount of gas available to dissolve in the water, which can be estimated using the ideal gas equation. After pure water calibration, the gas is injected from the top inlet by turning tab T3 open. We observe a jump in the pressure curve in Figure 4.3 corresponding to this event. The pressure decreases exponentially over time to a constant, which is the equilibrium of gas solubility at that pressure. Similar injecting processes were repeated, leading to similar jumps and decays in pressure in Figure 4.3. More gas dissolved with each repetition of this process. Studying the velocity change during the gas dissolution will help us to

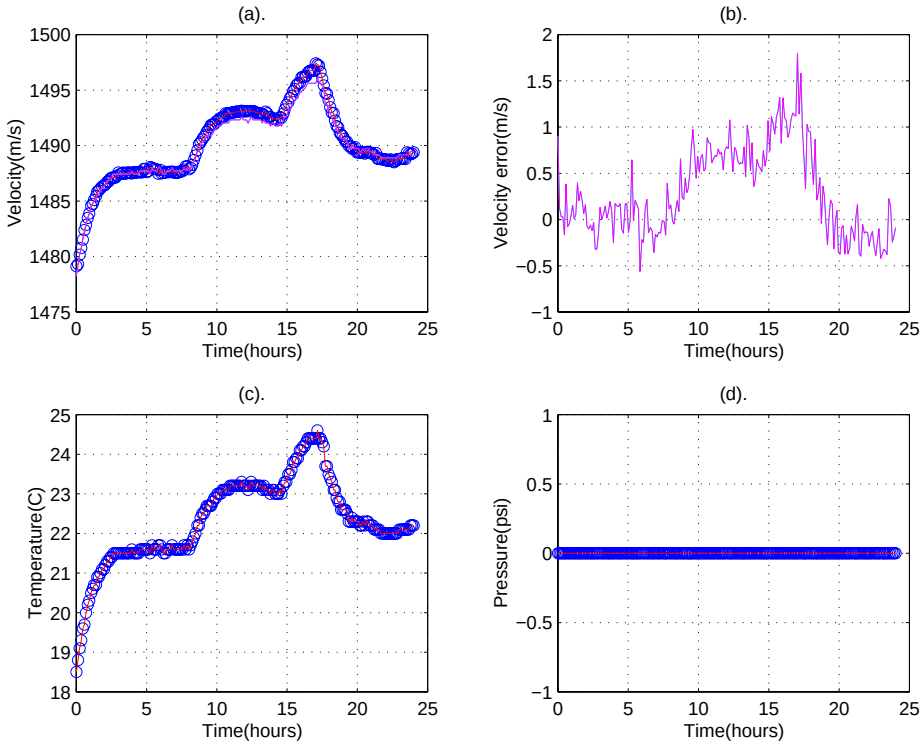

Figure 4.2: Result of pure water truncated from Figure 4.3.

understand the relation between gas concentration and velocity change in solutions, as we discuss in Section 4.3. More parameters will be derived from the measurements, as will be seen in Section 4.3.

4.3 Experimental Results

Our results show either increasing or decreasing velocity with increasing concentration of dissolved gas to different solvent. The results will be presented first for water as a solvent, then for decane.

4.3.1 Water-based Solutions

Solution of CO_2

Figure 4.3 shows the recorded data for CO_2 dissolving in pure water for about 170 hours continuously. The time interval between two data points has been set to a

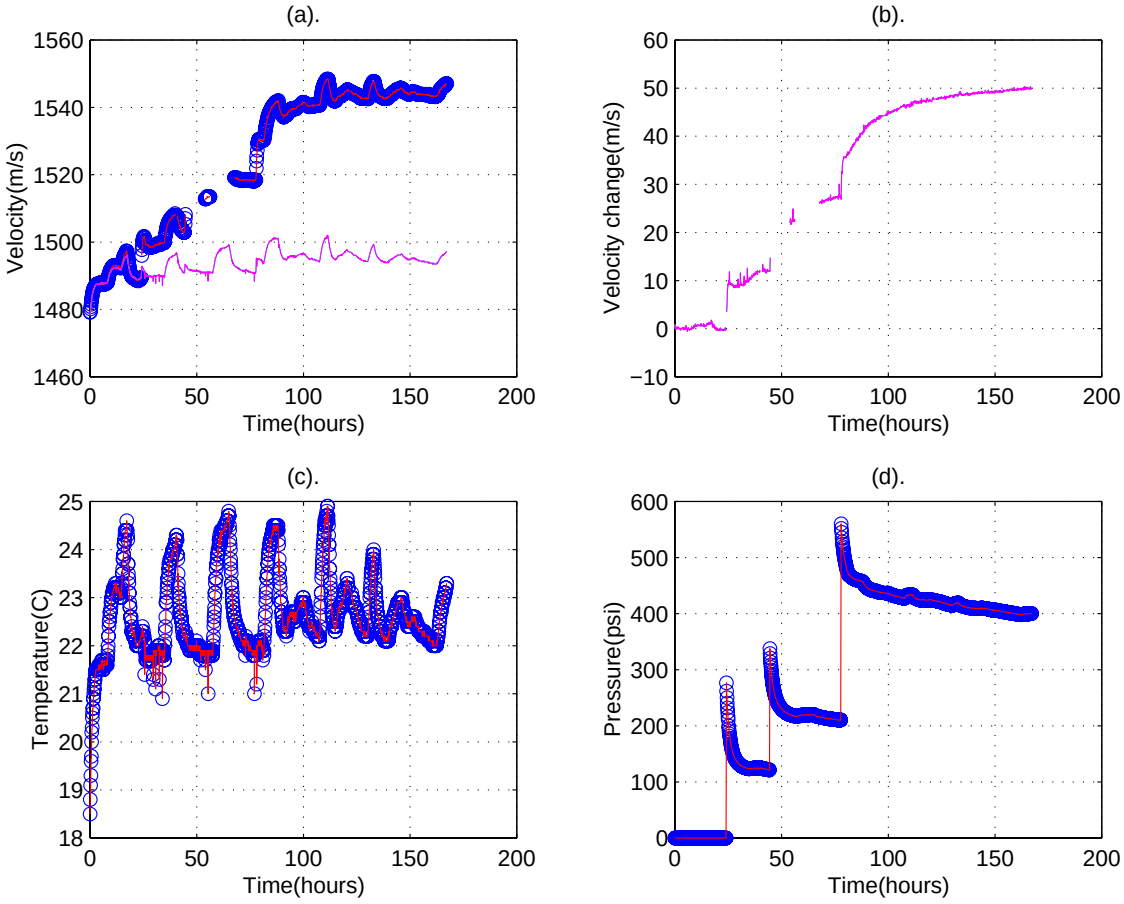

Figure 4.3: Results for CO_2 dissolving into water. (a) velocity as a function of time at the conditions of temperature at (c) and pressure at (d), where solid line and circle points are the velocity of pure water and the measured velocity of gas dissolution, respectively; (b) velocity difference between measured data and empirical relation (subtract empirical from measured data in Figure 4.3a); (c) real time temperature; (d) real time pressure (1 bar deducted).

minimum of about 6 minutes. To avoid the complexity of operation, the measurement cell (Cell-II) is kept outside the temperature bath, at ambient room temperature. Figure 4.3c shows the record of room temperature changes within the cell. The first few dozen points show a temperature increase, because the evacuation of the measurement cell decreased its initial temperature. The temperature in the laboratory has around 3 degrees of long term fluctuation. Figure 4.3d gives the pressure change inside the cell in real time. As discussed in Section 4.1, some abrupt pressure changes occurred as the CO_2 was introduced suddenly. The first interval shows that pressure is 0 psi, since no gas was added immediately after the cell was evacuated. The second interval shows an abrupt pressure increase to around 270psi when CO_2 was initially added; then we stopped the flow from the gas cylinder immediately, creating a closed system between Cell-I and Cell-II. The pressure gradually decreased with time to a constant value, because more and more gas dissolved into the water. Figure 4.3a gives the results of velocity measurements in Cell-II. The solid line in Figure 4.3a is the corresponding velocity in pure water at the temperature and pressure recorded in Figures 4.3c and 4.3d, according to an empirical relation (Chen, 1978). The circles in Figure 4.3a give the measured velocity during gas dissolution in real time. Figure 4.3b shows the velocity change between our measurement and the pure water empirical standard in Figure 4.3a. This curve should be the pure effect of gas dissolution. We can see that the velocity tends to increase as more and more gas is dissolved into the pure water.

It is very important for us to know how much gas is actually dissolved into the water at each recorded data point, so we can relate the velocity data with the solute concentration, in which we are most interested. To that end, we reorganize the data from Figure 4.3d to estimate the amount of gas dissolved. According to the ideal gas equation,

$$PV_0 = nRT. \tag{4.3}$$

We assume V_0 is constant, since the fluid expansion with solution is negligible. P is the partial pressure of gas and can be approximated to equal the total pressure if the fluid vapor pressure is a small term. Using the instantaneous filling pressure as our

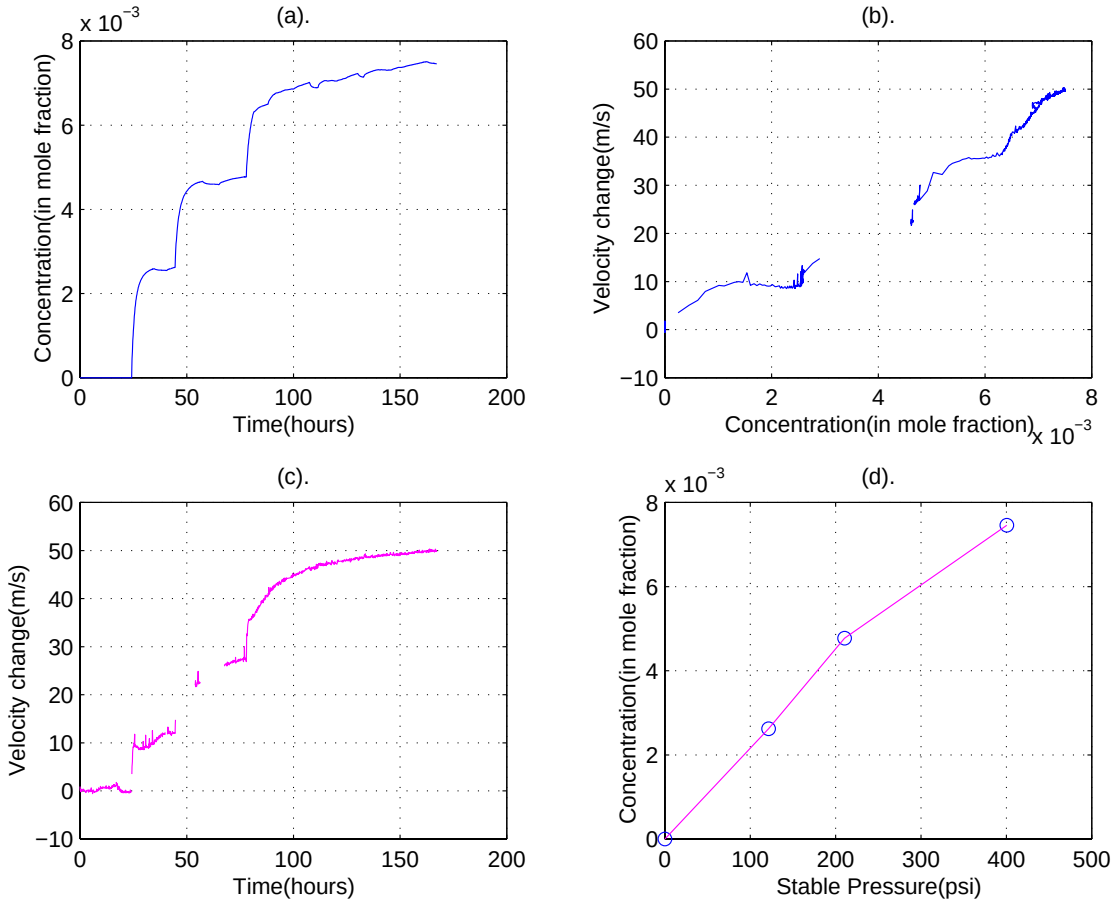

Figure 4.4: Derived result for CO_2 dissolving into water: (a) real time concentration at gas solution; (b) velocity change vs. concentration by combining (c) and (a); (c) measured velocity change by gas solution; (d) concentration at stable gas pressure.

baseline, we can use the gradual pressure drop, ΔP, to determine Δn, the amount of gas dissolved into solution:

$$\Delta P V_0 = \Delta n R T, \tag{4.4}$$

and,

$$\Delta n = (V_0/RT)\Delta P. \tag{4.5}$$

The gas concentration in mole fraction can be expressed as follows:

$$\chi = (n_0 + \Delta n)/n_w = \chi_0 + (V_0/n_w RT)\Delta P, \tag{4.6}$$

where n_w is the total amount of water in moles, and n_0 is the initial amount of gas dissolved in the water. The solution concentration, c, in mole fraction is used to manipulate the data in Figure 4.3d. The results are shown in Figure 4.4. Figure 4.4c gives a few points of concentration relating Figure 4.4a and Figure 4.3d at stable pressures of three different curves at Figure 4.3d. The linear polynomial fit for $\ln(\chi)$ and $\ln(P)$ is shown in Figure 4.4c, which gives,

$$\chi = 6.0251 \times 10^{-4} P^{0.7535}, \tag{4.7}$$

where P is in bars. The value for $\chi(P = 1) = 6.0251 \times 10^{-4}$ is consistent with the handbook solubility value: $\chi = 6.25 \times 10^{-4}$ at $T = 22°C$ and $P = 1$ bar (Table 4.1). The velocity change (black line) caused by gas solution is shown in Figure 4.4b, and the polynomial fit for the data is in Figure 4.5. The linear fit for the logarithm of the data (shown in Figure 4.5) is as follows:

$$\ln \Delta v = 9.781 + 1.2037 \ln \chi, \tag{4.8}$$

$$\Delta v = 1.77 \times 10^4 \chi^{1.20}. \tag{4.9}$$

Also shown in Figure 4.4b are the velocity change for pure water (dashed red line) caused by pressure and the total velocity effect (red solid line) for the open system.

Solution of Methane (CH_4)

Similarly, Figure 4.6 presents the results for CH_4 dissolving in pure water. Figure 4.6c gives the temperature and pressure in real time during velocity measurement (Figure 4.6a) when methane is dissolved. Methane has a very low solubility in water, which is about 2×10^{-5} in mole fraction at 25°C and 1 bar, which is an order of magnitude smaller than for CO_2. We used slightly higher pressures of methane than

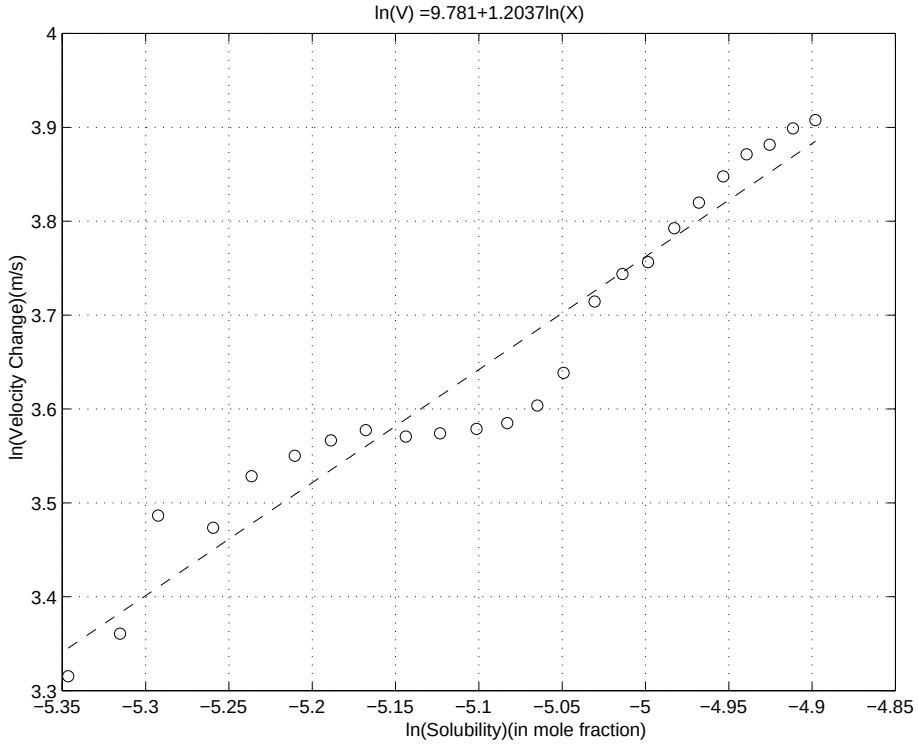

Figure 4.5: Velocity with concentration fit for CO_2 dissolving into water.

of CO_2, hoping to force solution of significant concentrations so we could obtain a measurable velocity effect. The difference in velocity from that of pure water under the same temperature and pressure conditions is given in Figure 4.6b, where the deviation of the pure water empirical velocity (solid line in Figure 4.6a) caused by pressure has been removed to make velocity change continue at the pressure jump points in Figure 4.6d. From the results, we can see that methane gas dissolved into pure water causes a slight increase in velocity.

Solution of Nitrogen (N_2)

Nitrogen gas had a solubility on the same order as that for methane in water, as in Table 4.1. We followed a similar procedure as for methane, and our results are presented in Figure 4.7. Results were similar results to those for methane: the velocity increased slightly after gas was dissolved.

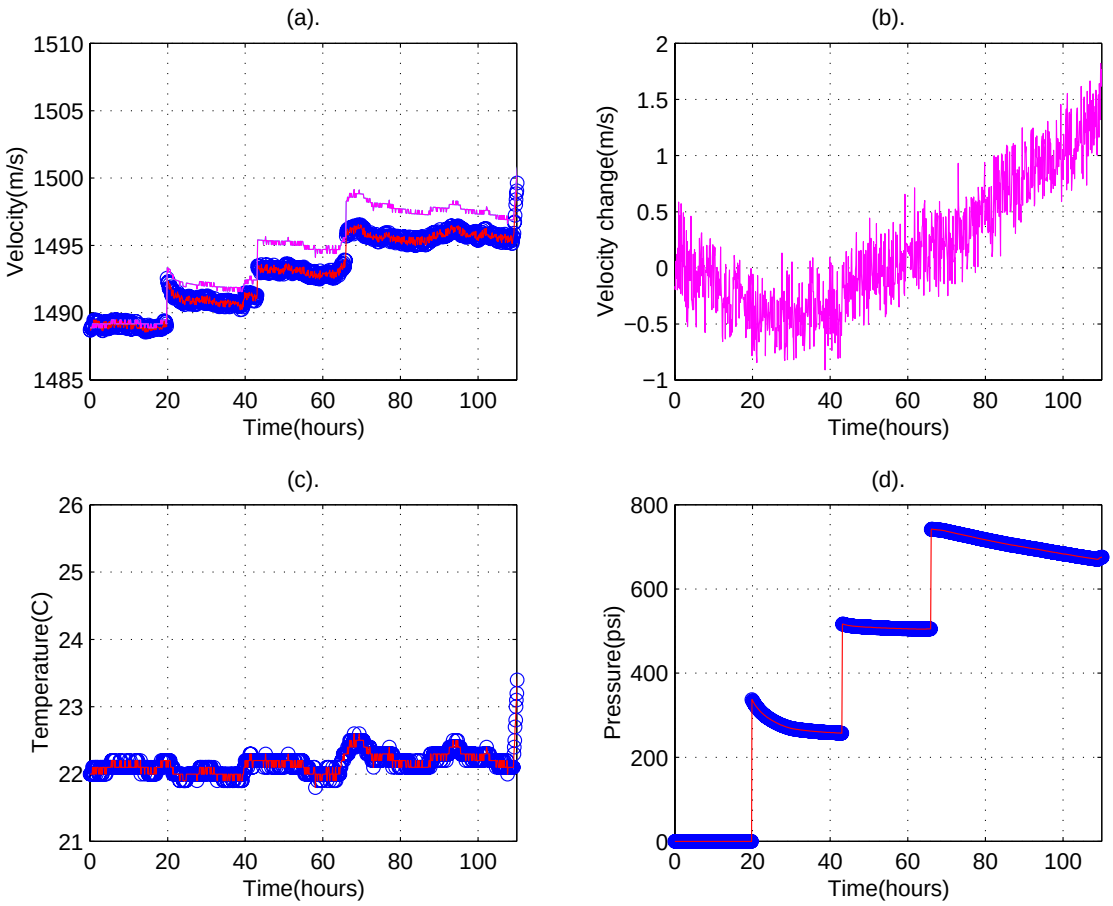

Figure 4.6: Results for CH_4 dissolving into water (see description in Figure 4.3)

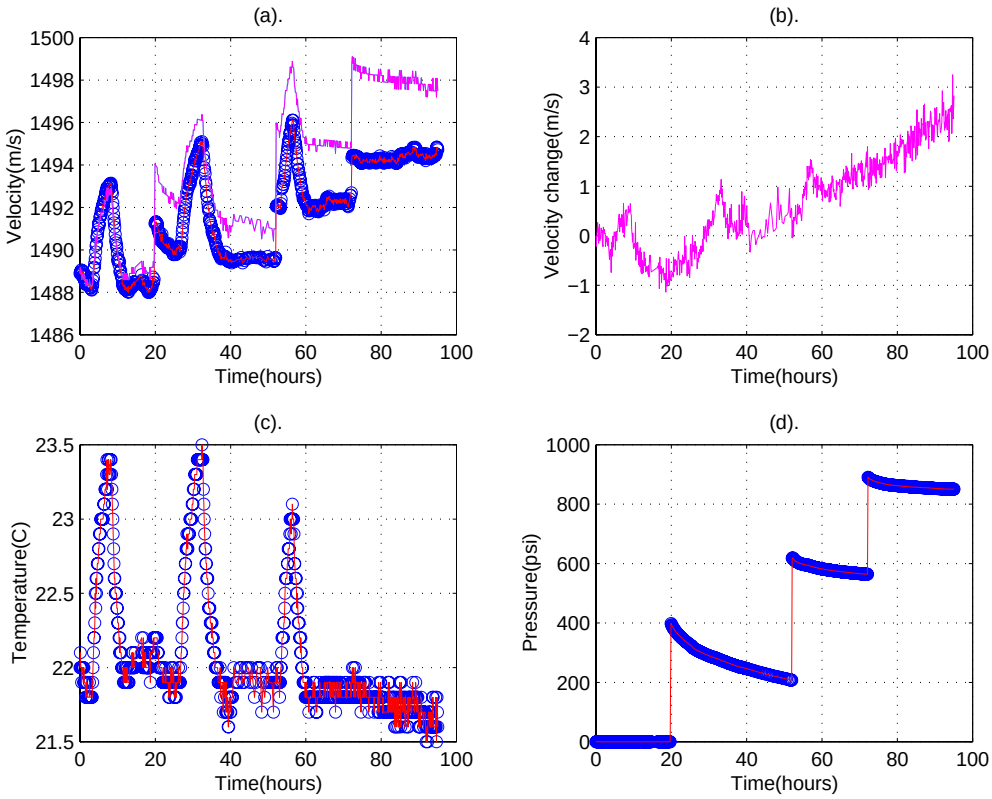

Figure 4.7: Results for N_2 dissolving into water (see description in Figure 4.3)

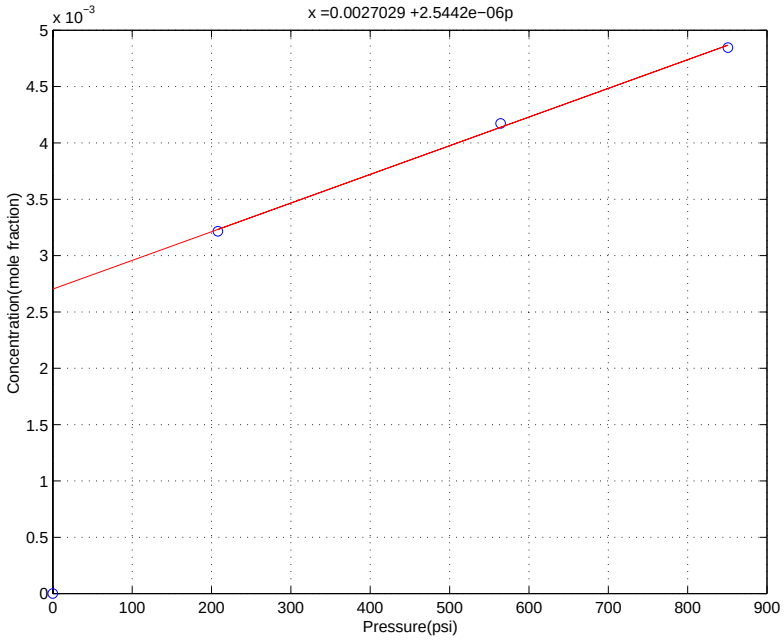

Figure 4.8: Concentration vs. pressure for N_2 dissolving into water.

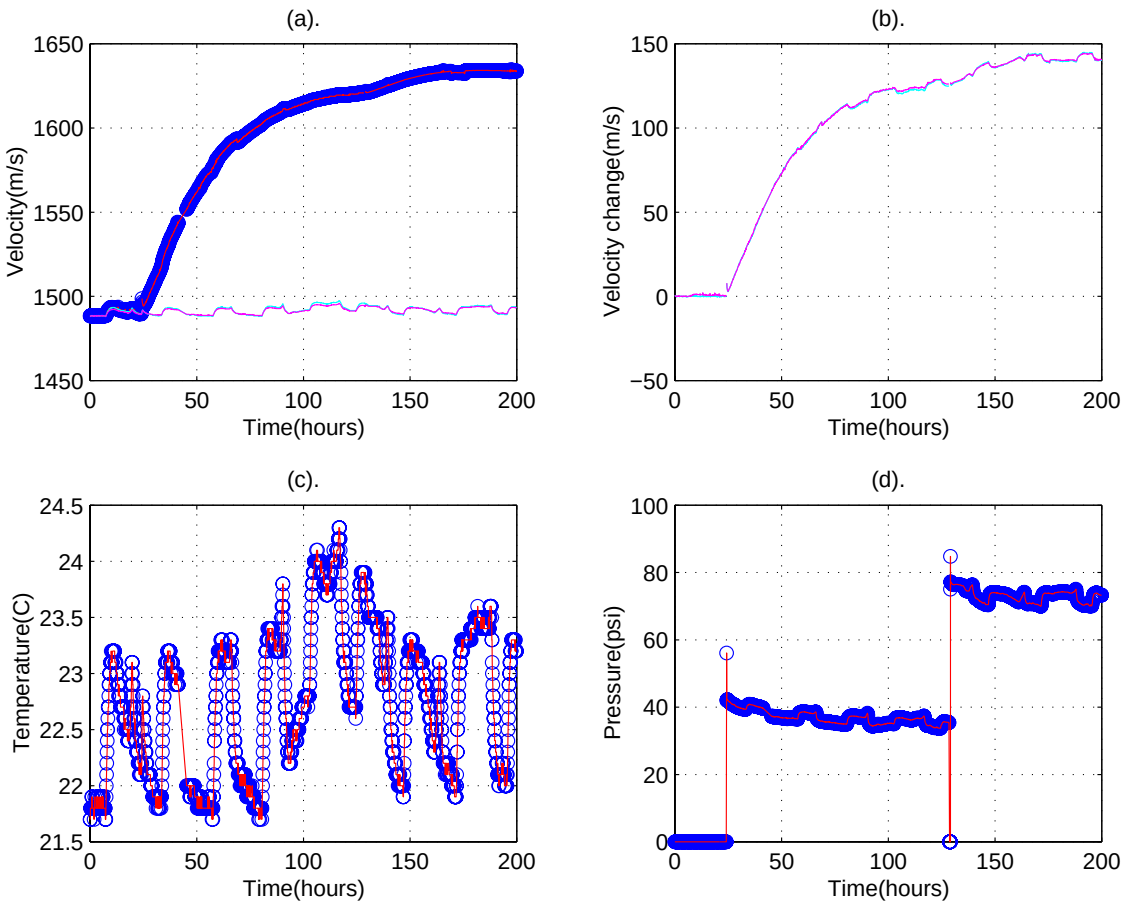

Figure 4.9: Results for NH_3 dissolving into water (see description in Figure 4.3)

Figure 4.8 shows the solubility vs. pressure for N_2 in water, which is calculated as described in the discussion of CO_2, by using the ideal gas equation with the pressure curve in Figure 4.7d. The linear fit for the available three points gives, after eliminating the the erroneous y-intercept in χ at $P = 0$,

$$\chi = 3.18 \times 10^{-5} P(bar)\,.$$

A specific point of solubility in the above relation, $\chi(P = 1) = 3.18 \times 10^{-5}$, does not differ much from the handbook value of 1.83×10^{-5}.

Solution of Ammonia (NH_3)

As we saw in Table 4.1, ammonia (NH_3) is highly soluble in water. Figure 4.9 presents the data for the solution of ammonia in pure water. We see that the velocity increases as the gas dissolves into the water, as was the case for CO_2. Some specifications are shown in Figure 4.9. The gas pressure for ammonia is very low compared to the other gases, because of its high solubility. The pressure curve in Figure 4.9d shows a rapid pressure drop after NH_3 contacts water, which indicates that the contact dissolving rate is much faster. This case is not as simple as the solution of a pure gas, though; ammonia undergoes a chemical reaction in the presence of water. Thus, we cannot use the same method as we used with CO_2 to estimate the amount of gas in solution. Figure 4.9a shows the velocity has a similar behavior as in CO_2, except that the increase was larger. The temperature sensitivity, however, is smaller for NH_3. The larger pressure did not cause a linear change in velocity difference, either because the velocity linearity relation failed under the large solubility condition, or because solubility may not be linear as pressure increases.

4.3.2 Decane-based Solutions

Solution of Methane (CH_4)

Figure 4.10 shows the results of CH_4 dissolving into decane ($C_{10}H_{22}$). The injection of CH_4 caused the velocity to drop dramatically. The fluctuation of the empirical pure decane reference velocity, as in the case of pure water in Figure 4.10a, reflects the recorded temperature fluctuation from Figure 4.10c. The first continuous step in Figure 4.10d was recorded using pure decane with no dissolved gas. Using the data measured in this period, we extracted the velocity vs. temperature relation for pure decane, using the same procedure we used in Section 3.5. We also removed the purely pressure-dependent velocity change, using the procedures developed in Section 3.5 and the pressure data in Figure 4.10d. Figure 4.10b shows the velocity with the temperature and pressure effects removed. The abrupt jumps in Figure 4.10d were caused by each injection of pressurized CH_4. Dissolving of CH_4 into decane caused the slow decrease in pressure toward a stable value. Velocity in Figure 4.10b decreased

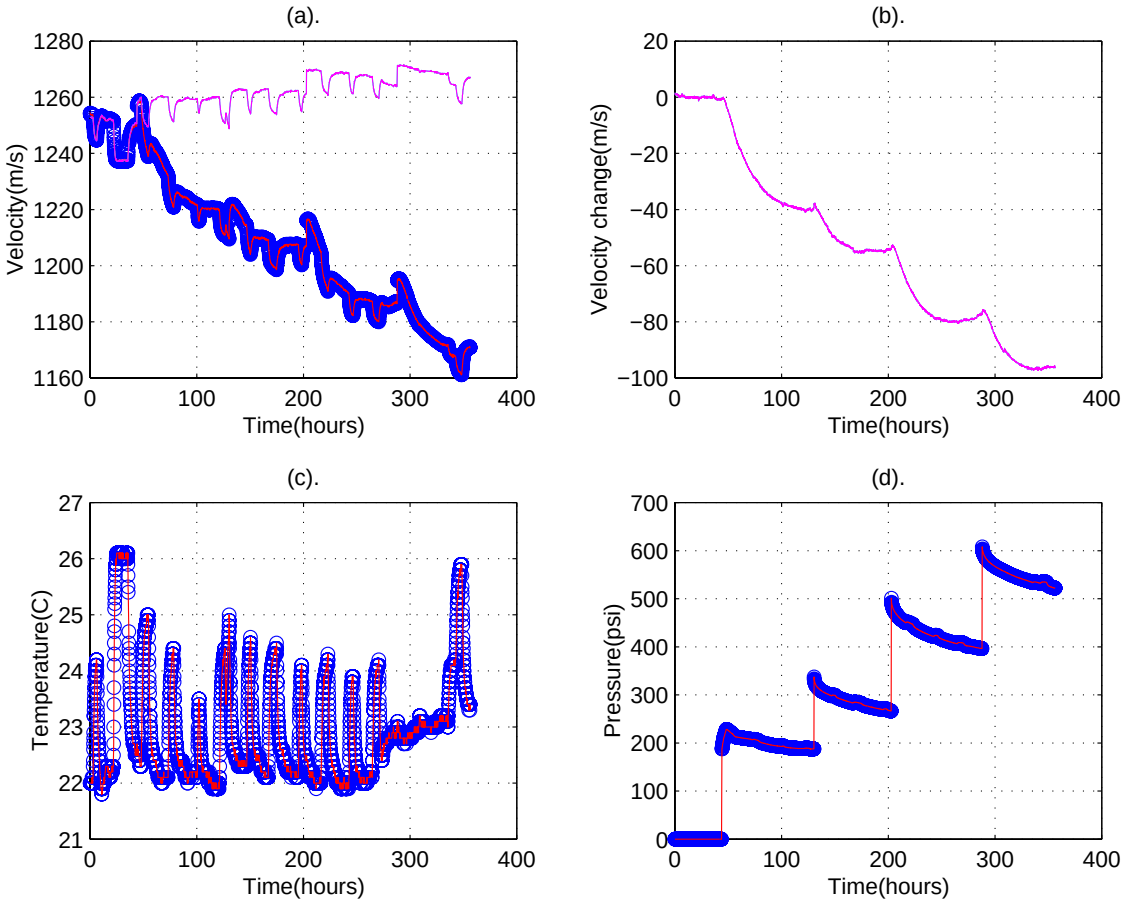

Figure 4.10: Measured results for CH_4 dissolving into decane (see description in Figure 4.3)

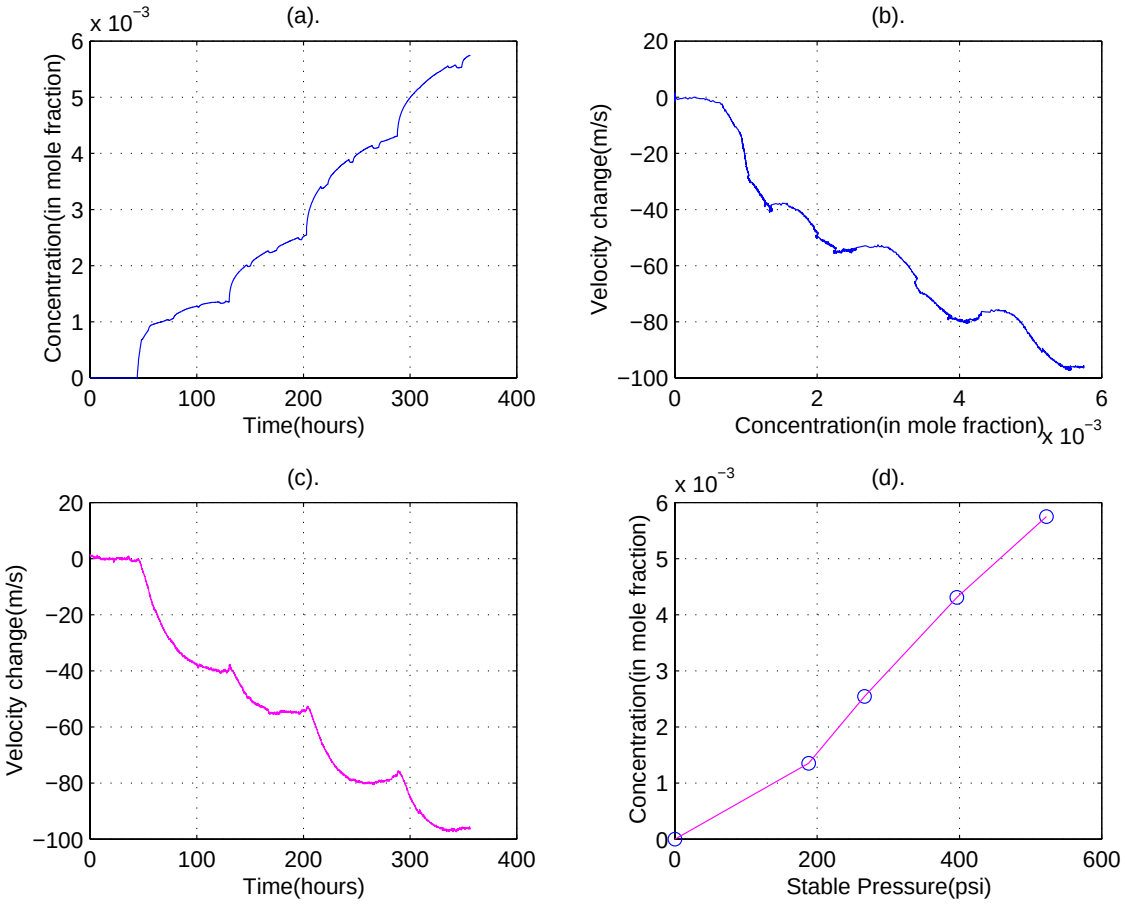

Figure 4.11: Derived results for CH_4 dissolving into decane (see description in Figure 4.4)

because of this increased gas dissolution. To better understand the pure effect of gas dissolving, the data is reorganized to reflect the mole fraction concentration of gas in solution, as presented in Figure 4.11.

The linear fit for solubility with pressure is presented in Figure 4.12, extracted in the way described in the previous section:

$$\chi = 1.64 \times 10^{-4} P(bar)\,. \tag{4.10}$$

The velocity vs. concentration fit from the data is shown in Figure 4.13, which gives the relation,

$$\Delta v = -6.20 \times 10^{4} \chi^{1.235}\,. \tag{4.11}$$

Solution of Carbon Dioxide (CO_2)

Figure 4.14 gives the results of CO_2 dissolving into decane. Similarly, a big change in velocity occurs after CO_2 is dissolved. Figure 4.15 shows the relation between gas concentration and pressure at equilibrium condition. A linear fit to their logarithmic value gives the solubility relation:

$$\chi(P) = 8.8 \times 10^{-4} P(bar)^{0.75479}.$$

Figure 4.16 shows the velocity dependence on concentration and the logarithmic fit to the data, given by the following equation:

$$\Delta v = -4.27 \times 10^{3} \chi^{0.775}. \tag{4.12}$$

Solution of Nitrogen (N_2)

Figure 4.17 gives the results of N_2 dissolving into decane. There is a decrease in velocity as the gas dissolves, as shown in Figure 4.17b.

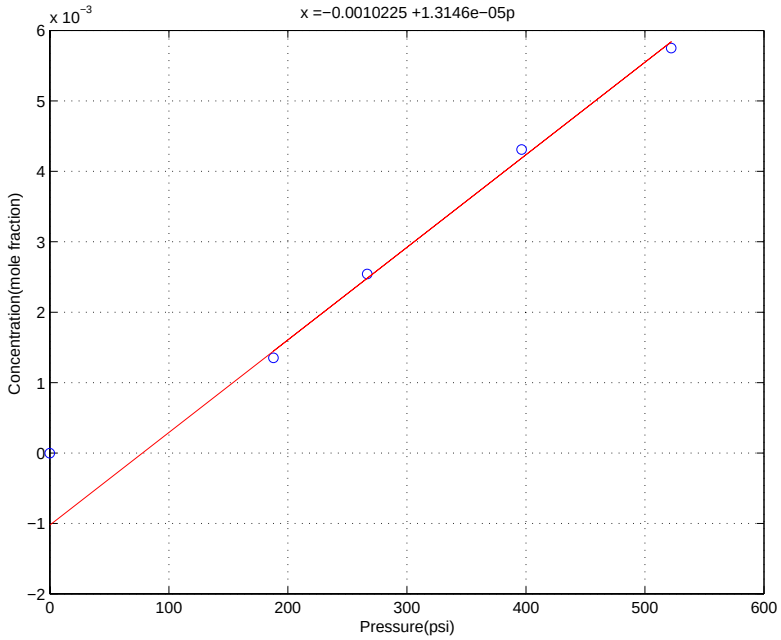

Figure 4.12: Concentration with pressure for CH_4 dissolving into decane

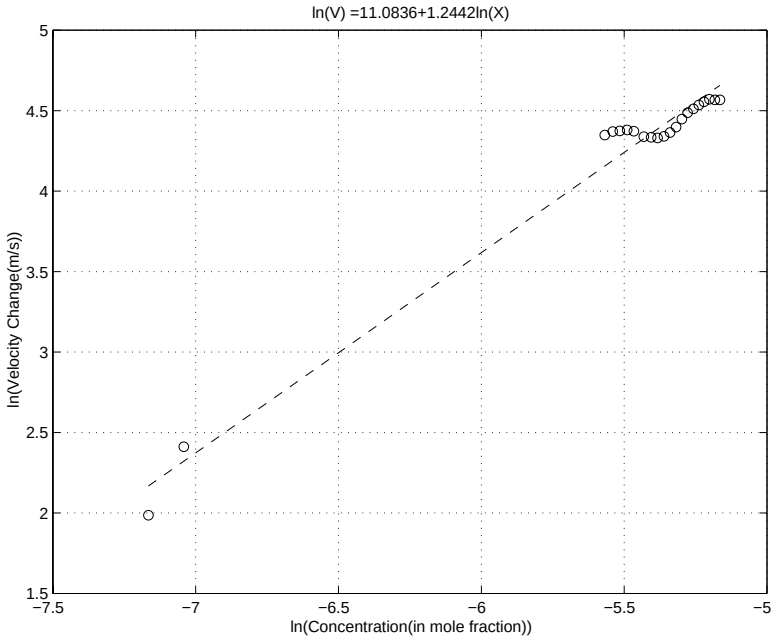

Figure 4.13: Velocity with concentration for CH_4 dissolving into decane

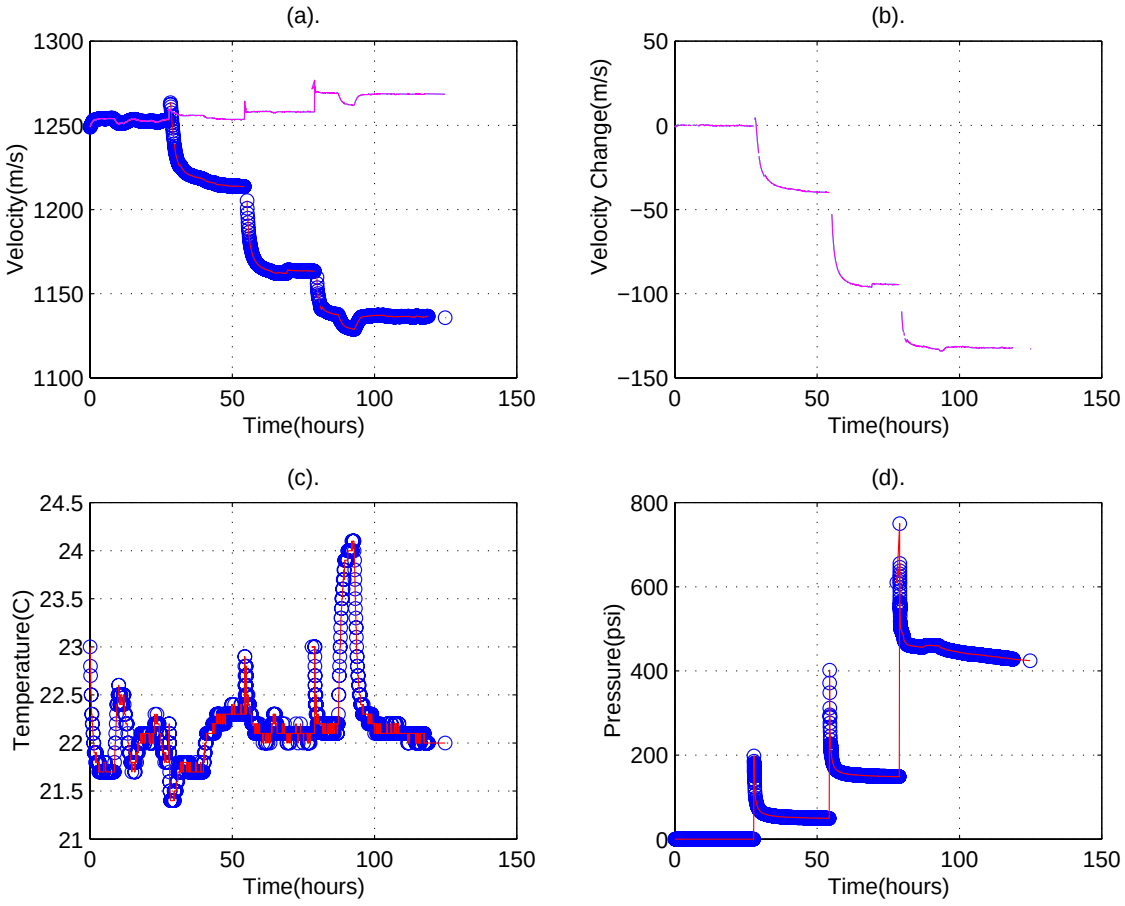

Figure 4.14: Measured results for CO_2 dissolving into decane (see description in Figure 4.3)

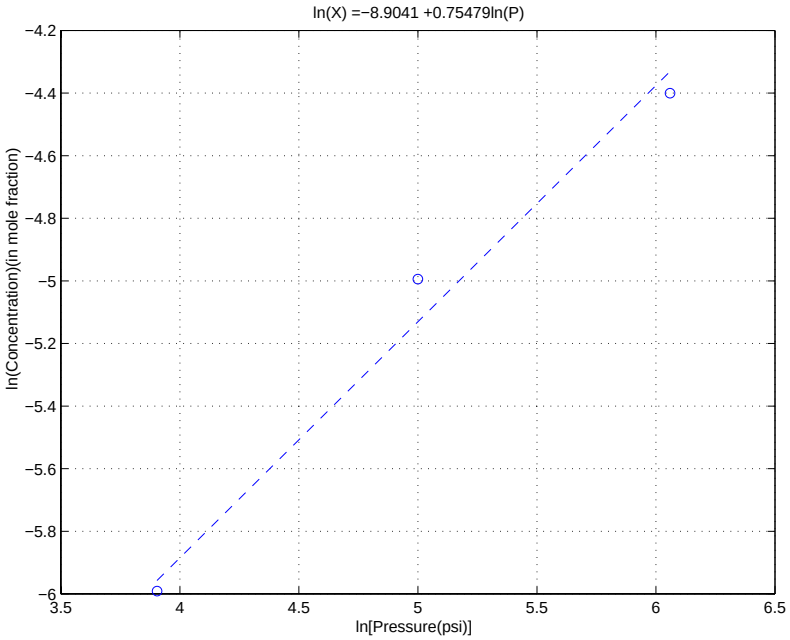

Figure 4.15: Concentration vs. pressure for CO_2 dissolving into decane

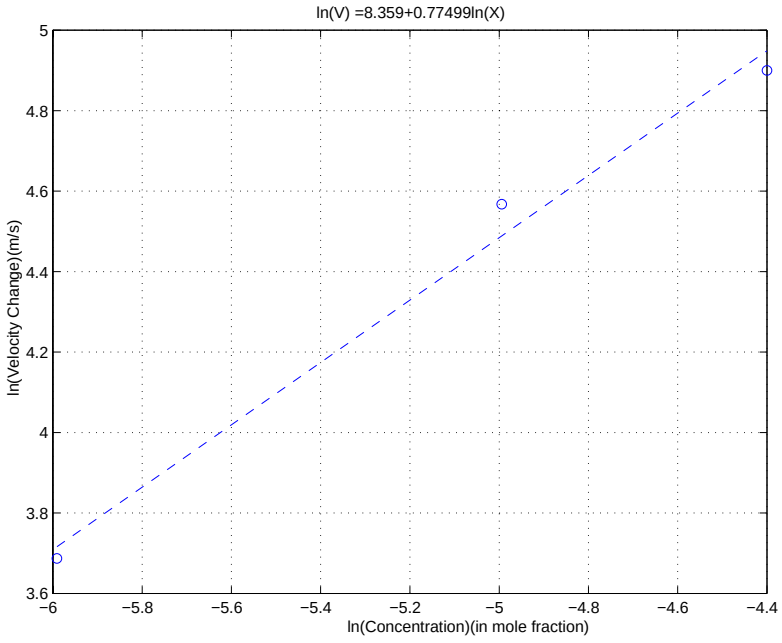

Figure 4.16: Velocity vs. concentration for CO_2 dissolving into decane

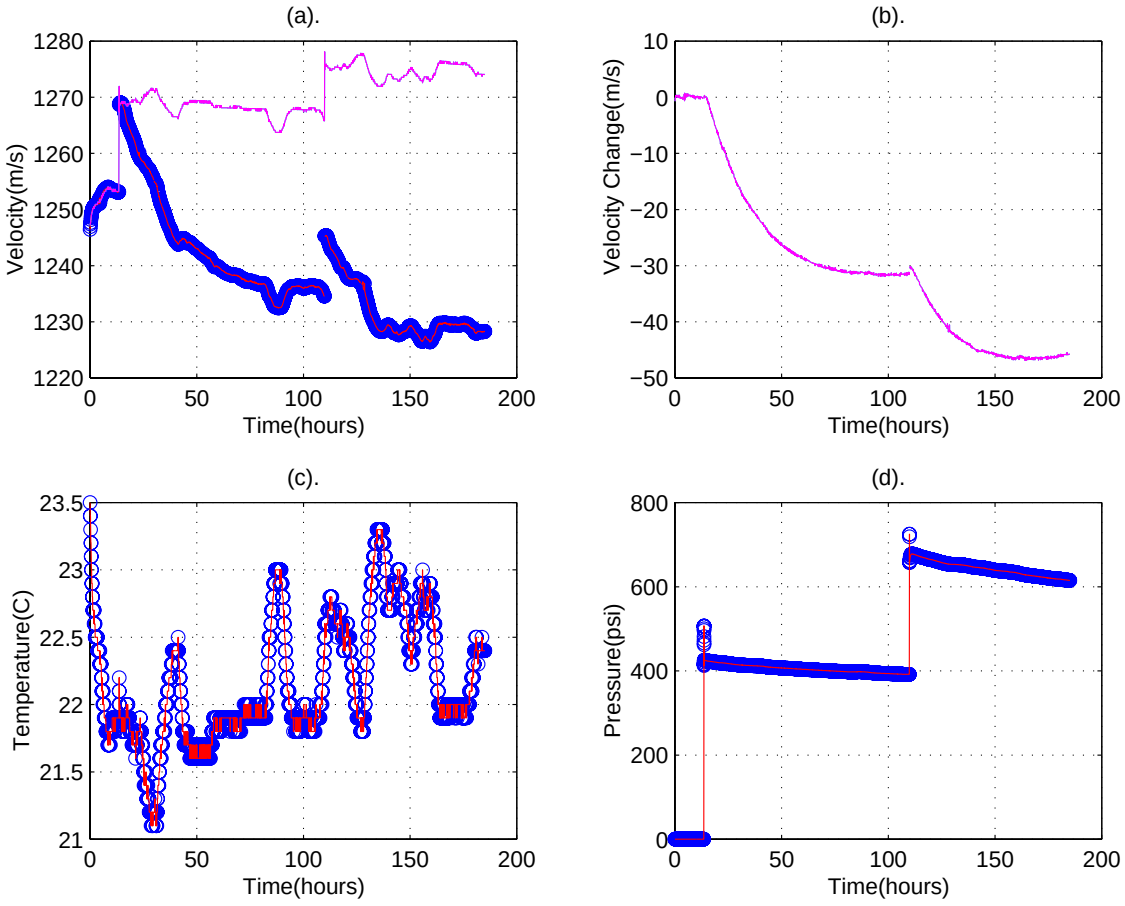

Figure 4.17: Measured results for N_2 dissolving into decane (see description in Figure 4.3)

4.3.3 Results Summary

We produced original velocity measurements for the solution of various gases into two very different solvents, water and decane. The qualitative results of velocity change with increasing concentration are listed in Table 4.2, where the notation of $++$ means increasing significantly, $+$ means increasing slightly, $--$ means decreasing significantly, and - means decreasing slightly. The numbers inside the parentheses are the figures in which the detailed results are displayed.

Solvent/Solute	CO_2	CH_4	N_2	NH_3
Water	$++$ (Figure 4.3)	$+$ (Figure 4.6)	$+$ (Figure 4.7)	$++$ (Figure 4.9)
Decane	$--$ (Figure 4.14)	$--$ (Figure 4.11)	$--$ (Figure 4.17)	N/A

Table 4.2: Summary of measurement results of sound speed in solution.

4.4 Dynamic Analysis

The results shown in the last section describe the dynamic process of gases dissolving into fluids and changing the fluid sound speed simultaneously. Qualitatively, we knew the dependence of velocity on gas concentration in solution. However, to better understand how the data vary for different solutions, we need to study them explicitly.

What we need to determine is the quantitative relation between velocity and gas concentration in the dynamic process of gas injection; then we will further explore what governs the velocity trend in each case.

The rough relation between velocity and gas concentration is given in Equation 4.9 and Equation 4.11 for the cases with significant velocity change: CO_2 in water and NH_3 in decane, respectively.

4.4.1 Time Dependence of Velocity Change

As we see from the original recording of data in Figure 4.3, etc., the time coordinate t is in hours. It takes a long time for a simple step to reach equilibrium. Apparently, the dissolution of gas into the fluids is a slow process. In the procedure described in Section 4.2, the gas was injected from the top, then freely dissolved when the gas and fluid contacted each other. The fluid was apparently heterogeneous in gas distribution. When it reached equilibrium, the velocity and the pressure reached constant values.

In an attempt to understand the process, we guessed that the sound speed varied exponentially with concentration. The data were redisplayed by plotting the y-axis on a logarithmic scale. We used the data with large changes in velocity shown in Figure 4.3, Figure 4.9, and Figure 4.10. We assumed one free dissolving process for analysis, with the following relation:

$$\Delta v = \Delta v_0 (1 - e^{-\alpha t}) \,,$$

or

$$\ln(\Delta v_0 - \Delta v) - \ln \Delta v_0 = -\alpha t \,.$$

Applying this equation to the data in Figure 4.18a, Figure 4.19a, and Figure 4.20a gives the results in Figure 4.18b, Figure 4.19b, and Figure 4.20b, respectively. We find that each process has the same linear relation after the exponential operation. Especially in Figure 4.20b, we see that the curve for each separate pressurization step shows the same slope, which means each addition of gas has the same effect. We therefore need to pick only one process for further analysis, which we do in the next section.

4.4.2 Dissolving Processes (Diffusion model)

Considering the control processes used, the single-phase sample of the solution could not become homogeneous instantly. Some physical processes underly this. Simplified

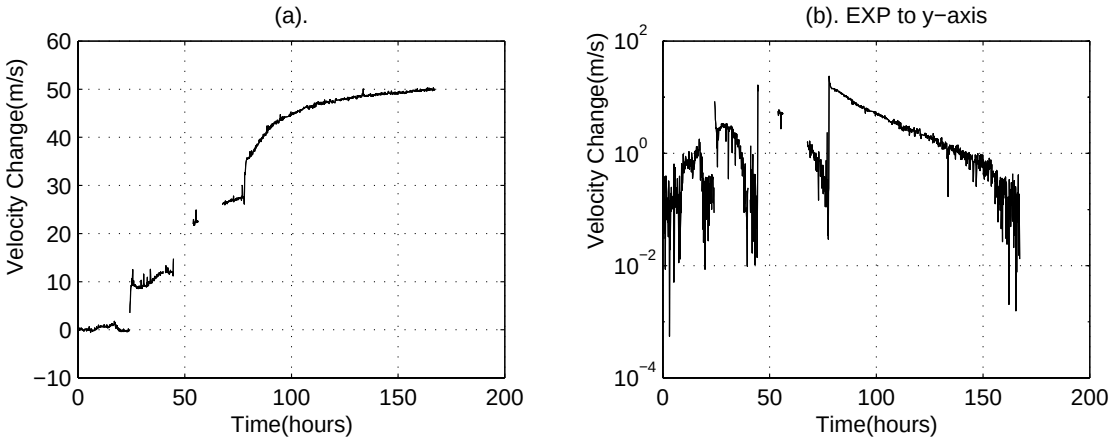

Figure 4.18: Velocity change for CO_2 dissolving into water: (a). from Figure 4.3, (b). logarithmic y-plot of (a).

diffusion mechanics is discussed here, assuming as a boundary condition that the gas-fluid interface has a constant gas concentration at the saturation point for the given temperature and pressure. To simplify the problem, we assume that the surface gas concentration, which in fact changes when pressure changes, stays constant. The cell is considered to be one dimensional and the side boundaries are removed to infinity. The influence of the transducer in the middle of the cell is omitted as well. The fine structure of the reflectors as shown in Figure 4.1 is not considered, either. Because of the rigid reflector in the bottom, an image cell, symmetric to the bottom, is set up to solve the problem. No chemical reaction is considered during the gas diffusion. The solution is listed in Appendix A. The boundary conditions are:

$$C_0 = 0,$$

and

$$C_1 = \chi C_{water}.$$

The diffusion coefficient can be estimated from Appendix B. The diffusion coefficients of solvent/solute pairs are listed in Table 4.3. The distribution of gas concentration will be solved explicitly.

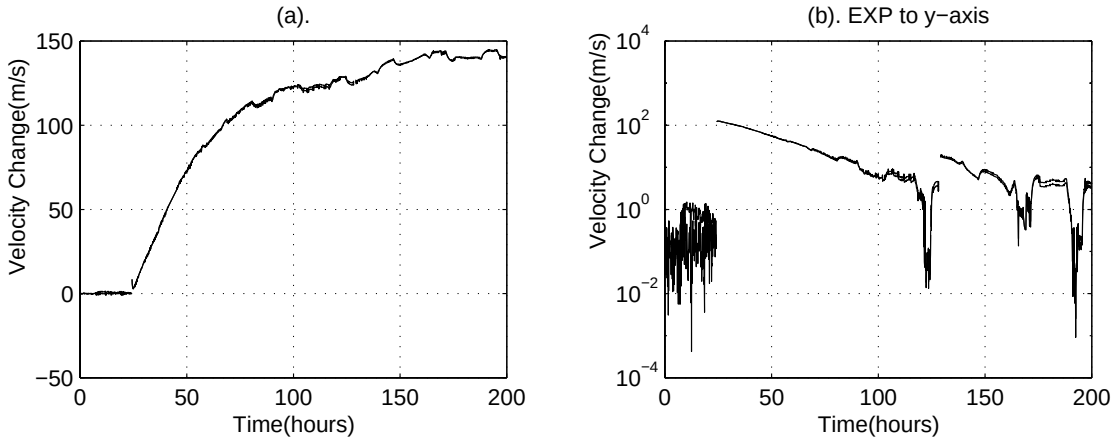

Figure 4.19: Velocity change for NH_3 dissolving into water (see description in Figure 4.18)

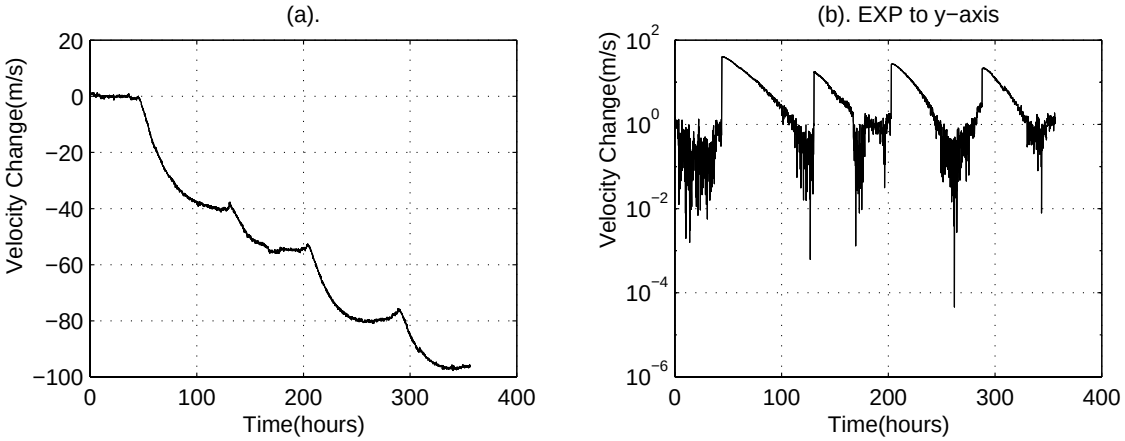

Figure 4.20: Velocity change for CH_4 dissolving into decane (see description in Figure 4.18)

Solvent/Solute	CO_2	CH_4	N_2	NH_3
Water	3.0×10^{-9}	2.213×10^{-9}	2.144×10^{-9}	3.542×10^{-9}
Decane	3.384×10^{-9}	3.677×10^{-9}	3.563×10^{-9}	3.993×10^{-9}

Table 4.3: Diffusion Coefficient of solvent/solute pairs under room conditions ($T = 25^oC, P = 1$ bar) (Units in m^2/s).

We need to convert the time-dependent gas distribution to sound speed, so we can compare the results of this model with our experiment. Assume a linear relation between velocity change and gas content, say:

$$v = v_0 \pm \alpha \chi^f, \tag{4.13}$$

where α is the solubility coefficient for velocity, v_0 is the velocity with zero gas concentration, and χ is gas concentration in mole fraction.

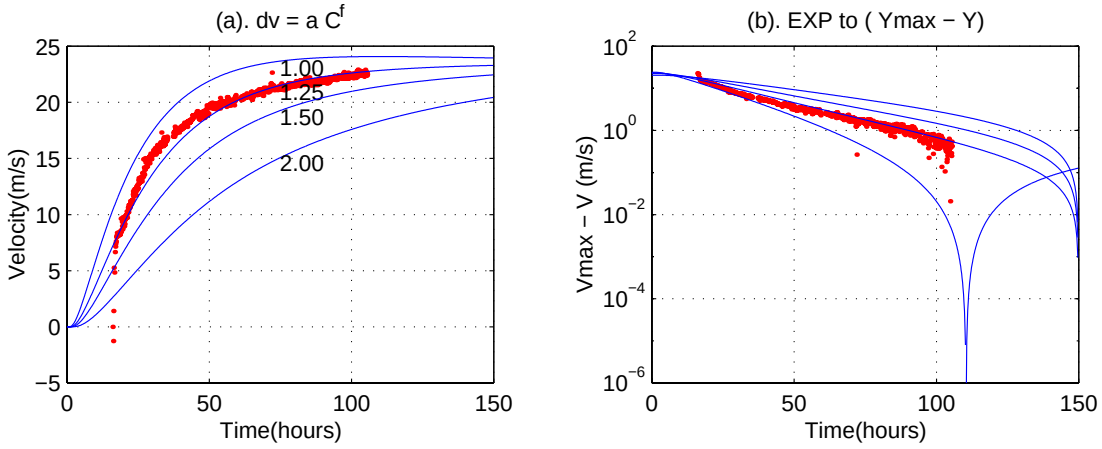

Figure 4.21: Diffusion simulation for CO_2 dissolving into water: (a) Velocity vs. time: solid lines are calculated results with different f-factors (number below each curve), dotted line is measured data from one process of gas solution; (b) logarithmic y-axis plot of (a).

We calculated the related parameters with a large velocity dependence on concentration, and simulated the average result under the experimental conditions as a

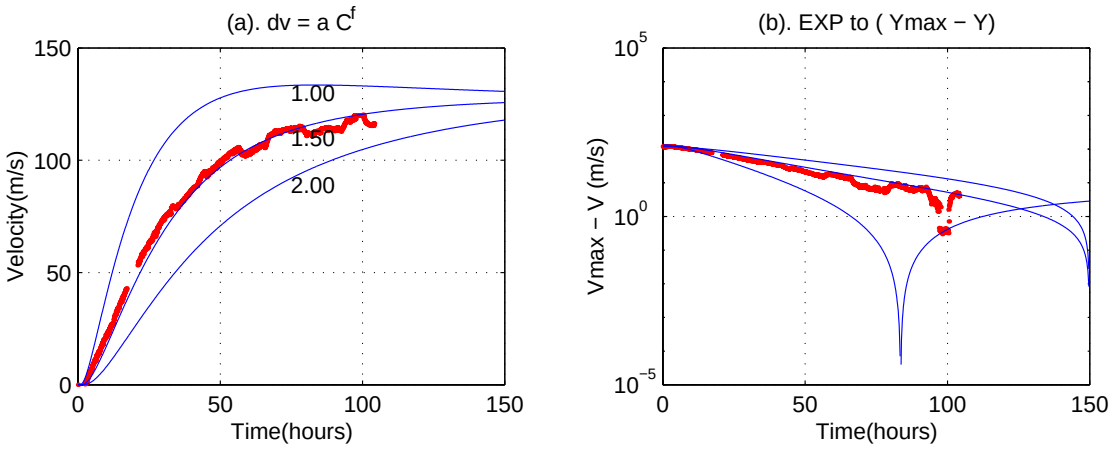

Figure 4.22: Diffusion simulation for NH_3 dissolving into water (see description in Figure 4.21)

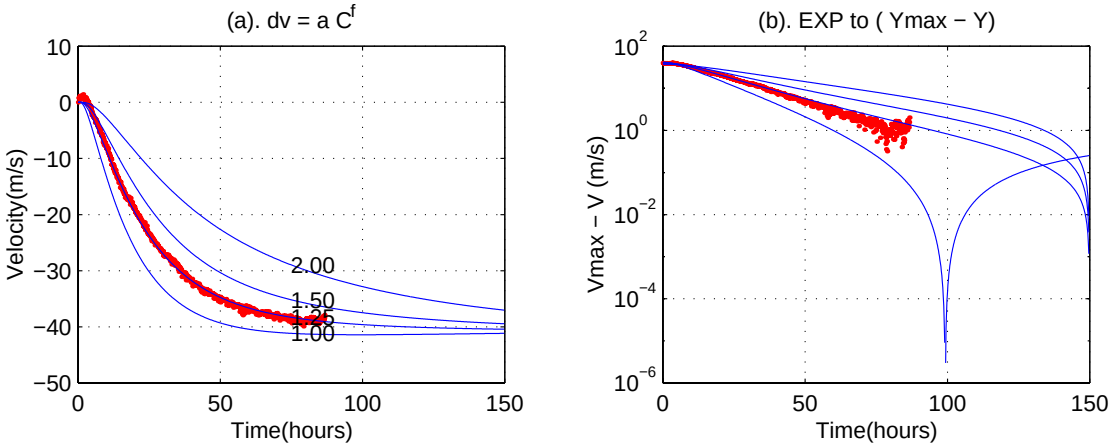

Figure 4.23: Diffusion simulation for CH_4 dissolving into decane (see description in Figure 4.21)

function of time. Figure 4.21, Figure 4.22 and Figure 4.23 give the comparison between the diffusion simulation results and a selected experiment curve related to Figure 4.18, Figure 4.19 and Figure 4.20, respectively, which show large velocity changes with increasing concentration. Each of the figures has two graphics. The solid lines in (a) give simulation results for different f-factors, and the dotted line shows the results for a single dissolving period in the experiment. (b) gives the logarithmic y-axis plot of (a).

We follow the same procedure for the other solvent/solute pairs, as follows. For CO_2 dissolving in water under an equilibrium pressure of $\Delta P = 200psi$, at which the concentration has been normalized to 1, we find:

$$\Delta v_{CO2-H_2O} = 23.0C^{1.25}\,,$$

where C is a related concentration with normalization.

For NH_3 dissolving into water under an equilibrium pressure of $\Delta P = 37psi$, at which the concentration has been normalized to 1:

$$\Delta v_{NH_3-H_2O} = 125C^{1.5}\,.$$

For CH_4 dissolving into decane at an equilibrium pressure of $\Delta P = 190psi$, at which the concentration has been normalized to 1:

$$\Delta v_{CH_4-C_{10}H_{22}} = -40C^{1.25}\,.$$

By using the above relations for velocity change with gas concentration, the simulation results fit quite well with the experimental data:

$$C = \chi(P)C_{water}.$$

where $\chi(P)$ is solute concentration in mole fraction at pressure P.

Then the velocity change with gas concentration for CO_2 in water at $P_0 = 200$ psi

using Equation 4.7, is as follows

$$\Delta v_{CO_2-H_2O} = 23.0(\frac{\chi}{\chi(P_0)})^{1.25} \quad (4.14)$$

$$= 1.79 \times 10^4 \chi^{1.25} . \quad (4.15)$$

For NH_3 in water at $P_0 = 37$ psi,

$$\Delta v_{NH_3-H_2O} = 125(\frac{\chi}{\chi(P_0)})^{1.5} . \quad (4.16)$$

For CH_4 in decane at $P_0 = 190$ psi, using Equation 4.10,

$$\Delta v_{CH_4-C_{10}H_{22}} = -40(\frac{\chi}{\chi(P_0)})^{1.25} \quad (4.17)$$

$$= -7.18 \times 10^4 \chi^{1.25}. \quad (4.18)$$

4.5 Conclusion

This chapter studied the velocity effects of gas-fluid solutions, and is the most important part of this thesis. We selected samples based on our interest in the oil industry. We discovered a new behavior for sound speed in fluid as a function of dissolved gas concentration. We further derived the velocity and concentration relations quantitatively, and realized the physical process under experimental conditions.

While conventional wisdom holds that it can only decrease, we found that the velocity can either increase or decrease when different gases are dissolved into different fluids. Some gases dissolving into water may cause the water velocity to increase. For example, the solutions of CO_2 and NH_3, two gases with high solubility in water, produced the same trend of significant velocity increase. Similar gases dissolving into hydrocarbons may cause velocity to decrease, as we saw in real oil samples. CH_4, CO_2, and N_2, which have high solubility in decane, produced significant decreases in velocity after dissolving into decane.

The dynamic process of gas solution was recorded continuously to accurately obtain the data and to further understand the relation between gas concentration and velocity change. The solution process for gas under the experimental conditions showed an exponential behavior with respect to time. Velocity as a function of temperature, pressure and further gas concentration is given after data analysis.

A diffusion model used to simulate the gas dissolving processes showed consistent results with experiment data. The relation between velocity change and gas concentration was derived by combining the model and real data. Some formulae were given for different sample combinations with significant velocity differences.

Appendix

A. Diffusion Model

The experiment setup after introducing the image plane can be solved as a case of unsteady diffusion in a flat plane with negligible surface resistance. (Geankoplis, 1993) Figure 4.24 is a simple sketch of the problem and its boundary conditions. It has a symmetry plane on x_1. The basic equation is as follows:

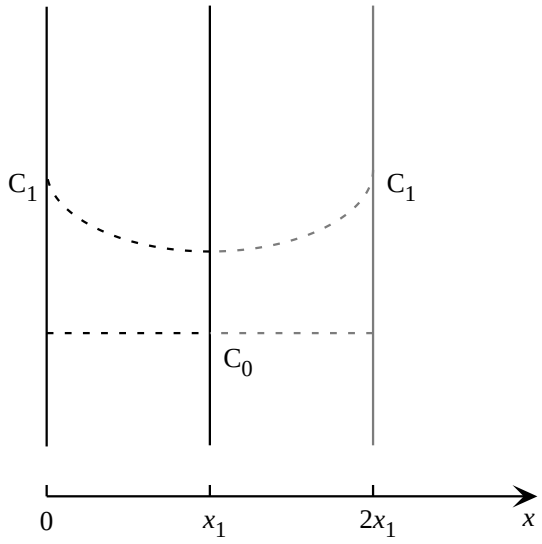

Figure 4.24: Sketch for diffusion in a flat plate

$$\frac{\partial C}{\partial t} = D\frac{\partial^2 C}{\partial x^2}, \tag{4.19}$$

$$C(x,0) = C_0, \tag{4.20}$$

$$C(0,t) = C_1, \tag{4.21}$$

$$C(2x_1,t) = C_1. \tag{4.22}$$

Substituting

$$Y \equiv \frac{C_1 - C}{C_1 - C_0},$$

the equation becomes:

$$\frac{\partial Y}{\partial t} = D\frac{\partial^2 Y}{\partial x^2}, \tag{4.23}$$

$$Y(x,0) = 1, \tag{4.24}$$

$$Y(0,t) = 0, \tag{4.25}$$

$$Y(2x_1,t) = 0. \tag{4.26}$$

The solution of this equation in Fourier series is as follows:

$$Y = \frac{C_1 - C}{C_1 - C_0} = \frac{4}{\pi}\sum_{n=0}^{\infty}\frac{1}{2n+1}exp(-\frac{(2n+1)^2\pi^2 X}{4})sin\frac{(2n+1)\pi x}{2x_1}, \tag{4.27}$$

where $X = Dt/x_1^2$ (dimensionless) and C = concentration at point x and time t.

B. Diffusion Coefficient

The Wilke-Chang gave an empirical formula for the diffusion coefficient, D_{AB}, where solute A is diluted in solvent B. This solution is useful for general purposes, especially when the direct data are not available.

$$D_{AB} = 1.173 \times 10^{-16}(\varphi M_B)^{1/2}\frac{T}{\mu_B V_A^{0.6}}, \tag{4.28}$$

where M_B is the molecular weight of solvent B, μ_B is the viscosity of B in Pa·s, V_A is the solute molar volume at the boiling point (Le Bas, 1915), and φ is an association parameter of the solvent. (Geankoplis, 1993)

Table 4.4 lists some typical values of molar volume related to this study, which will be used to calculate the molecular molar volume when unavailable.

Atom	Atomic Volume $(m^3/kgmol)10^3$	Material	Molecular Volume $(m^3/kgmol)10^3$
C	14.8	N_2	25.6
H	3.7	CO_2	34.0
O(Doubly bonded)	7.4	NH_3	25.8
N(Doubly bonded)	15.6	O_2	25.6

Table 4.4: Atomic or molecular molar volume at boiling point (Le Bas, 1915)

Chapter 5

Theoretical Analysis

5.1 Introduction

The previous three chapters described the experimental procedures and results for fluids and fluid-gas solutions. Velocity after gas dissolution decreases when hydrocarbons are the solvents and increases when the solvent is water. The anomalous behavior for gas aqueous solutions seemed contrary to the 'common' understanding of gas-fluid solutions. With careful calibration of the measurement system and our precise experimental procedure, we are quite confident in our results. Therefore, we must think further to explain the anomalous phenomena and find a reasonable model to interpret the anomalies.

Water is a unique substance in that it has unusually high melting and critical points for its molecular weight, and it has a complicated thermal expansion profile and heat capacity. It has been found that these anomalous properties are due to its strong hydrogen bonds and its specific structure, but there is no universally accepted model. Molecular interaction plays an important role in determining the state of a substance under a given temperature and pressure. The non-bonded interaction between molecules is known as van der Waals interaction, which is fundamental in analyzing the formation or association of bulk materials. In solution study, the interaction between solvent and solute can be described simply in term of the Van der Waals forces. Hydrophobic interaction has been found in the study of aqueous

solutions of nonpolar solutes. This special effect is known to cause some anomalous properties and form special structures in biochemistry.

Thermodynamics describes only the average properties of a macro-system, not the microscopic structure and properties of the system. Thermodynamics is a powerful tool to study the interactions between solute and solvent by comparing the presumed model with experimental quantities.

We use both molecular interaction and thermodynamic relations to understand the physical properties, such as solubility and acoustic velocity, of gas solutions. The pure solvent's structure and the solute-solvent interaction are the key to interpreting any normal or unusual properties.

5.2 Molecular Interactions

Ladd (1994) summarized the types of intermolecular forces and their energy functions, presented here in Table 5.1.

5.2.1 Conformational Analysis

Molecular mechanics uses a classical physics approach to ascribe the energy of a particular conformation to specific bonding parameters. The total steric energy of the molecule as calculated by molecular mechanics is the sum of a number of different kinds of interactions (Carroll, 1998):

$$E_{steric} = E(r) + E(\theta) + E(\Phi) + E(d), \tag{5.1}$$

where each term is discussed below.

E(r) is the energy of stretching or compressing an individual bond,

$$E(r) = 0.5k_r(\triangle r)^2(1 + CS\triangle r), \tag{5.2}$$

where k_r is the force constant of deformation, $\triangle r$ is the deformation of bond length from the ideal, and CS is a cubic stretching constant.

Interaction	Energy functions	Explanation
Covalent	$\int \phi_1 \phi_2 d\tau$	ϕ_1 and ϕ_2 are wave function of atoms
Metallic	$\int \phi_1 \phi_2 d\tau$	
Charge-charge	$\frac{Q_1 Q_2}{(4\pi\epsilon_o)r}$	Q is point charge, ϵ_o is the permittivity of a vacuum (8.854×10^{-12} farad/m), r is the distance of separated charges
Charge-dipole(fixed)	$-\frac{Q\mu cos\theta}{(4\pi\epsilon_o)r^2}$	μ is dipole moment, θ is angle of dipole vector to their center vector
Charge-dipole(free)	$-\frac{Q^2\mu^2}{6(4\pi\epsilon_o)^2 k_B T r^4}$	k_B is Boltzmann constant (1.38×10^{-23}J/K), T is absolute temperature (K)
Dipole(Fixed)-Dipole(Fixed)	$-\frac{\mu_1\mu_2(2cos\theta_1 cos\theta_2 - sin\theta_1 sin\theta_2 cos\phi)}{(4\pi\epsilon_o)r^3}$	ϕ is the angle of relative rotation of μ_1 and μ_2 with respect to the dipole axis
Dipole(free)-Dipole(free)	$-\frac{2\mu_1^2\mu_2^2}{3(4\pi\epsilon_o)^2 k_B T r^6}$	(Keesom energy)
Charge-nonpolar species	$\frac{Q^2\alpha}{2(4\pi\epsilon_o)^2 r^4}$	α is the polarizability of the nonpolar species
Dipole(fixed)-nonpolar species	$-\frac{\mu^2\alpha(3cos^2\theta+1)}{2(4\pi\epsilon_o)^2 r^6}$	
Dipole(free)-nonpolar species	$-\frac{\mu^2\alpha}{(4\pi\epsilon_o)^2 r^6}$	(Debye energy)
Nonpolar species-nonpolar species	$-\frac{3\alpha_1\alpha_2 h\nu_1\nu_2}{2(\nu_1+\nu_2)(4\pi\epsilon_o)^2 r^6}$	(London dispersion energy) $h\nu$ is the first ionization energy
Hydrogen bonding	$\sim -\frac{1}{r^2}$	r is the closest non-bonded distance between two non-hydrogen atoms

Table 5.1: Type of intermolecular forces (Reproduced with permission from Ladd, 1994. Copyright 1994 Prentice-Hall, Inc.)

$E(\theta)$ is the energy of distorting a bond angle from the ideal,

$$E(\theta) = 0.5k_\theta(\triangle\theta)^2(1 + SF(\triangle\theta)^4), \tag{5.3}$$

where $\triangle\theta$ is the deviation from ideal bond angles, k_θ is a force constant, and SF is a distorting constant.

$E(\Phi)$ is the torsional strain (due to non-staggered bonds),

$$E(\Phi) = 0.5V_0(1 + cos(3\Phi)), \tag{5.4}$$

where V_0 is the rotational energy barrier, and Φ is the torsional angle.

$E(d)$ is the energy from van der Waals forces, discussed separately in the following section.

5.2.2 Van der Waals Interactions

Van der Waals interaction is a non-bonded interaction arising from the structure of an atom or molecule. It consists of two parts, attractive and repulsive. The attractive force is dominant at long range, where there is no overlap of electron clouds between the molecules. It consists of electrostatic, induction, and dispersion forces. Electrostatic forces arise from the interaction of the dominant electric moments of the molecules. Induction forces arise from the permanent electric moments of one molecule with induced moments of another. Dispersion forces, also called London forces, arise from the correlated movement of electrons in neighboring molecules.

The repulsive force is a short range one. It takes effect in the spaces where there is a significant overlap of the electron distribution of two separate molecules, and it comes from the violation of the Pauli exclusion principle.

Several models and potential functions have been developed for short range interaction study. A hard sphere model was used to refer to 'excluded volume' by van der Waals' equation. The square-well model takes account of both attractive and repulsive aspects. However, the most useful expressions in practical analysis are the Lennard-Jones model and the Exponential-6 model. The Lennard-Jones potential

gives:

$$U(r) = 4\varepsilon_L[(\delta/r)^{12} - (\delta/r)^6]. \tag{5.5}$$

where δ is the effective (hard-sphere) diameter and r is the distance of two molecules. $-\varepsilon_L$ is the minimal potential of molecular interaction. At $r_e = 2^{1/6}\delta$, intermolecular force $-dU(r)/dr = 0$ and $U_{min}(r_e) = -\varepsilon_L$.

The Exponential-6 potential gives :

$$U(r) = A\exp(-Br) - Cr^6, \tag{5.6}$$

where A and B are constants of the repulsion function, and C is the constant of the attraction function.

5.2.3 Hydrogen Bonding

Hydrogen is unique among the elements in that all of its electron density is used in bonding when it is combined with other elements. By sharing electron density with a neighboring atom, the hydrogen nucleus is relatively exposed on the side opposite the bond. Hydrogen bonding is a weak electrostatic interaction between a hydrogen atom and an electro-negative atom bearing at least one lone pair of electrons. Typically, the hydrogen atom covalently bonded to one of these heteroatoms is also associated with another heteroatom (N, O, P, S). (Fox, 1994)

Because water is such an important and unusual fluid, much effort has gone into explaining its properties. The proposed concept of hydrogen bonding gave a clear picture of the unique structure of water and explained the properties of water. The hydrogen bond is formed between the covalently bonded hydrogen in one molecule and the oxygen with lone pairs of electrons in another molecule, and is symbolized as $O - H \cdots O$.

The hydrogen bond contains contributions from the following forces: (1) electrostatic attraction, (2) delocalization energy (charge transfer), (3) dispersion, and (4) exchange repulsion (Franks, 1972). The Lippincott-Schroeder potential function

(Lippincott, 1955) for a hydrogen bond $X - H \cdots Y$ is:

$$U = U_1 + U_2 + U_3 + U_4, \tag{5.7}$$

where U_1 is the potential function for the X-H bond, U_2 for the $H \cdots Y$ bond, U_3 is the van der Waals repulsion between the two oxygen atoms, and U_4 the electrostatic attraction between the oxygens:

$$U_1 = D(1 - \exp(-\frac{n(r - r_o)^2}{2r})),$$

$$U_2 = -D^* \exp(-\frac{n^*(R - r^* - r_o^*)^2}{2(R - r^*)}),$$

$$U_3 = Ae^{-bR},$$

$$U_4 = Be^{-m},$$

where D and D^* are the strengths of the X-H and $X \cdots Y$ bonds; A, B, b, and mm are constants; n and n^* are related to the ionization potentials of atoms; r_o and r_o^* are normal inter-nuclear distances without the hydrogen bond; r and r^* are the distances with hydrogen bond; and R is the $X \cdots Y$ distance.

The simplest postulation for the water cluster structure is found by considering the hydrogen bond in its dimer structure (Figure 5.1), which is the most stable geometry. This symmetry gives a dimerization energy of about $D_e \sim 6$ kcal/mol (Bene, 1970). Further study gives the possible stable structure of the water cluster to be a trimer, tetramer and so on. There has been no universally accepted view to date.

Samoilov (1965) suggested an interstitial model for liquid water. A hydrogen-bond network is formed containing cavities in which the other species–single non-hydrogen-bounded water molecules–reside. Liquid water is similar to ice in structure but has molecules in the cavities, which leads to a higher density. When ice melts, some of the molecules break their hydrogen bonds with the lattice and move into neighboring cavities.

Pople (1951) suggested a distorted hydrogen-bond model for liquid water. The original structure is assumed to be that of ice-I with fixed coordination and hydrogen

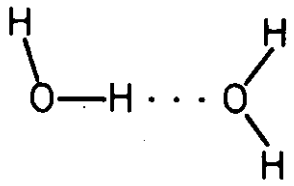

Figure 5.1: Dimer structure of water hydrogen bond

bond angles.

5.2.4 Hydrophobic Interaction

Hydrophobic interaction is the phenomenon by which apolar groups are driven to associate because of their ordering effect on the local aqueous environment. The typical graphic expression for hydrophobic hydration and hydrophobic interactions is shown in Figure 5.2. The hydrophobic interaction is generally treated as a partial reversal of the solution process:

$$solute(apolar solvent) \rightarrow solute(aqueous).$$

The effect of solute concentration should be gradually to remove the anomalous physical properties observed in the limit of "infinite dilution". Hydrophobic hydration is the entropically unfavorable solution of apolar molecules or residues in water. Inert solutes promote the structuring of the neighboring water molecules (Franks, 1975).

The extra contribution of the solvent to this force is given by Gibbs free energy caused by hydrophobic interaction, $\delta G^{HI}(R)$. The property of water as a medium in which nonpolar molecules attract each other is called hydrophobic interaction (Ben-Naim, 1980).

$$\triangle G(R) = U_{ss}(R) + \delta G^{HI}(R),$$

where $U_{ss}(R)$ is the van der Waals interaction of solutes with distance, R, in vacuum.

Hydrophobic solutes have a special behavior at low concentrations of solute (see

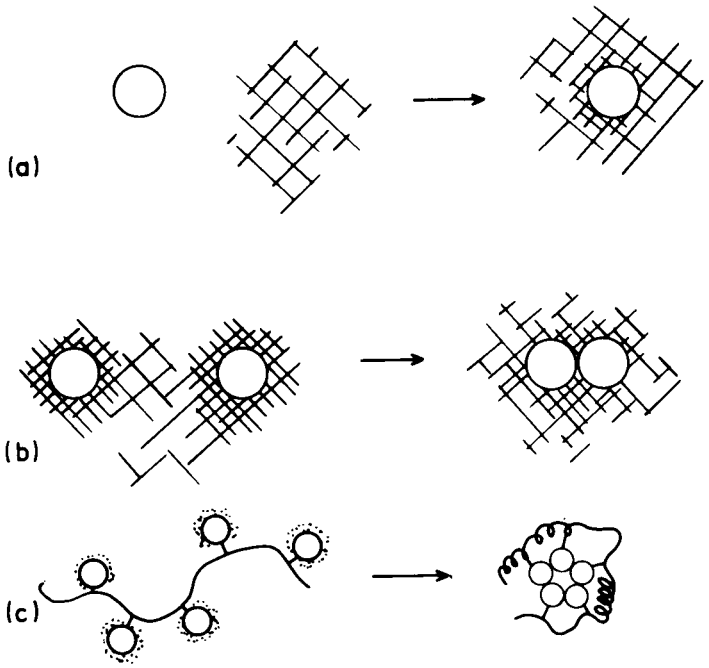

Figure 5.2: Diagrammatic representation of (a) hydrophobic hydration and (b)-(c) hydrophobic interactions; (b) Kauzmann-Nemethy-Scheraga contact interaction, (c) globular protein folding (Reprinted with permission from Franks, 1975. Copyright 1975 Plenum Press.)

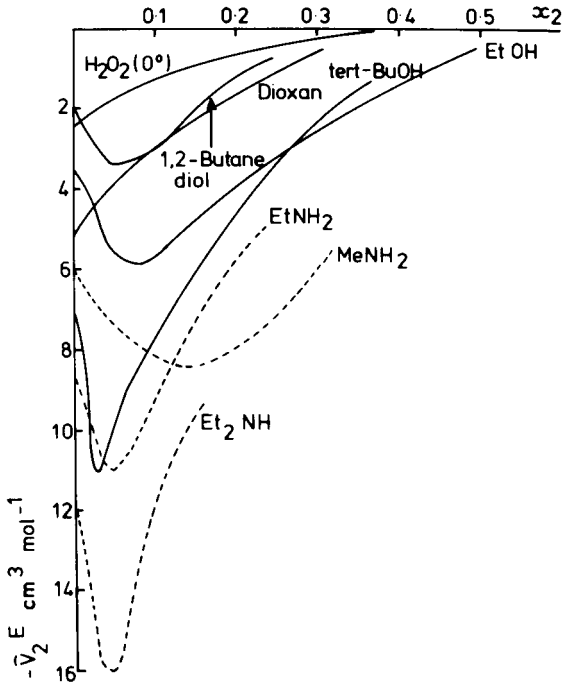

Figure 5.3: Excess molar volume $\overline{V}_2^E(x_2)$ curve at 25^o. The positions and depth of the minima depend on temperature, size, and configuration of the hydrophobic group (Reprinted with permission from Franks, 1975. Copyright 1975 Plenum Press.)

Figure 5.3). At low concentration ($x_2 < x_2^{'}$), the molar volume $-\overline{V}_2^E(x_2)$ shows an abnormal decrease. When the concentration increases to $x_2 > x_2^{''}$, $-\overline{V}_2^E(x_2)$ behaves normally and increases. There is a minimum between $x_2^{'}$ and $x_2^{''}$. The effect of solute concentration should be gradually to remove the anomalous physical properties observed in the limit of "infinite dilution". The anomalies–properties changed in the direction opposite to what we would expect–originate from the hydrophobic hydration phenomenon, at low concentrations, with $x_2 < x_2^{'}$ (Franks, 1975).

The presence of solute molecules should stabilize the four-bonded water network because of the additional van der Waals contacts. In contrast, a nonpolar molecule next to an unbonded water molecule is considered unfavorable compared to pure water, since water-water dipole interactions are stronger than dipole/induced-dipole interactions between water and a solute (Hagler, 1972). Nonpolar dissolved molecules bind with their solvent cluster to form a single group. Hydrophobic interaction tends to make those groups attract each other.

5.3 Thermodynamics of Liquid Mixture

5.3.1 Thermodynamic Quantities

The most important and most common thermodynamic variables for a system are the change in enthalpy $\triangle H$, change in entropy $\triangle S$, and the Gibbs free energy $\triangle G$. These are related as follows:

$$\triangle G = \triangle H - T\triangle S, \tag{5.8}$$

where T is the absolute temperature. Chemical potential is defined as follows:

$$\mu_i = (\frac{\partial G}{\partial n_i})_{P,T,n_{j\neq i}}, \tag{5.9}$$

where n_i is the mole concentration of i^{th} component, and μ_i is chemical potential of the i^{th} component. When dealing with solute and solvent mixtures, it is convenient to use the excess thermodynamic quantities, such as G^E, H^E, S^E, V^E (molar volume) as the measures of non-ideality. The excess quantity is defined as the difference between the measured quantity and the value in an ideal solution:

$$X^E = \triangle X - \triangle X_{id}, \tag{5.10}$$

where an ideal solution can be defined to obey Raoult's law over the whole range of concentration. X can be any physical variable. The partial molar quantity $\overline{X}_i$ is defines as:

$$\overline{X}_i = (\frac{\partial X}{\partial n_i})_{T,P,n_{j\neq i}}, \tag{5.11}$$

where n_i is the number of moles of component i in the mixture. The expression "$j \neq i$" means all components except i.

Frequently measured quantities are heat capacity $\triangle C_P$, the coefficients of thermal expansibility, α, and compressibility, β:

$$\triangle C_P = (\frac{\partial H}{\partial T})_P, \tag{5.12}$$

$$\alpha = (\frac{\partial V}{V \partial T})_P, \tag{5.13}$$

$$\beta_S = -(\frac{\partial V}{V \partial P})_S, \tag{5.14}$$

where β_S is adiabatic compressibility; by substituting subscript T for S, β_T becomes isothermal compressibility. They obey the following thermodynamic relation:

$$\beta_T = \beta_S + \frac{TV\alpha^2}{C_P}. \tag{5.15}$$

Ultrasonic sound speed in a fluid can be expressed by the thermodynamic relation:

$$v^2 = \frac{\beta_S^{-1}}{\rho}, \tag{5.16}$$

where v is sound speed and ρ is density.

5.3.2 Miscibility and Solubility

Completely dissolved mixtures will form a single phase. The range of miscibility of a solute in a solvent reflects the solubility pair. If the mixture is completely homogeneous, the Gibbs free energy of the mixture (G_m) is less than the sum of the Gibbs free energies of the separate components ($G_{A,m}, G_{B,m}$). Then we have,

$$\triangle G_{mix}(x) = G_m(x) - xG_{A,m} - (1-x)G_{B,m}, \tag{5.17}$$

where $x = n_A/(n_A + n_B)$ is the mole fraction of the A component. The quantity $\triangle G_{mix}(x)$ must have a single minimum in its whole miscible range. Figure 5.4 gives a graphic expression for completely miscible and partially miscible cases.

The transfer of an essentially hydrophobic solute from the gas state into aqueous solution is accompanied by a positive free energy change which originates mainly from the unfavorable entropy associated with such a transfer (Ben-Naim, 1974). This energy change is represented by the following equation:

$$\triangle \mu_S^o(g \to l) = -kT \ln(\gamma), \tag{5.18}$$

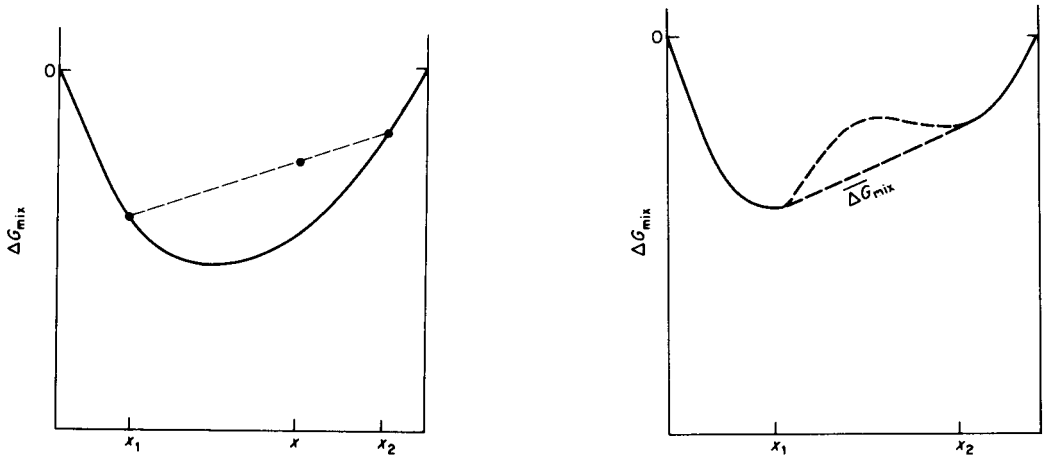

Figure 5.4: Diagrammatic representation of the Gibbs free energy at (a) completely miscible and (b) partial miscible (Reprinted with permission from Murrell, 1982. Copyright 1982 John Wiley & Sons Limited.)

where $\gamma = (\rho_S^l/\rho_S^g)_{eq} = V^g/V^l$ is the Ostwald absorption coefficient, meaning a volume V^g of gas dissolved in a given volume V^l of liquid. The value of $\triangle\mu_S^o$(in water) for methane in water is 1.747 kcal/mol and in ethanol is 0.325 kcal/mol at 10^oC.

The scaled particle theory gives two processes to determine solubility: the formation of a cavity in the solvent capable of accommodating a solute molecule, and an interaction term. The Henry's law solubility χ is given by (Franks, 1972):

$$\ln\chi = (\mu_c/RT) + (\mu_i/RT) + \ln(RT/V), \tag{5.19}$$

where the subscripts c and i represent cavity formation and interaction, respectively, and V is the molar volume of the solvent.

5.4 Results Analysis

Whenever two molecules in the gas state have low kinetic energy, they can become trapped by their intermolecular attraction for each other. When the temperature decreases, more gas molecules are in their low kinetic energy states. The kinetic

energy for free gas molecules, E_k, is as follows:

$$E_k = \frac{1}{2} m \overline{v}^2 = \frac{3}{2} k_b T, \tag{5.20}$$

where T is the absolute temperature, k_b is Boltzmann's constant, m is the molecular weight, and $\overline{v}$ is the average velocity of the molecule. From the Lennard-Jones potential curve (Equation 5.5) in Figure 5.5, we see that molecules with kinetic energy $E_k < \epsilon$, can not escape from molecular interaction. When temperature decreases, more and more gas molecules are trapped to form larger molecule clusters, then begin to condense and form a liquid state. The larger the absolute value of ϵ in the L-J function, the more readily a material becomes liquid at the same conditions of temperature and pressure. Thus the molecular interaction plays an important part in determining the equilibrium state.

Molecular interaction also plays an important role for solubility in liquid. A stronger molecular interaction causes the enthalpy term to be more negative ($-\epsilon$ in Figure 5.5 becomes larger). The positive value of $\triangle \mu_S^o$ caused by the entropy term is decreased by considering the enthalpy contribution, and the solubility increases according to Equation 5.18.

5.4.1 Aqueous Solutions

Section 5.2.2 showed that hydrogen bonding in water causes many unusual fluid properties. Hydrogen bonding makes water more structured in its liquid state than normal fluids. The anomalous properties of water can be interpreted by considering this special structure. We extend the simple interstitial model to understand the anomalous behavior in velocity–described in the previous chapter–when gas is dissolved into water.

Structure of Water

We start from a two-dimensional model as in Figure 5.6, where L-cules are molecules that build up the lattice, and H-cules hold interstitial sites in the lattice (Samoilov, 1965; Ben-Naim, 1974). X-ray diffraction has revealed this structure.

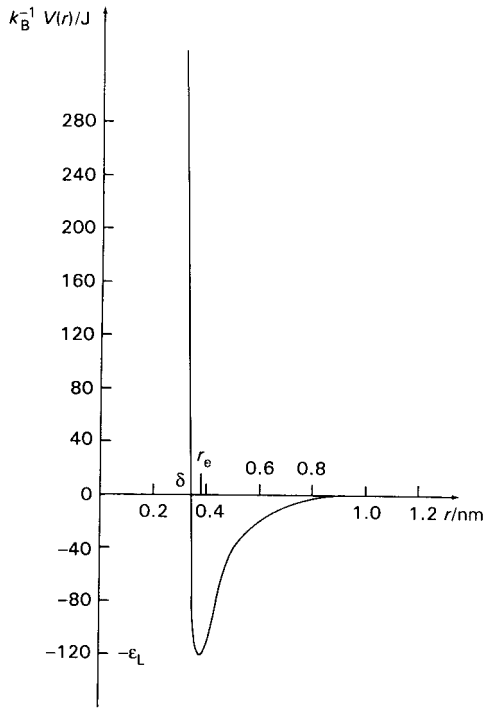

Figure 5.5: Diagrammatic representation of the potential function of molecular interaction (Reproduced with permission from Ladd, 1994. Copyright 1994 Prentice-Hall, Inc.)

Free molecules may occupy vacancies, the sites of L-cules, in water. This causes the anomalous behavior in density when temperature is increased beyond the melting point, and the density maximum is seen at 4^oC. Temperature dependence of the molar volume of water can be interpreted by combining the two competing effects (Eisenberg, 1969): (1) the open structure weakens or breaks down, thus reducing the volume, and (2) the amplitude of anharmonic intermolecular vibrations increases, thus enlarging the volume. Lower temperature leads to a more open structure in water. Most of the water molecules take part in the hydrogen bond structure, and fewer free water molecules exist; thus more vacancies are formed with fewer free molecules to occupy vacant L-cule sites. Therefore, the density of ice is even lower than that of liquid water. When the temperature is increased to slightly higher than melting point, some hydrogen bonds break and more free water molecules form. The

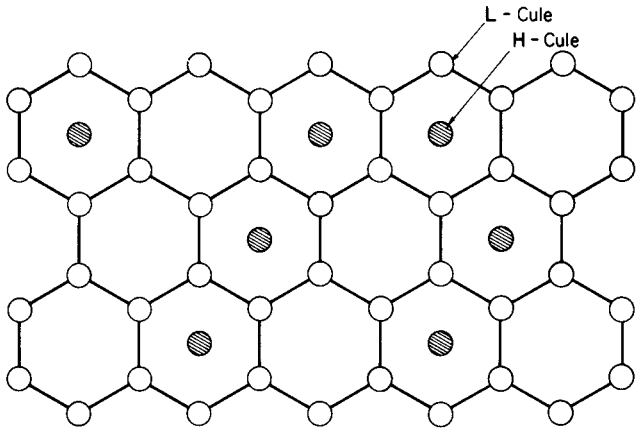

Figure 5.6: Schematic illustration of an interstitial model for water in two dimensions. L-cules are molecules that build up the lattice, whereas the H-cules hold interstitial sites in the lattice. (Reprinted with permission from Ben-Naim, 1974. Copyright 1974 Plenum Press.)

cavities in L-cule sites are then partially occupied, and this effect dominates compared to the enlarging effect of increased vibration. Thus, water density increases. When the temperature is further increased, the vibration effect becomes dominant, and the density starts decreasing. The higher the temperature increase, the greater the enlarging effect.

Water shows anomalously low compressibility compared to normal fluids below some characteristic temperature (46^oC for β_T and 65^oC for β_S). The cavities are occupied more and more because of the increase of the free water molecules to fill into the vacancies when temperature increases, and the molecules in the cavities interact with their surrounding structure making the entire system stronger. This effect causes the compressibility to decrease. When temperature increases, the hydrogen bonds are weakened and more water molecules are free. More cavities are deformed and fewer cavity sites are available. This effect causes the compressibility to increase. These two competing effects lead to a balance at the characteristic temperature above.

Effects of Gas Dissolving

We interpreted the anomalous phenomena in pure water and concluded that the anomalies stem from the special hydrogen bond structure of water. We saw anomalies in our sound speed measurements in Figure 4.3, Figure 4.6, Figure 4.7 and Figure 4.9 when gas was dissolved into water. From the measurement results, CO_2 and NH_3 had a large sound speed increase, whereas CH_4 and N_2 showed little difference.

CH_4 and N_2 are nonpolar molecules with low solubility in water. Apparently as an effect of the molecular interaction described at the beginning of this section, nonpolar molecules interact weakly with polar water. Therefore, their solubility is small according to Equation 5.18. CO_2 has no dipole moment, but it has a quadrupole moment. Therefore, CO_2 has a stronger interaction with the water molecule than nonpolar CH_4 and N_2. The solubility of CO_2 is much higher. NH_3 has a dipole moment, has a lone pair of electrons, and can form hydrogen bonds; it also undergoes a chemical reaction with water. Thus, NH_3 has the highest solubility among the gases we considered.

Because the process involves two phases, gas dissolving into water has limited miscibility. The range of miscibility depends on the gas solubility. Therefore, the solid curve shown in Figure 5.17 applies over only a small range. The miscible range can be extended by changing the conditions, such as decreasing temperature or increasing pressure, to increase the gas solubility.

The amount of gas molecules dissolving into water is generally small. Nonpolar gas and even polar gas apparently satisfy the low-concentration assumption ($\chi < \chi^{'}$) of Section 5.2.3, where $\chi^{'}$ is around 0.1 for aqueous solution. χ, which is on the order of 10^{-4} for CH_4 and N_2, is very small compared to $\chi^{'}$. When these dissolving molecules occupy the vacancies in the water structure, the weak molecular interaction with water clusters should cause anomalies in water properties, but the results are not apparent, since the filled vacancies are so few and the interaction weak. The compressibility or sound-speed change is negligible when nonpolar gas dissolves in liquid water.

CO_2 and NH_3, conversely, have stronger molecular interactions with the polar water network. The presence of those solute molecules in the vacancies in the water

structure stabilizes the water cluster. Still, those solutes have a weaker interaction than the interaction between unbonded water and the water dipole. Although CO_2 and NH_3 have higher solubility than nonpolar CH_4 and N_2, they still satisfy the low-concentration assumption ($\chi < \chi^{'}$) at our experimental conditions, room temperature and higher pressure. The vacancies in the water structure trap solutes easily. Most of the solutes fill up the vacancies in the water cluster rather than bond to free water molecules. Stabilization in a four-bonded water network is dominant. Thus the compressibility or sound speed will behave anomalously, as the experimental results reveal.

This interpretation can be seen from experimental evidence of water-ethanol mixtures by D$^{'}$Arrigo (1988). Figure 5.7 gives his measurement results of sound speed for water-ethanol mixtures. Pure ethanol has a lower velocity than pure water. The anomalous behavior is apparent in Figure 5.7a. At low concentration ($\chi < \chi^{'} \approx 0.1$), velocity increases while solute concentration increases at the measured temperature. The higher the temperature is, the lower the peak of the velocity, as the available vacancies are fewer and more water clusters are broken. When the solute concentration increases to fill the total available water vacancies, the velocity does not increase any more, and the cluster begins to weaken because of the weaker interaction between solute and unbonded water molecules. The mixture will show normal fluid characteristics.

5.4.2 Hydrocarbon Solvents

Liquid hydrocarbons behave normally, since they have a single structure determined by van der Waals interactions. The heavier the molecule is, the stronger the intermolecular attraction is. Usually, hydrocarbons with carbon number larger than 5 are in the liquid state at room conditions. Hydrocarbons with carbon number less than 4, such as methane (C_1) and propane (C_2), are in the gas state at room conditions. Only the low kinetic-energy gas molecules can be trapped by hydrocarbon fluids, with the solubility depending on the strength of the interaction between the gas molecule

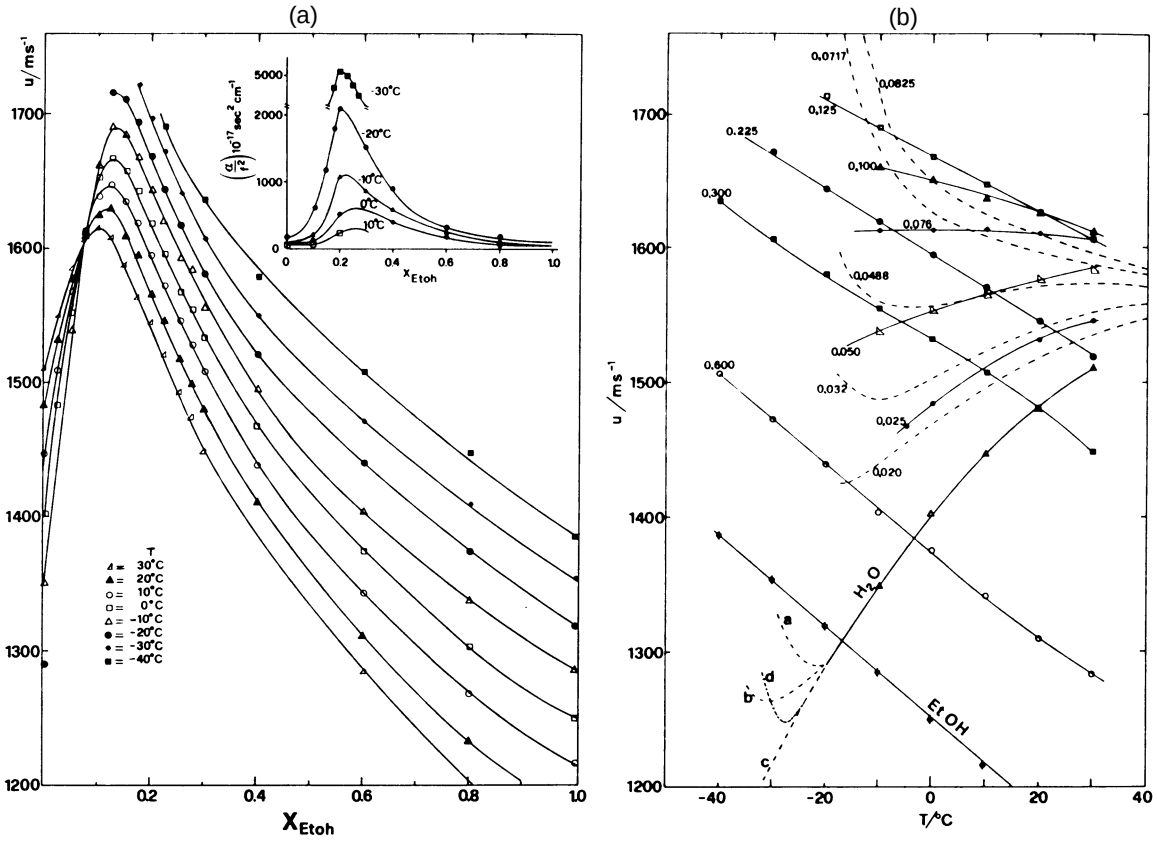

Figure 5.7: The velocity of ethanol aqueous solution vs. (a) solute concentration (x-mole fraction), and (b) temperature for some selected concentrations (Reprinted with permission from D'Arrigo, 1988. Copyright 1988 American Institute of Physics.)

and the hydrocarbon fluid. We focus on the behavior of alkane hydrocarbon fluids and their mixtures with the gases CH_4, CO_2, and N_2. CH_4 and N_2 are non-polar molecules. Their interactions with liquid hydrocarbons are mainly nonpolar-nonpolar interactions, which are also called London dispersion energies, as seen in Table 5.1. The solubility of these gases shows a similar order except that the similarity of CH_4 to the hydrocarbon solvent makes CH_4 more stable. CO_2 has a quadrupole moment, which contributes to the total interaction energy. The solubility of CO_2 in decane (C_{10}) will be larger than that of nonpolar gases by Equation 5.18. The gas solution in hydrocarbon fluid causes weakening of the heavier molecular interaction of the pure fluid. The physical properties behave according to the normal trend: sound speed will decrease when concentration increases. The experimental results appear in Figure 4.10, Figure 4.14, and Figure 4.17. We assumed the molar volume of solutions, because of free solute molecule and free solvent molecule interaction and their random distribution, to be as follows:

$$\overline{V}_m(x) = (1-x)\overline{V}_l + x\overline{V}_g, \tag{5.21}$$

where subscripts m, l, and g corresponded to mixture, solvent, and solute respectively; x is the solute concentration in mole fraction. According to Equation 5.14, then,

$$\begin{aligned} \beta_{S,m}(x) &= \frac{1}{\overline{V}_m(x)}[(1-x)\beta_{S,l}\overline{V}_l + x\beta_{S,g}\overline{V}_g] && (5.22) \\ &= \beta_{S,l} + (\beta_{S,g} - \beta_{S,l})x\frac{\overline{V}_g}{\overline{V}_m(x)}, && (5.23) \end{aligned}$$

where $\beta_{S,m}$, $\beta_{S,l}$ and $\beta_{S,g}$ are the adiabatic compressibility of the mixture, solvent and solute, respectively. As $\beta_{S,g} - \beta_{S,l} > 0$ for gas solution, then

$$\beta_{S,m}(x) \geq \beta_{S,l}\,.$$

The adiabatic compressibility of the mixture is larger than that of the pure fluid when gas is dissolved into the fluid.

5.5 Conclusion

This chapter focuses on the theoretical study of fluids and fluid-gas mixtures. The purpose of this chapter is to find a model to interpret the normal and abnormal results we obtained from experiment, and further to understand the underlying mechanics. The study is based on unbonded molecular interactions. Van der Waals forces dominate in the usual condensed phase, either fluid or real gas. The competition between intermolecular potential and thermal excitation because of temperature, as well as pressure, determines the degree of condensation. Certainly the entropy contribution is also important in determining the final phase.

We found that the anomalous properties of pure water come mainly from two factors: hydrogen bonding and a special cluster network. A two-dimensional interstitial structure, found in the ice-I structure, was proposed to simplify the analysis. Filling the cavities of the water cluster makes the entire system denser; also the filling solutes interact with the surrounding structure to strengthen the network. Temperature increase weakens the bonding network and breaks some cages, so that fewer cavities and more free water molecules exist, making the system tend towards normal. The competition of those two effects leads to a transition from abnormal to normal fluid behavior. This model interprets the anomalies in density and sound speed, which interested us in this study. Using this model, gas aqueous solutions should show similar anomalies. External solutes filling the cavities of the network may strengthen the entire network while keeping the cavities unchanged. Strongly interacting solutes, such as CO_2 and NH_3, give significant abnormalities in sound speed, as we saw from experiment.

Unlike water, hydrocarbon fluids behave normally. Van der Waals interaction between free solute and free solvent molecules dominates in the solution. Temperature increase weakens the unbonded structure. Compressibility decreases when gases, which have weaker interaction than heavier fluid molecules, are dissolved into the solvent. Our experimental results from decane mixed with solute gases CH_4, CO_2, and N_2 corroborate this analysis.

Chapter 6

Conclusion

The purpose of this thesis is to study the acoustic properties of reservoir fluids. We study both pure fluid samples and gas-fluid solutions. The samples, fluid solvents of water and decane and gas solutes of CO_2, CH_4, N_2, and NH_3, are selected not only for simplicity but also because they have practical applications. Our study proceeds from experimental to theoretical as follows:

- System Design & Construction: A phase-interference method was developed for velocity measurement, where double impulses and double reflectors were combined to fulfill the interference requirements. I built the entire measurement system myself, including most of the electrical and mechanical design, to allow efficient and convenient measurements. The velocity measurement has a relative error of $\pm 0.02\%$. The calibration or real measurement uncertainty is the best verification for our system setup.

- Experimental Measurement: The experimental results range from pure fluids to gas-fluid solutions. The pure fluid measurement is important not only for obtaining the data and calibrating the system, but also for developing a proper measurement algorithm. Two fluid solvents, water and decane, were measured during mixing with typical gas solutes, selected as above. The velocity change with gas dissolution was found to have opposite trends for the two fluids. For gas aqueous solution, the sound speed of the solution increases with increasing

concentration. Velocity increases up to 50 m/s ($\approx 3\%$) and 140 m/s ($\approx 9\%$) for CO_2 aqueous solution and NH_3 aqueous solution respectively. These results were obtained at room temperature ($\approx 22^oC$) with CO_2 saturated vapor pressure of 400 psi (where CO_2 concentration in mole fraction is about 0.8%), and NH_3 saturated vapor pressure of 70 psi. Velocity increases only slightly for CH_4 and N_2 aqueous solutions (only 1.5 m/s for CH_4 and 2.5 m/s for N_2 at saturated vapor pressures of 700 psi and 850 psi, respectively). Conversely, for gases dissolved in decane, the sound velocity of the solution decreases with increasing concentration. Velocity decreases about 100 m/s for CH_4 ($\approx 8\%$), 130 m/s for CO_2 ($\approx 10\%$), and 47 m/s for N_2 ($\approx 4\%$) at saturated vapor pressures of 500 psi, 400 psi, and 600 psi, respectively. The empirical relation between velocity and concentration was given in the measurement range. A dynamic analysis was carried out to understand the real diffusion process.

- Theoretical Model: Theoretical analysis was based on molecular interaction. Van der Waals interaction plays an important role in analysis of a normal fluid, such as decane. Hydrogen bonding between water molecules makes water exhibit special properties. A interstitial model was used to explain water's anomalous behavior.

Our study makes three original contributions:

- A robust system was built to take highly accurate measurements, and a reliable experimental method was developed to measure the dynamic velocity change in a fluid-gas solution.

- Reverse trends in velocity were discovered when gas dissolved into water and decane.

- A mechanism was proposed based on the interstitial structure of water to interpret its anomalous properties during gas dissolution.

Our results and contributions not only give the properties of the samples themselves, but also can be extended to predict the properties in some other interesting

fields. Gas hydrates provide an example. According to the interstitial structure of water, more and more hydrogen bonded units with vacancies are formed when temperature decreases. The velocity of pure water or ice decreases with decreasing temperature. When solute molecules of gas occupy the interstitial vacancies, the velocity will increase compared to pure water under the same conditions. The more the vacancies are filled by solute molecules, the more apparent will be the increase. The velocity will increase until all of the vacancies are filled; then it will behave normally, i.e., start to decrease, as more gas is dissolved. The amount of gas in solution depends on the temperature and molecular interaction between the solute and the water. When gas hydrate forms, many gas molecules occupy the interstitial positions, and the velocity will be greater than the velocity of pure water ice.

Further study can be developed experimentally and theoretically. The results in our experiment cover only a small range of gas concentrations. Further study can expand the range of concentrations by decreasing temperature and using efficient agitation. Theoretically, a general relation between acoustic properties and gas concentration may be determined using molecular interaction. Combining the gas dissolving mechanism and hydrophobic interaction may be useful in some applications, such as understanding the process of CO_2 flooding.

Bibliography

A.G.A. (American Gas Association), 1965. *Gas engineers handbook.* the Industrial Press, New York.

Bark, L.S., 1964. *Tables of the velocity of sound in sea water.* New York, Macmillan.

Battino, R., 1987. *Solubility Data Series, Methane*, ed. Clever, H.L. and Young, C.L., **27/28**. Pergamon Press, Oxford.

Batzle, M. and Wang, Z., 1992. "Seismic properties of pore fluids". *Geophysics*, **57**(11), 1396.

Bene, J. Del and Pople, J.A., 1970. "Theory of molecular interaction. I. molecular orbital studies of water polymers using a minimal alater-type basis". *J. Chem. Phys.*, **52**, 4858.

Ben-Naim, A., 1980. *Hydrophobic Interactions.* Plenum, New York.

Ben-Naim, A., 1974. *Water and aqueous solutions.* Plenum, New York.

Bhatia, A.B., 1967. *Ultrasonic Absorption.* Oxford at the Clarendon Press.

Blaney, B.L. and Ewing, G.E., 1976, "Van der Waals Molecules". *Ann. Rev. Phys. Chem. 1976.* **27**, 553.

Burger, K., 1983. *Solvation, ionic and complex formation reactions in non-aqueous solvents.* Elsevier Scientific Pub. Co., Amsterdam.

Carroll, F.A., 1998. *Structure and Mechanism in organic chemistry.* Brooks/Cole Publishing Company.

Chen, C.T., et al., 1978. "Speed of sound in NaCl, $MgCl_2$, Na_2SO_4, and $MgSO_4$ aqueous solutions as functions of concentration, temperature, and pressure". *J. Acoust. Soc. Am.*, **63**, 1795.

Clark, V.A., 1992. "The effect of oil under in-situ conditions on the seismic properties of rocks". *Geophysics*, **57**(7), 894.

Colgate, S.O., *et al.*, 1992. "Sonic speed and critical point measurements in ethane by the acoustic resonance method". *Fluid Phase Equil.*, **76**, 175.

Colgate, S.O., et al., 1990. "Experimental ideal gas reference state heat capacities of gases and vapors". *J. Chem. Eng. Data*, **35**(1), 1.

D'Arrigo, G. and Paparelli, A., 1988. "Sound propagation in water-ethanol mixtures at low temperatures. I. Ultrasonic velocity". *J. Chem. Phys.*, **88**, 405.

Eisenberg, D. and Kauzmann, W., 1969. *The structure and properties of Water.* Oxford University Press.

Ferris, H.G., 1952. "The free vibration of a gas contained with a spherical vessel". *J. Acoust. Soc. Am.*, **24**(1), 57.

Fine, R.A. and Millero, F.J., 1973. "Compressibility of water as a function of temperature and pressure". *J. Chem. Phys.*, **59**(10), 5529.

Fogg, P.G.T. and Gerrard, W., 1991. *Solubility of gases in liquids.* John Wiley & Sons, New York.

Fox, M.A. and Whitesell, J.K., 1994. *Organic chemistry.* Jones and Bartlett Publishers, Boston.

Franks, F., 1972. *Water, a comprehensive treatise (Vol. I).* Plenum, New York.

Franks, F., 1975. *Water, a comprehensive treatise (Vol. IV).* Plenum, New York.

Geankoplis, C.J., 1993. *Transport processes and unit operations (3rd ed.).* Engelwood Cliffs, N.J.

Gregory, J.K., et al., 1997. "The water dipole moment in water clusters". *Science*, **275**, 814.

Hagler, A. T., et al., 1972. "Structure of liquid water. Statistical thermodynamic theory". *J.Phys. Chem.*, **76**, 3229.

Horne, R.A., 1972. *Water and aqueous solution, structure thermodynamics, and transport processes.* Wiley-interscience, New York.

Kortbeek, P.J., *et al.*, 1985. "Apparatus for sound velocity measurements in gases up to 10 k bar: Experimental data for argon". *Rev. Sci. Instrum.*, **56**, 1269.

Kvenvolden, K.A., 1988. "Methane hydrate - A major reservoir of carbon in the shallow geosphere". *Chemical Geology*, **71**, 41.

Ladd, M., 1994. *chemical Bonding in Solids and Fluids.* Ellis Horwood, New York.

Latimer, A.H. and Rodebush, H. A., 1920. "Polarity and ionization from the standpoint of the lewis theory of valence". *J. Am. Chem. Soc.*, **42**, 1419.

Le Bas, G., 1915. *The molecular volumes of liquid chemical Compounds.* David McKay Co., New York.

Lippincott, E.R. and Schroeder, R., 1955. "One-dimensional model of the hydrogen bond". *J. Chem. Phys.*, **23**, 1099.

Liu, K., et al., 1996. "Water Clusters". *Science*, **271**, 929.

McCain, W.D., 1990. *The properties of petroleum fluids (2nd ed.).* PennWell, Tulsa.

Mehl, J.B. and Moldover, M.R., 1981. "Precision Acoustic Measurements with a Spherical Resonator: Ar and C_2H_4". *J. Chem. Phys.*, **74**(1), 4062.

Michelson, A.A., 1902. *Light Waves and Their Uses.* Univ. of Chicago Press, Chicago.

Montel, Francois, 1993. "It's a gas, or is it?". *ELF supplement*, **4**, 4.

Murrell, J.N. and Boucher, E.A., 1982. *Properties of liquids and solutions.* John Wiley & Sons Ltd., New York.

Odutola, J.A. and Dyke, T.R., 1980. "Partial deuterated water dimers: microwave spectra and structure". *J. Chem. Phys.*, **72**, 5062.

Orr, F.M., 1995. *Thermodynamics*. PE251 course notes, Stanford University.

Pople, J.A., 1951. "Molecular association in liquids II. A theory of the structure of water". *Proc. Roy. Soc. Lond.*, **A205**, 163.

Samoilov, O.Ya., 1965. *Structure of aqueous electrolyte solutions and the hydrate of ions*. Plenum, New York.

Sloan, E.D., 1990. *Clathrate hydrates of natural gases*. Marcel Dekker, New York.

Stillinger, F.H., 1980. "Water revisited". *Science*, **209**, 451.

Wang, Z., Nur, A. and Batzle, M.L., 1988. "Acoustic velocities in petroleum oils". *Society of Petroleum Engineers (SEP) paper 18163*. Proc. 63rd Soc. Petr. Eng. Tech. Conf., Formation Eval. Res. Geol. Section, 571.

Williams, J. and Lamb, J., 1958. "On the measurement of ultrasonic velocity in solid". *J. Acoust. Soc. Am.*, **30**(4), 308.

Wilson, W.D., 1959. "Speed of sound in distilled water as a function of temperature and pressure". *J. Acoust. Soc. Am.*, **31**, 1067.